

Zhang et al.: Identification of soil-cooling rains in southern France from soil temperature and soil moisture observations, Atmos. Chem. Phys. Discuss., <https://doi.org/10.5194/acp-2018-929>.

RESPONSE TO REVIEWER #2

2.2 [General comments

There is one point that is however not clear for me. The authors presents some simulations based on the ISBA land surface model, that does not include a representation of heat exchanges due to water mass movement, to show that it is not able to reproduce the observed change in soil temperature. To perform these simulations, the authors use the SAFRAN reanalysis that has a low temporal resolution for rainfall (hourly) and a spatial resolution of 8x8 km². This resolution may not allow the forcing to capture very localized rainfall events. If in situ meteorological data are available, why didn't the authors use them?

Specific comments

1/ p.4, lines 10-14; p.8 lines 10-16: why do you use SAFRAN reanalysis and not the in situ collected meteorological data? The low resolution of SAFRAN is probably not adapted to capture the high spatial and temporal variability of rainfall that is relevant if you want to relate the forcing to temperature and soil moisture local variations.]

Response 2.2:

The shown ISBA simulations represent the current state of hourly operational land surface monitoring, available over whole of metropolitan France. The message we want to convey is that the best possible operational simulations currently available are not able to represent the impact of intense precipitation on the soil temperature profile. The ISBA land surface model needs to be improved. The SAFRAN atmospheric analysis could also probably be improved by using more in situ observations together with high resolution atmospheric simulations. This is work in progress. Unfortunately, local meteorological data do not include all the atmospheric variables needed to force the ISBA land surface model. Using locally observed precipitation together with other variables from SAFRAN would not be technically correct. Therefore, properly disentangling SAFRAN and ISBA shortcomings is not possible now. We understand that this can be confusing for the readers: **the ISBA simulations were moved to the Supplement, including Figure 6.**

2.3 [2/ Section 3.3: the location of this section is strange. Why didn't you put it in an appendix?]

Response 2.3:

Section 3.3 was moved to an appendix.

2.4 [3/ Section 4.2: this section is very detailed. It could be shortened. Fig. 9 could also be put in the supplementary materials.]

Response 2.4:

Section 4.2 was shortened: last paragraph of this section and Fig. 9 were moved to the supplement. The content of old Fig. 9 was summarized in new Table 4.

Table 4. Characteristics of the 122 intense soil-cooling rains.

Characteristic	Event count or fraction
M or MM climate	107
O or SO climate	15
Spring	17
Summer	82
Autumn	19
Winter	4
Starting time at daytime (9:00 am – 21:00 pm)	83 %
Duration less than 2 hours	80 %
Minimum $\Delta T_{5\text{cm}}$ values ranging from -3 to -1.5 °C 12 min ⁻¹	82 %
Maximum number of events per year per station	2.7

2.5 [4/ Section 5.2. This section is somehow frustrating: the authors have gathered all the data to test the impact of cold rainfall temperature on the soil temperature and water content and the reader is expecting to see such a simulation using the ISBA model. Adding a representation of heat exchanges due to water mass movement into the model could be done in order to complement the paper. It would also give more strength to the conclusions on whether rainfall cooling matters or not.]

Response 2.5:

The following discussion was included in Section 5.2:

“Now, the ISBA model has no representation of heat exchanges due to water mass movement. This process needs to be introduced in ISBA. We think that data from a fully instrumented site including direct measurements of rain water temperature are needed to completely address this issue and to validate the upgraded model version. Such an experiment would give insights to understand when, where and why soil cooling occurs or not and would be valuable to help model development. In particular, the precipitation-induced sensible heat flux is not limited to intense precipitation and the impact of this process on the surface energy budget needs to be investigated in all conditions.”

RESPONSE TO REVIEWER #3

3.1 [General comment: This paper presents an assessment of soil-cooling rain events in South of France and is based on observations recorded during 9 years, a long enough period to allow robust statistics. The paper is mostly a description of the dataset which is stratified in different ways. The dataset and the method are generally well described and the argument is quite relevant. The modelling aspects are less satisfactory, for instance, the comparison between ISBA and the observations is not convincing since ISBA does not represent the cooling process and the quality of the forcing is poor (duration and intensity of the rain events). On one hand the discussion of the results could have been shortened may be summarizing some of them in tables, on the other hand insights to understand when, where and why soil cooling occurs or not would have been valuable to help model development. For instance section 5.2 starts well "Does soil cooling matter" but at the end of the section it is not clear what is the added value of the paper to answer this question.]

Response 3.1:

See also Responses 2.2 and 2.5.

The ISBA simulations were moved to the Supplement, including Figure 6.

The following discussion was included in Section 5.2:

“Now, the ISBA model has no representation of heat exchanges due to water mass movement. This process needs to be introduced in ISBA. We think that data from a fully instrumented site including direct measurements of rain water temperature are needed to completely address this issue and to validate the upgraded model version. Such an experiment would give insights to understand when, where and why soil cooling occurs or not and would be valuable to help model development. In particular, the precipitation-induced sensible heat flux is not limited to intense precipitation and the impact of this process on the surface energy budget needs to be investigated in all conditions.”

3.2 [Minor comments The meaning of the sentence starting line 29 in section 3.1 is not clear.]

Response 3.2:

“The missing data fraction across seasons (Table S1) is used to correct the estimation of the possible number of intense soil-cooling rainfall events, their frequency and the mean time lag between two events.”

This sentence refers to Table 1. **It was rephrased and moved to Section 2, where Table 1 is presented:**

“Table 1 also presents the frequency of intense soil-cooling events (see Sections 3 and 4). Since a noticeable fraction of observed T5cm or VSM5cm data is missing, the number of marked soil-cooling rainfall events could be underestimated. The missing data fraction across

seasons (Table S1) is used to correct the estimation of the possible number of intense soil-cooling rainfall events, their frequency and the mean time lag between two events in Table 1.”

3.3 [Section 3.2 l. 24 : Why the precipitation induced sensible heat flux dominates the heat exchange, is it possible to evaluate it and compare with the heat conduction?]

Response 3.3:

The following discussion was included in Section 5.1:

“In Eqs. (2) and (3), it is assumed that the precipitation-induced sensible heat flux dominates heat exchanges in the topsoil layer. Since soil properties are known, the mean PH value can be estimated from Eq. (2) for the intense soil-cooling events used to retrieve Train (see Table 5). For the 10 events of Table 5 occurring at summertime, this flux ranges from 408 to 1009 W m⁻², with a mean value of 648 W m⁻². These PH flux values are very high and represent large fractions of absolute values of the net radiation Rnet (i.e. the amount of energy available for surface heat exchanges, driven by the incoming solar radiation, that could be simulated without accounting for PH). They are probably often much larger than Rnet because the Rnet energy budget component is generally small during rainfall events, in relation to the low incoming solar radiation. Moreover, 7 events out of 10 occur at nighttime or at dusk (see Supplement), i.e. in small Rnet value conditions. The Rnet variable is not measured at SMOSMANIA stations. Typical measured summertime values of the maximum daily Rnet over the grassland site of Meteopole-Flux in southwestern France (Zhang et al. 2018) range from about 200 W m⁻² during cloudy rainy days to 5 about 700 W m⁻² in clear sky conditions. At nighttime, absolute Rnet values rarely exceed 100 W m⁻².”

3.4 [Section 4.1 When speaking about the minimum deltaT5cm using absolute values may render easier the reading:: even if it's correct: "larger than -0.5C" is a bit confusing.]

Response 3.4:

“are larger than -0.5 °C in 12 minutes” was replaced by “do not depart much from 0 °C in 12 minutes” (now in Supplement P. 28).

3.5 [Panels in Figure 6 are partially commented, if they are not essential they have to be removed or put in the supplementary materials. By the way, units are original!]

Response 3.5:

Figure 6 was moved to the Supplement (now Figure S25).

Identification of soil-cooling rains in southern France from soil temperature and soil moisture observations

Sibo Zhang^{1,2}, Catherine Meurey¹, and Jean-Christophe Calvet¹

¹CNRM (Université de Toulouse, Météo-France, CNRS), Toulouse, France

5 ²now at: Qian Xuesen Laboratory of Space Technology, China Academy of Space Technology (CAST), Beijing, China

Correspondence to: Jean-Christophe Calvet (jean-christophe.calvet@meteo.fr)

Abstract. In this study, the frequency and intensity of soil-cooling rains is assessed using in situ observations of atmospheric and soil profile variables in southern France. Rainfall, soil temperature and topsoil volumetric soil moisture (VSM) observations, measured every 12 minutes at 21 stations of the SMOSMANIA (Soil Moisture Observing System -
10 Meteorological Automatic Network Integrated Application) network, are analyzed over a time period of 9 years, from 2008 to 2016. The spatial and temporal statistical distribution of the observed rainfall events presenting a marked soil-cooling effect is investigated. It is observed that the soil temperature at a depth of 5 cm can decrease by as much as 6.5 °C in only 12 minutes during a soil-cooling rain. We define marked soil-cooling rains as rainfall events triggering a drop in soil temperature at a depth of 5 cm larger than 1.5 °C in 12 minutes. Under Mediterranean and Mediterranean-mountain climates,
15 it is shown that such events occur up to nearly 3 times a year, and about once a year on average. This frequency decreases to about once every 3.5 years under semi-oceanic climate. Under oceanic climate, such pronounced soil-cooling rains are not observed over the considered period of time. Rainwater temperature is estimated for 13 cases of marked soil-cooling rains using observed changes within 12 min in soil temperature at a depth of 5 cm, together with soil thermal properties and changes in VSM. On average, the estimated rainwater temperature is generally lower than the observed ambient air
20 temperature, wet-bulb temperature, and topsoil temperature at a depth of 5 cm, with mean differences of -5.1 °C, -3.8 °C, and -11.1 °C, respectively. The most pronounced differences are attributed to hailstorms or to hailstones melting before getting to the soil surface. Ignoring this cooling effect can introduce biases in land surface energy budget simulations.

1 Introduction

Over natural and agricultural land surfaces, the frequency and intensity of rainfalls govern soil moisture dynamics from
25 topsoil layers to the root-zone. While these processes are represented in land surface models (LSMs) (e.g. Decharme et al., 2013), sensible heat input from liquid water into the soil and its impact on the soil temperature profile is often overlooked (Wang et al., 2016). For example, current versions of the ISBA (Interactions between Soil, Biosphere, and Atmosphere) LSM developed by Centre National de Recherches Météorologiques (CNRM) neglect the precipitation-induced sensible heat flux (P_H). Rainwater temperature is rarely measured and raindrop temperature is not explicitly simulated in atmospheric
30 models (Wei et al., 2014).

The impact of neglecting this process was investigated in recent studies, in the context of global atmospheric simulations. Wang et al. (2016) showed that the impact on land surface temperature was relatively small in LMDZ simulations (less than 0.3 °C) but they considered mean annual air temperature differences only. Wei et al. (2014) showed that accounting for precipitation-induced sensible heat helps reducing biases in land surface air temperature simulated by the Community Earth System Model 1 (CESM1). Focusing on the winter season in the northern hemisphere, they found a pronounced effect (up to 1 °C) on land surface air temperature in their simulations. In both studies, it was assumed that rainwater temperature was equal to the air wet-bulb temperature. This assumption is valid for rain drops in thermal equilibrium with the ambient air (Kinzer and Gunn, 1951). Both studies tended to show a soil-cooling effect over France but for some regions at higher latitudes a soil-warming effect was simulated.

At the field scale, Kollet et al. (2009) simulated the impact of a rainfall event on soil temperature at a depth of 5 cm ($T_{5\text{cm}}$) over a grassland site in the Netherlands. They showed that accounting for precipitation-induced sensible heat in their simulations triggered a drop in $T_{5\text{cm}}$ of more than 1 °C on a single rainfall event. The simulated surface energy fluxes were markedly influenced by this soil-cooling event during several days. In particular, the ground heat flux was affected during nearly one month. They suggested that this effect could be more pronounced in regions affected by strong convective rainfall events. They did not measure rainwater temperature and they assumed that it was equal to the air wet-bulb temperature. Rainwater temperature was measured in 1947 by Byers et al. (1949) at Wilmington, Ohio, USA. They analyzed the data from 7 storms and concluded that 3 types of events could be distinguished according to rainwater temperature values within minutes after the rain onset: close to air temperature, close to wet-bulb temperature, and lower than air temperature by as much as 10 °C. They attributed the latter kind of event to hail melting before reaching the surface.

More than 70 years after Byers et al. (1949) performed their experiment, we were not able to find other examples in the open literature of the analysis of ground rainwater temperature observations. Such measurements are usually not performed in networks of ground meteorological stations.

The objectives of this study are to assess (1) the frequency of soil-cooling rains across contrasting climatic areas in southern France using in situ observations of atmospheric and soil profile variables, (2) the feasibility of estimating rainwater temperature using soil temperature profile measurements, (3) the difference between rainwater temperature and the ambient air temperature or wet-bulb temperature and the topsoil temperature, ~~(4) the impact of neglecting precipitation-induced sensible heat in the soil temperature simulations of a LSM~~ (moved to Section 5.2).

We use the in situ soil temperature and volumetric soil moisture (VSM) measurements collected by the SMOSMANIA (Soil Moisture Observing System - Meteorological Automatic Network Integrated Application) network in southern France (Calvet et al., 2007, 2016), over a 9-year time period from 2008 to 2016. The soil profile measurements are made at a high sampling frequency of one observation every 12 min and the accumulated precipitation is available at the same frequency. This permits investigating intense precipitation events and their impact on topsoil variables, together with the retrieval of rainwater temperature in certain conditions. ~~We perform and use soil temperature and soil moisture simulations of the ISBA~~

~~(Interactions between Soil, Biosphere, and Atmosphere) LSM to show the impact on the simulated topsoil temperature of neglecting the precipitation-induced sensible heat flux. (Moved to Section 5.2)~~

The observations and the model simulations are presented in Sect. 2. Methods for selecting marked soil-cooling rains and for estimating rainwater temperature are described in Sect. 3. The statistical distribution of soil-cooling rains, and estimates of rainwater temperature are presented in Sect. 4. The results are discussed in Sect. 5. The main conclusions are summarized together with prospects for further research in Sect. 6.

2 Data

The SMOSMANIA network was implemented in southern France by Meteo-France, the French national meteorological service, in order to monitor in situ soil moisture and soil temperature in contrasting soil and climatic conditions at operational automatic weather stations (Calvet et al., 2007). The SMOSMANIA network is composed of 21 stations forming an Atlantic-Mediterranean transect shown in Fig. 1. Soil and climate types for the 21 stations of the SMOSMANIA network are presented in Table 1. Station full names are given in Table S1 (see Supplement). The 3 westernmost stations are close to the Atlantic Ocean and present an oceanic climate. Further east, 6 stations present a semi-oceanic climate. The 12 easternmost stations are close to the Mediterranean sea and present a Mediterranean climate. Among them, five are located at altitudes above sea-level (a.s.l.) higher than 400 m a.s.l. over complex, mountainous terrain, in the Corbières (MTM) and Cévennes (LGC, MZN, BRN, BRZ) mountainous areas. Two stations (MZN and BRZ) of the Cévennes area are located higher than 600 m a.s.l. and present lower mean monthly minimum and maximum temperatures (T_{\min} and T_{\max} , respectively) than the other stations. While T_{\min} can be 2 to 3 °C below freezing level at wintertime at MZN and BRZ, T_{\min} is always higher than 1 to 5 °C above freezing level at the other stations. The T_{\max} values do not exceed 21 °C and 24 °C at MZN and BRZ, respectively, while T_{\max} at the other stations can reach 26 to 30 °C. Oceanic, semi-oceanic, and Mediterranean climates are characterized by contrasting precipitation regimes, with maximum monthly precipitation occurring at wintertime, at spring, and in the autumn, respectively (see Sect. 4.1). It must be noticed that Mediterranean stations are often affected by severe convective precipitation events such as thunderstorms and hailstorms, especially in the autumn (Ruti et al., 2016). This is true for stations located in mountainous areas, but also for those located in the foothills of Corbières (NBN), Cévennes (PZN, PRD, VLV, MJN), and Monts de Vaucluse (CBR). Table 1 also presents the frequency of intense soil-cooling events (see Sections 3 and 4). Since a noticeable fraction of observed $T_{5\text{cm}}$ or $\text{VSM}_{5\text{cm}}$ data is missing, the number of marked soil-cooling rainfall events could be underestimated. The missing data fraction across seasons (Table S1) is used to correct the estimation of the possible number of intense soil-cooling rainfall events, their frequency and the mean time lag between two events in Table 1. (Response 3.2)

In general, the soil around the stations is covered by grass. The soil properties were measured for each station as described in Calvet et al. (2016). In the SMOSMANIA network, VSM and soil temperature are measured every 12 min at four depths (5, 10, 20 and 30 cm) using ThetaProbe and PT100 sensors, respectively. The soil moisture (temperature) observations are recorded with a resolution of 0.001 m³ m⁻³ (0.1 °C). The data are available to the research community through the

International Soil Moisture Network website (ISMN, 2018). In this study, the sub-hourly observations of VSM and soil temperature were used over 9 years from 2008 to 2016.

Additionally, the SMOSMANIA network consists of preexisting automatic weather stations operated by Météo-France, measuring atmospheric variables. We used a number of meteorological observations such as the maximum and minimum air temperatures in an hour at 2 m, the hourly mean relative humidity (RH) of the air, and the accumulated rainfall every 12 min. A small fraction (less than 4 %) of the rainfall data is missing at each station. For most of the stations, a larger fraction of the VSM and soil temperature observations is missing. The mean fractions of missing data for all stations are 0.11 and 0.15 for VSM and $T_{5\text{cm}}$, respectively. The mean fraction of missing data for either VSM or $T_{5\text{cm}}$ is 0.17. More details on missing data for each station, including the seasonal distribution of missing data, are given in Figs. S1, S2, and in Table S1 (see the Supplement). For stations presenting a fraction of missing data larger than 0.1, the fraction of missing data is relatively evenly distributed across seasons. Missing data are slightly more frequent at wintertime and at spring. The maximum fraction of missing VSM at 5 cm is 0.23 at the SBR station, and the maximum fraction of missing $T_{5\text{cm}}$ is 0.47 at the VLV station (Fig. S1). The scaled missing data fraction of either VSM or $T_{5\text{cm}}$ is shown in Fig. S2 and Table S1 for each season.

~~In addition to in situ observations, soil temperature and VSM simulations at depths of 5, 10, 20 and 30 cm were performed using the ISBA (Interactions between Soil, Biosphere, and Atmosphere) LSM within the SURFEX (version 8.0) modeling platform (Masson et al., 2013). The ISBA configuration and the hourly SAFRAN atmospheric analysis (Durand et al., 1993, 1999) we used to force the model at a spatial resolution of 8 km x 8 km are described in Lafont et al. (2012) and Decharme et al. (2013). In this study, ISBA simulation of topsoil soil moisture and soil temperature profiles for the grassland plant functional type are considered. (moved to Supplement)~~

3 Methods

3.1 Identification of intense soil-cooling

In situ rainfall observations are used to identify various types of rainfall events in six steps summarized in Table 2. In a first stage, a rainfall event is defined as a continuous time series of non-zero accumulated liquid precipitation values at time intervals of 12 minutes. Then we only keep the fully documented rainfall events with available soil temperature and VSM observations at a depth of 5 cm. Another stage of data sorting (step 3 in Table 2) is needed to ensure that rainwater is not completely intercepted by vegetation and is able to actually reach the soil. Because of the method used to count rainfall events, only about 5 % of the rainfall events exceed 5 mm and have a significant impact on the topsoil VSM. Among these marked rainfall events, we sort out (step 4) those affecting $T_{5\text{cm}}$ by more than 1 °C. In order to assess the precipitation-induced sensible heat flux (P_H) on the topsoil temperature, we then select marked soil-cooling rainfall events (step 5) presenting at least one marked drop of $T_{5\text{cm}}$ of at least -1.5 °C in 12 min. No other meteorological factor can trigger such rapid changes in topsoil temperature.

Finally, a few cases are selected (step 6) for the assessment of the rainwater temperature retrieval (Sect. 3.2), in conditions where the topsoil VSM profile is sufficiently affected by the rainwater.

~~Since a noticeable fraction of observed T_{5cm} or VSM_{5cm} data is missing, the number of marked soil-cooling rainfall events could be underestimated. The missing data fraction across seasons (Table S1) is used to correct the estimation of the possible number of intense soil-cooling rainfall events, their frequency and the mean time lag between two events.~~

3.2 Estimation of rainwater temperature

In the SMOSMANIA network, rainwater temperature is not measured. We investigate whether it is realistic to postulate that the rainwater temperature can be estimated using in situ topsoil VSM_{5cm} and T_{5cm} observations within a topsoil layer of depth $\Delta z = 0.1$ m. We focus on marked soil-cooling rainfall events corresponding to a drop in topsoil temperature associated to a rise in VSM values. This condition is not always satisfied in practice because the soil temperature probes and the soil moisture probes at a given soil depth are not located at exactly the same place. In order to limit the impact of spatial heterogeneities in the infiltration of rainwater into the soil, we consider intense precipitation events able to markedly wet the topsoil soil moisture (VSM_{5cm}) together with the deeper soil layer (VSM_{10cm}) during the drop in T_{5cm} . The in situ VSM observations at a depth of 10 cm (VSM_{10cm}) are used to ensure that the rainwater really penetrates into the soil and affects the topsoil layer as a whole. Among 122 rainfall events presenting intense soil-cooling, 101 events have available VSM_{10cm} observations, and only 50 events present an increase in VSM_{10cm} larger than $0.05 \text{ m}^3 \text{ m}^{-3}$. Within these 50 rainfall events, we only select 13 events for which the rise in VSM_{5cm} corresponds to the rise in VSM_{10cm} and to the drop in T_{5cm} within the same 12-minute slot (step 6 in Table 2). Firstly, the soil heat capacity at a depth of 5 cm at time t (C_{5cm}^t , in units of $\text{J m}^{-3} \text{ K}^{-1}$) is estimated using the volumetric soil moisture at a depth of 5 cm at time t , VSM_{5cm}^t (in units of $\text{m}^3 \text{ m}^{-3}$):

$$C_{5cm}^t = C_{water} VSM_{5cm}^t + C_{min} f_{min} + C_{SOM} f_{SOM} \quad (1)$$

where C_{water} , C_{min} , C_{SOM} are heat capacity values of water, soil minerals, and soil organic matter (SOM) (4.2×10^6 , 2.0×10^6 , and $2.5 \times 10^6 \text{ J m}^{-3} \text{ K}^{-1}$, respectively). Their corresponding volumetric fractions at a depth of 5 cm (Table 3) are VSM_{5cm}^t , f_{min} and f_{SOM} . Soil minerals consist of sand, clay, silt and gravels. Values of the VSM at saturation at a depth of 5 cm VSM_{sat} (the porosity) is also listed in Table 3 for all stations. While the volumetric fractions of sand (f_{sand}), clay (f_{clay}) and silt (f_{silt}) were directly measured at a depth of 5 cm, the volumetric fraction of gravels (f_{gravel}) was derived from measurements made at a depth of 10 cm (Sect. 5.1).

During a short time period from time t_1 to t_2 (12 min in this study) of intense precipitation for which (P_{12}) the precipitation-induced sensible heat flux dominates heat exchanges in the topsoil layer, we can assume that the heat storage change in the topsoil layer, in units of J m^{-2} , corresponds to the change in temperature of the infiltrated rainwater as:

$$C_{5cm}^{t_1} (T_{5cm}^{t_1} - T_{5cm}^{t_2}) \Delta z = C_{water} (VSM_{5cm}^{t_2} - VSM_{5cm}^{t_1}) (T_{rain}^{t_2} - T_{rain}^{t_1}) \Delta z \quad (2)$$

One may assume that soil and incoming rainwater have reached thermal equilibrium at time t_2 . Houpeurt et al. (1965) showed that thermal equilibrium is nearly instantaneous for small soil mineral particles (e.g. about 10 seconds or less for particle size of less than 5 mm). With this assumption, the rainwater temperature at time t_2 ($T_{rain}^{t_2}$) is equal to the measured soil temperature at time t_2 ($T_{5cm}^{t_2}$), and the rainwater temperature just before reaching the soil at time t_1 ($T_{rain}^{t_1}$) can be estimated as:

$$T_{rain}^{t_1} = T_{5cm}^{t_2} - \frac{C_{5cm}^{t_1}}{C_{water}} \frac{(T_{5cm}^{t_1} - T_{5cm}^{t_2})}{(VSM_{5cm}^{t_2} - VSM_{5cm}^{t_1})} \quad (3)$$

10

It must be noticed that Eqs. (2) and (3) are valid for liquid rainwater only. During hailstorms, hailstones can melt at the soil surface and part of the heat extracted from the topsoil layer (left term in Eq. (2)) is used for ice melting. Hailstones may melt after getting to the soil surface or just before. It can be assumed that both liquid water resulting from hailstones melting at the surface and liquid rainwater getting to the soil together with hailstones are very close to freezing level ($T_f = 0^\circ\text{C}$) before infiltrating the topsoil layer. In this case, the quantity of hailstones (in kg m^{-2}) melting after getting to the soil surface, I , can be estimated as:

$$I = \frac{1}{L_f} \{ C_{5cm}^{t_1} (T_{5cm}^{t_1} - T_{5cm}^{t_2}) - C_{water} (VSM_{5cm}^{t_2} - VSM_{5cm}^{t_1}) (T_{5cm}^{t_2} - T_f) \} \Delta z \quad (4)$$

20 where $L_f = 3.34 \times 10^5 \text{ J kg}^{-1}$ is the latent heat of fusion. Since a fraction of the rain drops may exceed freezing temperature, I as calculated from Eq. (4) is a low estimate.

3.3 Nomenclature

- ~~T_{5cm} ($^\circ\text{C}$): in situ soil temperature at a depth of 5 cm;~~
- ~~ΔT_{5cm} ($^\circ\text{C 12 min}^{-1}$): T_{5cm} change every 12 min during a rainfall event;~~
- 25 • ~~T_{5cm} change range ($^\circ\text{C}$): maximum minus minimum T_{5cm} during a rainfall event, including 12 minute slots just after and before the rainfall event;~~
- ~~δT_{5cm} ($^\circ\text{C}$): T_{5cm} just after the rainfall event minus T_{5cm} just before the rainfall event;~~
- ~~VSM_{5cm} ($\text{m}^3 \text{ m}^{-3}$): in situ volumetric soil moisture (VSM) at a depth of 5 cm;~~
- ~~ΔVSM_{5cm} ($\text{m}^3 \text{ m}^{-3} \text{ 12 min}^{-1}$): VSM_{5cm} change every 12 min during a rainfall event;~~

- ~~VSM_{5cm} change range ($m^3 m^{-3}$): maximum minus minimum VSM_{5cm} during a rainfall event, including 12-minute slots just after and before the rainfall event;~~
- ~~δVSM_{5cm} ($m^3 m^{-3}$): VSM_{5cm} just after the rainfall event minus VSM_{5cm} just before the rainfall event;~~
- ~~A_z (m): depth of the topsoil layer (0.1 m in this study);~~
- ~~T_{ISBA} ($^{\circ}C$): ISBA soil temperature simulations at a depth of 5 cm;~~
- ~~ΔT_{ISBA} ($^{\circ}C 12 min^{-1}$): T_{ISBA} change every 12 min during a rainfall event;~~
- ~~T_{air} ($^{\circ}C$): observed ambient air temperature at 2 m;~~
- ~~T_{wb} ($^{\circ}C$): ambient wet bulb temperature at 2 m calculated using the Stull (2011) equation;~~
- ~~T_{rain} ($^{\circ}C$): estimated rain temperature;~~
- ~~RH (dimensionless): in situ air relative humidity at 2 m;~~
- ~~VSM_{sat} ($m^3 m^{-3}$): VSM at saturation (i.e. the soil porosity);~~
- ~~$\frac{VSM_{5cm}}{VSM_{sat}}$ (dimensionless): VSM_{5cm} to VSM_{sat} ratio or degree of saturation;~~
- ~~SOM : soil organic matter;~~
- ~~$f_{clay}, f_{gravel}, f_{min}, f_{sand}, f_{silt}, f_{SOM}$ ($m^3 m^{-3}$): volumetric fractions of clay, gravels, soil minerals, sand, silt, and SOM;~~
- ~~$C_{5cm}^t, C_{water}, C_{min}, C_{SOM}$ ($J m^{-3} K^{-1}$): heat capacity values of the topsoil layer at time t , water, soil minerals, and (SOM);~~
- ~~O, SO, M, MM : oceanic, semi-oceanic, Mediterranean, Mediterranean mountain climate conditions.~~

~~For the first 8 symbols, subscript 5cm stands for observations made at a depth of 5 cm.~~

~~In Table 2, marked rainfall events affecting T_{5cm} are defined with T_{5cm} change range $\geq 1^{\circ}C$. Intense soil cooling during a marked rainfall event is defined with minimum $\Delta T_{5cm} \leq -1.5^{\circ}C$ in 12 minutes.~~

~~In Table 1, the rescaled number of intense soil cooling events is calculated as:~~

$$N_{SR} = \frac{N_s}{(1-f_s)} \quad (5)$$

~~where N_s is the number of intense soil cooling events for one season at one station, and f_s is the proportion of missing data for the same season at the same station (see Table S1 and Fig. S2 in the Supplement). The f_s values for each season are estimated using the total missing data proportion for all seasons and the scaled seasonal distribution of the fraction of missing data. **(moved to Appendix)**~~

4 Results

4.1 Identification of soil-cooling rains

The various types of rainfall events considered in this study are listed in Table 2. Their frequency is indicated. After data sorting (step 3 in Table 2), only 5.5 % of the fully documented rainfall events can be considered as marked rainfall events, with accumulated precipitation and changes in VSM_{5cm} larger than 5 mm and $0.05 \text{ m}^3 \text{ m}^{-3}$, respectively. At the same time, this small fraction of rainfall events contributes as much as 57 % of the accumulated rainfall of all rainfall events. On average, 30 marked rainfall events are observed each year at each station.

Among these marked rainfall events, some have a notable impact on the soil temperature and soil moisture profiles. This is illustrated by Fig. 2, showing soil temperature and soil moisture measured at the PRD station from 21 to 25 August 2015 at depths of 5, 10, 20 and 30 cm. A sharp decrease in soil temperature associated to an increase in soil moisture can be observed around noon of 23 August 2015, along with a rainfall event. The most pronounced impacts of the rain are on the topsoil variables at a depth of 5 cm, but the whole soil profile is affected by the rain, down to a depth of 30 cm. This clearly shows the effects on soil temperature of a soil-cooling rain. **Figure 2 also presents the ISBA numerical simulation of the**

same soil variables. Since ISBA does not represent the heat exchange caused by the mass movement of rainwater, the simulated topsoil temperature is only driven by the surface energy budget, including the evaporation of rainwater intercepted by the vegetation, and by heat conduction from deeper soil layers. As a result, almost no soil temperature change is simulated while changes in soil moisture in response to the rain are simulated. In this example, the rainfall event as a whole is represented well by the SAFRAN atmospheric forcing used to force the ISBA model. In SAFRAN, the rainfall event lasts for 14 h, starting at 10:00 UTC and ending at 23:00 UTC. Over this period of time, the accumulated rainfall of SAFRAN rain is 86.4 mm, very close to the observed accumulated rainfall of in situ rain of 86.1 mm (note that this time period differs from the one used in Table 4). However, SAFRAN is not able to represent the sub-hourly variability of rainfall intensity. While the observed peak rainfall intensity value is 27.8 mm in 12 minutes at 12:36 UTC, SAFRAN indicates a rather constant intensity of about 6 mm h^{-1} **(moved to Supplement)**

The PRD station considered in Fig. 2 is characterized by a Mediterranean climate. The 21 stations of the SMOSMANIA network cover contrasting climate areas (Sect. 2) presenting a different seasonal distribution of precipitation. Figure 3 presents the average monthly rainfall amount across seasons (winter is from December to February) for each SMOSMANIA station over a 9-year period of time, from 2008 to 2016. Differences in the seasonal distribution of precipitation are very large. For the 9 westernmost stations (from SBR to SFL) the average monthly rainfall amount across seasons is rather homogenous, although stations under oceanic (O) climate tend to have more precipitation in winter and those under semi-oceanic (SO) climate in spring. For the other 12 stations (from MTM to CBR) under Mediterranean (M) and Mediterranean-mountain (MM) climate conditions, summer is generally drier than other seasons. On the other hand, the autumn is wetter than other seasons, especially in MM climate conditions. The maximum seasonal monthly mean precipitation rate is $272 \text{ mm month}^{-1}$ at the BRN station, and LGC, MZN, and BRZ stations, also under MM climate conditions, present values larger than

150 mm month⁻¹. The differences in rain intensity distribution are analyzed further in Fig. 4 for marked rainfall events (step 3 in Table 2). We can see that both accumulated rainfall and rain duration of individual marked rainfall events can be much larger for M and MM stations than for O and SO stations, especially in the autumn and in winter. The longest rain duration is 41 hours in winter, and the maximum accumulated rainfall during a single rainfall event is 370 mm in the autumn, at the same BRN station. On the other hand, most of the marked rainfall events of O and SO stations present less than 50 mm accumulated rainfall and last less than 12 h.

The statistical distribution of $\delta T_{5\text{cm}}$ ($T_{5\text{cm}}$ increase or decrease in topsoil temperature corresponding to a rainfall event) and the $T_{5\text{cm}}$ change range for marked rainfall events are shown in Fig. 5. In all climate conditions, the topsoil layer is cooler after a marked rainfall event with a probability of 80 %. The $\delta T_{5\text{cm}}$ difference values are larger than 1 °C or smaller than -1 °C with a probability of 25 %, only. More often than not, a cooling is observed in these conditions, rather than a warming. The probability of the $T_{5\text{cm}}$ change range to equal or exceed 1 °C is a bit larger: 28 %. This criterion was used to select marked rainfall events affecting $T_{5\text{cm}}$ (step 4 in Table 2). After data sorting, we obtain a total of 1577 events. This corresponds to about 8 events per year and per station. Because a lot of marked rainfall events can last several hours, $T_{5\text{cm}}$ change range values ≥ 1 °C can be explained by the diurnal cycle of the surface net radiation, rather than to the mass movement of rainwater. Since obvious soil-warming rainfall events are not detectable in our observations, we focus on soil-cooling events characterized by a sharp decrease of topsoil temperature (e.g. in Fig. 2) during the 12-min time interval of the soil profile observations. For this purpose, step 5 in Table 2 permits selecting 122 intense soil-cooling rains using minimum $\Delta T_{5\text{cm}}$ values ≤ -1.5 °C in 12 minutes. This corresponds to 0.65 events per year and per station. Figure 6 presents the statistical distribution of minimum $\Delta T_{5\text{cm}}$ observations, and the corresponding minimum $\Delta T_{5\text{cm}}$ values simulated by the ISBA model for the 1577 marked rainfall events affecting $T_{5\text{cm}}$. It appears that step 5 tends to remove the longest rainfall events and the selected rainfall events last less than 4 hours. The comparison between observed and simulated values shows that ISBA is not able to simulate $\Delta T_{5\text{cm}}$ values well. In particular, most of the simulated minimum $\Delta T_{5\text{cm}}$ values are larger than -0.5 °C in 12 minutes during intense soil cooling events, even for very intense ones with observed minimum $\Delta T_{5\text{cm}}$ values lower than -4 °C in 12 minutes. Figure 6 also shows that most of the 122 intense soil cooling events occur in M or in MM climate conditions. (moved to Supplement)

4.2 Frequency of intense soil-cooling rains

Characteristics of intense soil-cooling rains are summarized in Table 4 and in Fig. S23. (Response 2.4) Among the 122 identified intense soil-cooling events, 107 occur at stations under M or MM climates, only 15 under the O or SO climates. The spatial and seasonal distribution of these intense soil-cooling rainfall events is shown in Fig. 76 for each station of the SMOSMANIA network. Most of the intense soil-cooling rains (82) are in summer, while only 4 are found in winter. The latter are all for the same BRZ station, under MM climate conditions. In spring and during the autumn, 17 and 19 events are observed, respectively. At 6 stations, no intense soil-cooling rain is observed in 9 years, 3 are under O climate conditions (SBR, URG, CRD), 2 under SO climate conditions (CDM, MNT), and 1 under MM climate conditions (MZN). The PRD

and BRZ stations, under M and MM climate conditions, respectively, present the largest number of events, with a mean rescaled frequency of intense soil-cooling rains of 2.7 per year (Table 1). For the 12 M or MM stations (from MTM to CBR) the mean frequency of intense soil-cooling rains is once a year. More details are shown in Table 1. ~~The missing data fraction across seasons (Table S1) is used to correct the estimation of the possible number of intense soil-cooling rainfall events, their frequency and the mean time lag between two events.~~

More characteristics of these 122 intense soil-cooling rains are shown in Fig. 87. These events do not always correspond to a large amount of accumulated rainfall. Actually, about 80 % of these events present accumulated rainfall values smaller than 30 mm. About 80 % of these rains last less than 2 hours, and the longest rain duration is less than 5 hours. The mean hourly rain rate per event does not exceed 30 mm h^{-1} for 90 % of the events. This shows that extremely large amounts of rain or large precipitation intensity are not required to produce intense soil-cooling. Figure 87 also shows that while 82 % of intense soil-cooling rains present minimum $\Delta T_{5\text{cm}}$ values larger than $-3 \text{ }^{\circ}\text{C 12 min}^{-1}$, very low values (down to $-6.5 \text{ }^{\circ}\text{C 12 min}^{-1}$) can be observed. During intense soil-cooling rains, the minimum $\Delta T_{5\text{cm}}$ contributes to increase the $T_{5\text{cm}}$ change range. For 18 % of the events, the minimum $\Delta T_{5\text{cm}}$ represents more than 80 % of the $T_{5\text{cm}}$ change range. For 48 % of the events, the minimum $\Delta T_{5\text{cm}}$ represents more than 60 % of the $T_{5\text{cm}}$ change range. The statistical distributions of $\delta T_{5\text{cm}}$ and $\delta \text{VSM}_{5\text{cm}}$ are also shown in Fig. 87. For intense soil-cooling rains, $T_{5\text{cm}}$ is always lower after the rain than before. The major part (74 %) of the $\delta T_{5\text{cm}}$ values ranges between $-6 \text{ }^{\circ}\text{C}$ and $-2 \text{ }^{\circ}\text{C}$. For $\delta \text{VSM}_{5\text{cm}}$, 8 % of the values are slightly negative (the minimum observed $\delta \text{VSM}_{5\text{cm}}$ is $-0.006 \text{ m}^3 \text{ m}^{-3}$), and 21 % do not exceed $0.050 \text{ m}^3 \text{ m}^{-3}$. The maximum observed $\delta \text{VSM}_{5\text{cm}}$ is $0.3 \text{ m}^3 \text{ m}^{-3}$.

~~Figure 9 investigates the distribution of the starting time of the intense soil cooling rains at a resolution of 1 hour together with the corresponding average rain rate (in mm h^{-1}) across seasons. For the 4 winter events, the rain rate is relative small (less than 7.5 mm h^{-1}). Only 3 events are found with a rain rate larger than 50 mm h^{-1} , two in summer and one during the autumn. It can be seen that the intense soil cooling rains tend to occur at daytime. A large proportion (83 %) of the 122 intense soil cooling rains occur between 09:00 and 21:00 UTC, which is much larger than the fraction of 67 % observed for the 1577 marked rainfall events affecting $T_{5\text{cm}}$. The intense soil cooling rains are rather uniformly distributed between 09:00 and 21:00 UTC. (moved to Supplement)~~

4.3 Estimation of rain temperature from soil temperature and soil moisture observations

Among the 122 intense soil-cooling events, we found 13 cases presenting simultaneous marked changes in $T_{5\text{cm}}$, $\text{VSM}_{5\text{cm}}$, and $\text{VSM}_{10\text{cm}}$, within a 12-minute slot (step 6 in Table 2). Observed values of $\text{VSM}_{5\text{cm}}$, $T_{5\text{cm}}$, 2 m air temperature T_{air} at time t_1 and t_2 , and 2 m wet-bub temperature T_{wb} at time t_1 for these 13 example rains are listed in Table 45, together with the accumulated precipitation of the considered rainfall events and the peak rainfall intensity (mm 12 min^{-1}) of each rain. Among these 13 cases, 2 are under SO climate conditions (PRG and SFL), and 11 are under M and MM climate conditions (from LZC to CBR in Table 45). The latter include 5 cases from the same station, PRD. From a seasonal perspective, 2 cases occurred in spring (cases 9 and 12), one during the autumn (case 3), and the other 10 cases occurred in summer.

Table 45 also shows the rain temperature estimates at time t_1 (T_{rain}) derived from Eq. (3), and the amount of melted hail derived from Eq. (4). Interestingly, the only two cases occurring in spring (cases 9 and 12) correspond to melting hail events. Taking the PRD station case 9 as an example, the measured precipitation amount is 9.3 kg m^{-2} during a rainfall event of 36 min, with an average rain rate of 15.5 mm h^{-1} . From time t_1 to t_2 , the $T_{5\text{cm}}$ topsoil temperature decreases very fast from 17.9 to $12.6 \text{ }^\circ\text{C}$ ($-5.3 \text{ }^\circ\text{C}$ in 12 min), and the air temperature also decreases from 17.5 to $15.0 \text{ }^\circ\text{C}$ ($-2.5 \text{ }^\circ\text{C}$ in 12 min). During the same time lapse, $VSM_{5\text{cm}}$ increases by $+0.13 \text{ m}^3 \text{ m}^{-3}$. Storms with hail were reported in the press and in social media at many places of southern France on 23 April 2016, including close to the PRD region (Infoclimat, 2016). Using Eq. (4), one can estimate the amount of water originating from melting hail: about 1 kg m^{-2} . Soil temperature and soil moisture time series for all these 13 rain examples are shown in Figs. S3 - S15. Thunderstorms and hail were also reported for case 12 (Infoclimat, 2010).

Figure 408 shows the estimated T_{rain} vs. T_{air} and $T_{5\text{cm}}$ at time t_1 . While most of the T_{air} values range between 16 and $22 \text{ }^\circ\text{C}$, except for case 12 ($T_{\text{air}} = 4.3 \text{ }^\circ\text{C}$), the estimated T_{rain} present a larger variability, from 0 to $22.5 \text{ }^\circ\text{C}$. Excluding the two spring cases (9 and 12), the standard deviation of T_{rain} values in Table 45 is $4.6 \text{ }^\circ\text{C}$, much larger than for T_{air} , $1.9 \text{ }^\circ\text{C}$. For the 13 storms listed in Table 45, T_{rain} ($T_{5\text{cm}}$) tends to be lower (higher) than T_{air} , with a mean difference of $-5.1 \text{ }^\circ\text{C}$ ($+6.0 \text{ }^\circ\text{C}$). On average, T_{rain} is cooler than topsoil by $-11.1 \text{ }^\circ\text{C}$. T_{rain} is cooler than T_{wb} by $-3.8 \text{ }^\circ\text{C}$. For cases 2, 11, and 13, T_{rain} is close to T_{air} . For cases 1 and 3, T_{rain} is close to T_{wb} . The other cases present T_{rain} values much cooler than T_{air} and T_{wb} . In particular, T_{rain} is cooler than T_{air} by more than $5 \text{ }^\circ\text{C}$ for 5 cases (4, 5, 7, 9, 10), among which 3 cases (7, 9, 10) occurred at the PRD station. At time t_1 , RH ranges from 68% to 97% and $\frac{VSM_{5\text{cm}}}{VSM_{\text{sat}}}$ ranges from 20.7% to 63.8% . Soil-cooling rate $\Delta T_{5\text{cm}}$ values range from $-5.3 \text{ }^\circ\text{C}$ to $-1.5 \text{ }^\circ\text{C}$ in 12-min. The corresponding air cooling values are less pronounced, ranging from $-2.5 \text{ }^\circ\text{C}$ to $0.0 \text{ }^\circ\text{C}$. For case 9, $\frac{VSM_{5\text{cm}}}{VSM_{\text{sat}}}$ increases only by 27% during the considered 12-min slot. This is a relative small increase compared to other cases, less than the median value of 29% and much less than the maximum value of 58% observed for case 10 at the same station. Despite the moderate soil wetting in case 9, $T_{5\text{cm}}$ values presented the most pronounced decrease ($-5.3 \text{ }^\circ\text{C}$). The $T_{5\text{cm}}$ value at time t_2 also presented the largest difference with the estimated rain temperature ($+12.6 \text{ }^\circ\text{C}$).

5 Discussion

5.1 How accurate are rain temperature estimates?

In this study, an attempt is made to estimate rain temperature using observations in the topsoil layer. In Eqs. (2) and (3), it is assumed that the precipitation-induced sensible heat flux dominates heat exchanges in the topsoil layer. Since soil properties are known, the mean P_H value can be estimated from Eq. (2) for the intense soil-cooling events used to retrieve T_{rain} (see Table 5). For the 10 events of Table 5 occurring at summertime, this flux ranges from 408 to 1009 W m^{-2} , with a mean value of 648 W m^{-2} . These P_H flux values are very high and represent large fractions of absolute values of the net radiation R_{net} (i.e. the amount of energy available for surface heat exchanges, driven by the incoming solar

radiation, that could be simulated without accounting for P_H). They are probably often much larger than R_{net} because the R_{net} energy budget component is generally small during rainfall events, in relation to the low incoming solar radiation. Moreover, 7 events out of 10 occur at nighttime or at dusk (see Supplement), i.e. in small R_{net} value conditions. The R_{net} variable is not measured at SMOSMANIA stations. Typical measured summertime values of the maximum daily R_{net} over the grassland site of Meteopole-Flux in southwestern France (Zhang et al. 2018) range from about 200 W m^{-2} during cloudy rainy days to about 700 W m^{-2} in clear sky conditions. At nighttime, absolute R_{net} values rarely exceed 100 W m^{-2} . (Response 3.3)

Because Eqs. (3) and (4) include soil heat capacity (Eq. (1)), the static soil properties must be known together with the time-evolving VSM and soil temperature. In particular, the volumetric fraction of gravels is the most variable static soil characteristic in Table 3: f_{gravel} ranges from 0 to $0.41 \text{ m}^3 \text{ m}^{-3}$ at CRD and BRN stations, respectively. Among stations of the 13 rain retrieval cases in Table 45, f_{gravel} ranges from 0.05 to $0.34 \text{ m}^3 \text{ m}^{-3}$ at PZN and PRD, respectively. The fraction of gravels was not measured at a depth of -5 cm. Instead, values given in Table 3 are derived from gravimetric measurements made at -10 cm. In order to assess to what extent uncertainties on f_{min} values may affect the retrieved T_{rain} values, two numerical experiments (Exp1 and Exp2) were made using other soil characteristics than those listed in Table 3 (Control experiment):

- Exp1 used the reassembled static soil volumetric fractions of soil minerals and SOM at a depth of 5 cm assuming $f_{gravel} = 0 \text{ m}^3 \text{ m}^{-3}$. This was equivalent to considering fine earth only and the resulting f_{SOM} and f_{min} fractions were larger and smaller than in the Control experiment, respectively. This tended to increase C_{5cm}^t (Eq. (1)), and to decrease T_{rain} (Eq. (3)).
- Exp2 used the measured soil characteristics at a depth of 10 cm (Calvet et al., 2016). The impact of Exp2 on f_{SOM} , f_{min} , C_{5cm}^t , and T_{rain} varied a lot from one station to another.

Volumetric fractions of the topsoil elements used in Exp1 and Exp2 are listed in Tables S2 and S3, respectively. Differences in f_{SOM} and f_{min} values are listed in Table 56.

Differences in estimated T_{rain} values for Exp1 and Exp2 with respect to the Control are shown in Table 56. In Exp1, T_{rain} estimates tend to present slightly lower values, with differences down to $-0.3 \text{ }^\circ\text{C}$, and the median difference value is $-0.1 \text{ }^\circ\text{C}$, with a standard deviation of $0.1 \text{ }^\circ\text{C}$. In Exp2, T_{rain} differences range from $-1.23 \text{ }^\circ\text{C}$ to $+0.17 \text{ }^\circ\text{C}$, and the median difference value is $0 \text{ }^\circ\text{C}$, with a standard deviation of $0.4 \text{ }^\circ\text{C}$. Merging results from Exp1 and Exp2, 80 % of the statistical distribution of T_{rain} differences range between $-0.3 \text{ }^\circ\text{C}$ and $+0.1 \text{ }^\circ\text{C}$. The most marked changes in T_{rain} ($-0.50 \text{ }^\circ\text{C}$ and $-1.23 \text{ }^\circ\text{C}$) are observed for Exp2 (cases 1 and 4, at PRG and NBN stations, respectively). They correspond to the largest changes in f_{min} ($+0.070$ and $+0.105$, respectively). This gives an idea of the uncertainties on T_{rain} related to poorly known soil heterogeneities and to their impact on the soil characteristics measured in the field.

Another source of uncertainties is that the topsoil layer, from the soil surface down to a depth of -0.1 m , may not be completely affected by the rainfall event, or that the instruments positioned at a depth of -5 cm may not be able to sample mean values relevant for the topsoil layer. In order to limit this effect, we selected only 13 intense soil-cooling events by

imposing a marked change in VSM_{10cm} during the considered 12-min slot. If the latter condition is ignored, 32 soil-cooling events can be considered instead of 13, and we checked that similar results are found (not shown).

A limitation of the method used in this study is that the soil moisture and soil temperature probes at a depth of 5 cm are not placed at exactly the same location. We found some examples for which the VSM response to rain does not match with the drop in topsoil temperature (Figs. S18, S19, S20, S21 and S22). This limited the number of events for which rainwater temperature could be estimated.

More research is needed to develop techniques to measure rainwater temperature. Instruments similar to the rain-temperature equipment of Byers et al. (1949) could be developed. Our results show that using automatic temperature and volumetric moisture observations in a porous medium of known thermal properties has potential to estimate T_{rain} and possibly the amount of hailstones in real time.

5.2 Does soil-cooling matter?

We showed (e.g. Fig. 2) that the temperature of rain drops reaching the soil surface can impact the soil temperature profile during several hours. Investigating the impact on longer time periods would require using a LSM able to activate or deactivate the representation of sensible heat input from liquid water into the soil. This impact was investigated experimentally by Wierenga et al. (1975) through an irrigation experiment with cold and warm water (4.1 °C and 21.6 °C, respectively). They showed that 42 hours were needed before differences in soil temperature at a depth of 0.2 m were reduced to less than 1 °C, and more than 5 days below a depth of 0.5 m. They used quite large irrigation amounts of more than 120 mm. Figure 87 shows that accumulated rainfall during one event can exceed 120 mm in Mediterranean climate conditions (M and MM). Such events are not observed in O and SO conditions but less intense precipitation events can impact the surface energy budget, even if this is not obvious in the soil temperature time series. Figure 87 shows that intense soil-cooling events (step 5 in Table 2) are associated to rather uniformly distributed increases in topsoil VSM values. Actually, the statistical distribution of δVSM_{5cm} values tends to shift towards larger values at each data sorting step listed in Table 2. This is illustrated by Fig. 449 for steps 2, 3, and 4. For fully documented rainfall events (step 2), VSM_{5cm} does not increase for about 60 % of the rainfall events ($\delta VSM_{5cm} \leq 0 \text{ m}^3 \text{ m}^{-3} \text{ 12 min}^{-1}$). Two possible reasons are that (1) rainwater can be intercepted by vegetation and/or litter, especially when the rain is very slight and/or the soil ground is very dry, (2) VSM_{5cm} is close to saturation, so as to no VSM_{5cm} increase is observed. We found examples under the above two situations, shown in Fig. S16 (VSM_{5cm} is relatively small and the rainwater might be intercepted) and Fig. S17 (VSM_{5cm} is close to saturation). For steps 3 and 4, Fig. 449 shows that only 7 % to 9 % of VSM_{5cm} values do not increase. About the same proportion is observed for the 122 intense soil-cooling rains (Fig. 87).

Assessing the impact of neglecting precipitation-induced sensible heat in the soil temperature simulations of a LSM is a key issue. Developing LSMs able to represent the sensible heat input from liquid water into the soil is needed, as well as a way to diagnose rainwater temperature from atmospheric model simulations (Feiccabrino et al., 2015). We perform and use a Soil temperature and soil moisture simulations of from the ISBA (Interactions between Soil, Biosphere, and Atmosphere) LSM

are presented in the Supplement (Figs. S24 and S25). It is shown that ISBA simulations are not able to represent the response of soil variables to intense soil-cooling precipitation events. ~~to show the impact on the simulated topsoil temperature of neglecting the precipitation induced sensible heat flux.~~ Now, the ISBA model has no representation of heat exchanges due to water mass movement. This process needs to be introduced in ISBA. We think that data from a fully instrumented site including direct measurements of rain water temperature are needed to completely address this issue and to validate the upgraded model version. Such an experiment would give insights to understand when, where and why soil cooling occurs or not and would be valuable to help model development. In particular, the precipitation-induced sensible heat flux is not limited to intense precipitation and the impact of this process on the surface energy budget needs to be investigated in all conditions. **From Responses 2.5 and 3.1**

Attempts were made in a few studies to ~~represent-simulate this effect the~~ precipitation-induced sensible heat (e.g. Emanuel et al., 2008; Wang et al., 2016) but in general, it was assumed that T_{rain} was equal to T_{wb} . This study shows that T_{rain} can be much lower than T_{wb} during severe convective events and confirms the findings of Byers et al. (1949). Since severe convective events associated to the intense soil-cooling events observed in this study tend to become more and more frequent in relation to climate change (Feng et al., 2016), soil-cooling effects may play a role in the response of the Earth system to climate change. Moreover, rainwater temperature estimates from observation networks or from atmospheric model simulations could be beneficial for a number of applications such as urban heat island monitoring (e.g. Jelinkova et al., 2015), drink-water quality monitoring (e.g. Chubaka et al., 2018), the estimation of the emission rates of greenhouse gases by soils (e.g. Gagnon et al., 2018), or the quantification of soil erosion (e.g. Sachs and Sarah, 2017).

6 Conclusions

In situ rain-temperature measurements are rare. We used the soil moisture and soil temperature observations from the SMOSMANIA network over 9 years in southern France to assess the cooling effects on soils of rainfall events. The rainwater temperature was estimated using observed changes of topsoil volumetric soil moisture and soil temperature in response to the rainfall event. We found that most (72 %) marked rainfall events did not impact $T_{5\text{cm}}$ change range more than ± 1 °C. On the other hand, about 2 % of marked rainfall events triggered intense soil-cooling with drops in $T_{5\text{cm}}$ ($\Delta T_{5\text{cm}} \leq -1.5$ °C in 12 min. Such intense soil-cooling rains were mainly observed under Mediterranean climate conditions, in summer, at daytime. The average frequency of the occurrence of such events for the 12 Mediterranean stations was once a year. Among all these intense soil-cooling rains, the minimum observed value of $\Delta T_{5\text{cm}}$ was -6.5 °C in 12 min. Rain temperature estimates were obtained for 13 cases. They were generally lower than the ambient air temperatures, wet-bulb temperatures, and $T_{5\text{cm}}$ values (with mean differences of -5.1, -3.8, and -11.1 °C, respectively). In 5 cases, rain temperature estimates were much cooler than air temperature, by at least -5 °C and down to -17.5 °C, likely in relation to hailstones melting just before reaching the surface or melting at the surface of the soil. More research is needed to develop measurement techniques for rainwater temperature and perform such measurements in contrasting climate conditions.

Data availability.

The soil moisture (temperature) observations are available to the research community through the International Soil Moisture Network website (ISMN, 2018).

Acknowledgments.

This work is a contribution to the HyMeX program (<https://www.hymex.org/>). We thank our Météo-France colleagues for their support in collecting, checking and archiving the SMOSMANIA data: Annick Auffray, Catherine Bienaimé, Marc Bailleul, [Basile Baumann](#), Laurent Brunier, Jérôme Candiago, Anne Chaumont, Jacques Couzinier, Mathieu Créau, [Pierre Farges](#), Hélène Fillancq, [Noureddine Fritz](#), Philippe Gillodes, Sandrine Girres, Michel Gouverneur, Didier Grimal, Viviane Isler, Maryvonne Kerdoncuff, Matthieu Lacan, Pierre Lantuejoul, [Franck Lavie](#), William Maurel, Roland Mazurie, [Nicolas Naudet](#), Dominique Paulais, Bruno Piguet, Fabienne Simon, Dominique Simonpietri, Marie-Hélène Théron and Marie Yardin.

3.3

Appendix: Nomenclature

- T_{5cm} (°C): in situ soil temperature at a depth of 5 cm;
- ΔT_{5cm} (°C 12 min⁻¹): T_{5cm} change every 12 min during a rainfall event;
- T_{5cm} change range (°C): maximum minus minimum T_{5cm} during a rainfall event, including 12-minute slots just after and before the rainfall event;
- δT_{5cm} (°C): T_{5cm} just after the rainfall event minus T_{5cm} just before the rainfall event ;
- VSM_{5cm} (m³ m⁻³): in situ volumetric soil moisture (VSM) at a depth of 5 cm;
- ΔVSM_{5cm} (m³ m⁻³ 12 min⁻¹): VSM_{5cm} change every 12 min during a rainfall event;
- VSM_{5cm} change range (m³ m⁻³): maximum minus minimum VSM_{5cm} during a rainfall event, including 12-minute slots just after and before the rainfall event;
- δVSM_{5cm} (m³ m⁻³): VSM_{5cm} just after the rainfall event minus VSM_{5cm} just before the rainfall event;
- Δz (m): depth of the topsoil layer (0.1 m in this study);
- T_{ISBA} (°C): ISBA soil temperature simulations at a depth of 5 cm;
- ΔT_{ISBA} (°C 12 min⁻¹): T_{ISBA} change every 12 min during a rainfall event;
- T_{air} (°C): observed ambient air temperature at 2 m;
- T_{wb} (°C): ambient wet-bulb temperature at 2 m calculated using the Stull (2011) equation;

- T_{rain} (°C): estimated rain temperature;
- P_H (W m⁻²): precipitation-induced sensible heat flux;
- R_{net} (W m⁻²): net radiation flux;
- RH (dimensionless): in situ air relative humidity at 2 m;
- VSM_{sat} (m³ m⁻³): VSM at saturation (i.e. the soil porosity);
- $\frac{VSM_{5\text{cm}}}{VSM_{\text{sat}}}$ (dimensionless): $VSM_{5\text{cm}}$ to VSM_{sat} ratio or degree of saturation;
- SOM: soil organic matter;
- $f_{\text{clay}}, f_{\text{gravel}}, f_{\text{min}}, f_{\text{sand}}, f_{\text{silt}}, f_{\text{SOM}}$ (m³ m⁻³): volumetric fractions of clay, gravels, soil minerals, sand, silt, and SOM;
- $C_{5\text{cm}}^t, C_{\text{water}}, C_{\text{min}}, C_{\text{SOM}}$ (J m⁻³ K⁻¹): heat capacity values of the topsoil layer at time t , water, soil minerals, and (SOM);
- O, SO, M, MM: oceanic, semi-oceanic, Mediterranean, Mediterranean-mountain climate conditions.

For the first 8 symbols, subscript 5cm stands for observations made at a depth of 5 cm.

In Table 2, marked rainfall events affecting $T_{5\text{cm}}$ are defined with $T_{5\text{cm}}$ change range ≥ 1 °C. Intense soil-cooling during a marked rainfall event is defined with minimum $\Delta T_{5\text{cm}} \leq -1.5$ °C in 12 minutes.

In Table 1, the rescaled number of intense soil-cooling events is calculated as:

$$N_{sR} = \frac{N_s}{(1-f_s)} \quad (5)$$

where N_s is the number of intense soil-cooling events for one season at one station, and f_s is the proportion of missing data for the same season at the same station (see Table S1 and Fig. S2 in the Supplement). The f_s values for each season are estimated using the total missing data proportion for all seasons and the scaled seasonal distribution of the fraction of missing data.

References

- Byers, H. R., Moses, H., and Harney, P. J.: Measurement of rain temperature, *J. Meteorol.*, 6, 51-55, [https://doi.org/10.1175/1520-0469\(1949\)006<0051:MORT>2.0.CO;2](https://doi.org/10.1175/1520-0469(1949)006<0051:MORT>2.0.CO;2), 1949.
- 5 Calvet, J. C., Fritz, N., Froissard, F., Suquia, D., Petitpa, A. and Piguët, B.: July. In situ soil moisture observations for the CAL/VAL of SMOS: the SMOSMANIA network, In *Geoscience and Remote Sensing Symposium, IGARSS*, Barcelona, Spain, 23-28 July 2007, 1196-1199, <https://doi.org/10.1109/IGARSS.2007.4423019>, 2017.
- Calvet, J.-C., Fritz, N., Berne, C., Piguët, B., Maurel, W., and Meurey, C.: Deriving pedotransfer functions for soil quartz fraction in southern France from reverse modeling, *SOIL*, 2, 615-629, <https://doi.org/10.5194/soil-2-615-2016>, 2016.
- 10 Decharme, B., Martin, E. and Faroux, S.: Reconciling soil thermal and hydrological lower boundary conditions in land surface models, *Journal of Geophysical Research: Atmospheres*, 118, 7819-7834, <https://doi.org/10.1002/jgrd.50631>, 2013.
- ~~Durand, Y., Brun, E., Mérindol, L., Guyomarc'h, G., Lesaffre, B., and Martin, E.: A meteorological estimation of relevant parameters for snow models, *Ann. Geophys.*, 18(1), 65–71, <https://doi.org/doi:10.1017/S0260305500011277>, 1993.~~
15 **moved to Supplement**
- ~~Durand, Y., Giraud, G., Brun, E., Merindol, L., and Martin, E.: A computer-based system simulating snow pack structures as a tool for regional avalanche forecasting, *Ann. Glaciol.*, 45(151), 469–484, <https://doi.org/doi:10.1017/S0022143000001337>, 1999.~~
moved to Supplement
- Emanuel, K., Callaghan, J., and Otto, P.: A hypothesis for the redevelopment of warm-core cyclones over northern Australia, *Mon. Weather Rev.*, 136, 3863-3872, <https://doi.org/10.1175/2008MWR2409.s1>, 2008.
- 20 Feiccabrino, J., Graff, W., Lundberg, A., Sandström, N., and Gustafsson, D.: Meteorological knowledge useful for the improvement of snow rain separation in surface based models, *Hydrology*, 2, 266-288; <https://doi.org/10.3390/hydrology2040266>, 2015.
- Feng, Z., Leung L. R., Hagos, S., Houze, R. A., Burleyson, C. D., and Balaguru, K.: More frequent intense and long-lived storms dominate the springtime trend in central US rainfall, *Nature Comm.*, 7, 13429, 8 pp., <https://doi.org/10.1038/ncomms13429>, 2016.
- 25 Gagnon, S., Allard, M., and Nicosia, A.: Diurnal and seasonal variations of tundra CO₂ emissions in a polygonal peatland near Salluit, Nunavik, Canada, *Arctic Science* 4, 1–15, <https://doi.org/10.1139/as-2016-0045>, 2018.
- Houpeurt, A., Delouvrier, J., and Iffly, R.: Fonctionnement d'un doublet hydraulique de refroidissement, *La Houille Blanche*, 3, 239-246, available at: <https://www.shf-lhb.org/fr/articles/lhb/pdf/1965/03/lhb1965020.pdf> (last access: August 2018), 1965.
- 30 Jelinkova, V., Dohnal, M., and Pícek, T. : A green roof segment for monitoring the hydrological and thermal behavior of anthropogenic soil systems, *Soil Water Res.*, 10, 262-270, <https://doi.org/10.17221/17/2015-SWR>, 2015.

- Kinzer, G. D., and Gunn, R.: The evaporation, temperature and thermal relaxation-time of freely falling waterdrops, *J. Meteorol.*, 8, 71-83, [https://doi.org/10.1175/1520-0469\(1951\)008<0071:TETATR>2.0.CO;2](https://doi.org/10.1175/1520-0469(1951)008<0071:TETATR>2.0.CO;2), 1949.
- Kollet, S. J., Cvjanovic, I., Schüttemeyer, D., Maxwell, R. M., Moene, A. F., and Bayer, P.: The influence of rain sensible heat and subsurface energy transport on the energy balance at the land surface, *Vadose Zone Journal*, 8, 846-857, <https://doi.org/10.2136/vzj2009.0005>, 2009.
- ~~Lafont, S., Zhao, Y., Calvet, J. C., Peylin, P., Ciais, P., Maignan, F., and Weiss, M.: Modelling LAI, surface water and carbon fluxes at high resolution over France: comparison of ISBA-A_{gs} and ORCHIDEE, *Biogeosciences*, 9, 439-456, <https://doi.org/10.5194/bg-9-439-2012>, 2012. (moved to Supplement)~~
- Infoclimat, Website forum, Suivi du temps dans les regions Méditerranéennes (13 avril 2016), available at: <https://forums.infoclimat.fr/f/topic/349-suivi-du-temps-dans-les-r%C3%A9gions-m%C3%A9diterran%C3%A9ennes/?page=10>, (last access : August 2018), 2016.
- Infoclimat, Bilan météo du mardi 20 mars 2010, available at: <https://www.infoclimat.fr/actualites/bqs/11100/bilan-meteo-du-mardi-30-mars-2010.html>, (last access : August 2018), 2010.
- ISMN, International Soil Moisture Network, data available at: <https://ismn.geo.tuwien.ac.at/>, (last access : August 2018), 2018.
- ~~Masson, V., Le Moigne, P., Martin, E., Faroux, S., Alias, A., Alkama, R., Belamari, S., Barbu, A., Boone, A., Bouyssel, F., Brousseau, P., Brun, E., Calvet, J. C., Carrer, D., Decharme, B., Delire, C., Donier, S., Essaouini, K., Gibelin, A. L., Giordani, H., Habets, F., Jidane, M., Kerdraon, G., Kourzeneva, E., Lafaysse, M., Lafont, S., Lebeaupin Brossier, C., Lemonsu, A., Mahfouf, J. F., Marguinaud, P., Mokhtari, M., Morin, S., Pigeon, G., Salgado, R., Seity, Y., Taillefer, F., Tanguy, G., Tulet, P., Vincendon, B., Vionnet, V., and Voldoire, A.: The SURFEXv7.2 land and ocean surface platform for coupled or offline simulation of earth surface variables and fluxes, *Geosci. Model Dev.*, 6, 929-960, <https://doi.org/10.5194/gmd-6-929-2013>, 2013. (moved to Supplement)~~
- Ruti, P.M., Somot, S., Giorgi, F., Dubois, C., Flaounas, E., Obermann, A., Dell'Aquila, A., Pisacane, G., Harzallah, A., Lombardi, E., Ahrens, B., Akhtar, N., Alias, A., Arsouze, T., Aznar, R., Bastin, S., Bartholy, J., Béranger, K., Beuvier, J., Bouffies-Cloch , S., Brauch, J., Cabos, W., Calmanti, S., Calvet, J.-C., Carillo, A., Conte, D., Coppola, E., Djurdjevic, V., Drobinski, P., Elizalde-Arellano, A., Gaertner, M., Gal n, P., Gallardo, C., Gualdi, S., Goncalves, M., Jorba, O., Jord , G., L'Heveder, B., Lebeaupin-Brossier, C., Li, L., Liguori, G., Lionello, P., Maci s, D., Nabat, P., Onol, B., Rajkovic, B., Ramage, K., Sevault, F., Sannino, G., Struglia, M. V., Sanna, A., Torma, C., and Vervatis, V.: MED-CORDEX initiative for Mediterranean Climate studies, *Bull. Amer. Meteor. Soc.*, 97 (7), 1187-1208, <https://doi.org/10.1175/BAMS-D-14-00176.1>, 2016.
- Sachs, E., and Sarah, P.: Combined effect of rain temperature and antecedent soil moisture on runoff and erosion on Loess, *Catena*, 158, 213-218, <https://doi.org/10.1016/j.catena.2017.07.007>, 2017.
- Stull, R.: Wet-bulb temperature from relative humidity and air temperature, *J. Applied Meteorol. Climatol.*, 50, 2267-2269, <https://doi.org/10.1175/JAMC-D-11-0143.1>, 2011.

Wang, F., Cheruy, F., and Dufresne, J.-L.: The improvement of soil thermodynamics and its effects on land surface meteorology in the IPSL climate model, *Geosci. Model Dev.*, 9, 363–381, <https://doi.org/10.5194/gmd-9-363-2016>, 2016.

5 Wei, N., Y. Dai, M. Zhang, L. Zhou, D. Ji, S. Zhu, and L. Wang: Impact of precipitation-induced sensible heat on the simulation of land-surface air temperature, *J. Adv. Model. Earth Syst.*, 6, 1311–1320, <https://doi.org/10.1002/2014MS000322>, 2014.

Wierenga, P. J., Hagan, R. M., and Nielsen, D. R.: Soil temperature profiles during infiltration and redistribution of cool and warm irrigation water, *Water Resour. Res.*, 6, 230-238, 1975.

10 [Zhang, S., Calvet, J.-C., Darrozes, J., Roussel, N., Frappart, F., Bouhours, G.: Deriving surface soil moisture from reflected GNSS signal observations over a grassland site in southwestern France, *Hydrol. Earth Syst. Sci.*, 22, 1931–1946, <https://doi.org/10.5194/hess-22-1931-2018>, 2018.](https://doi.org/10.5194/hess-22-1931-2018)

Table 1. The environment characteristics for the 21 stations of the SMOSMANIA network and the frequency of intense soil-cooling during marked rainfall events from 2008 to 2016. The number of intense soil-cooling rains, the frequency and the mean time lag between two intense soil-cooling rains are rescaled according to the fraction of missing data across seasons (see Table S1). Stations are listed from (top) west to (bottom) east.

5

Station	Altitude (m)	Climate	Soil type	Number of intense soil-cooling events	Rescaled number of intense soil-cooling events	Rescaled frequency of intense soil-cooling events (year ⁻¹)	Rescaled mean time lag between two intense soil-cooling events (months)
SBR	81	Oceanic	Sand	0	0.0	0.0	-
URG	145	Oceanic	Silt loam	0	0.0	0.0	-
CRD	149	Oceanic	Sand	0	0.0	0.0	-
PRG	245	Semi-oceanic	Silty clay	2	2.0	0.2	54.0
CDM	174	Semi-oceanic	Silty clay	0	0.0	0.0	-
LHS	249	Semi-oceanic	Clay loam	6	6.2	0.7	17.4
SVN	158	Semi-oceanic	Loam	6	6.3	0.7	17.1
MNT	295	Semi-oceanic	Silt loam	0	0.0	0.0	-
SFL	330	Semi-oceanic	Loam	1	1.1	0.1	98.2
MTM	538	Mediterranean/Mountain	Clay loam	1	1.0	0.1	108.0
LZC	60	Mediterranean	Sandy clay loam	6	6.3	0.7	17.1
NBN	112	Mediterranean	Clay	4	4.1	0.5	26.3
PZN	30	Mediterranean	Sandy loam	3	3.1	0.3	34.8
PRD	85	Mediterranean	Clay loam	23	24.3	2.7	4.4
LGC	499	Mediterranean/Mountain	Loamy sand	11	11.4	1.3	9.5
MZN	1240	Mediterranean/Mountain	Sandy loam	0	0.0	0.0	-
VLV	41	Mediterranean	Sandy loam	3	3.4	0.4	31.8
BRN	480	Mediterranean/Mountain	Loamy sand	11	11.7	1.3	9.2
MJN	318	Mediterranean	Loam	15	16.3	1.8	6.6
BRZ	650	Mediterranean/Mountain	Clay loam	22	24.0	2.7	4.5
CBR	142	Mediterranean	Sandy clay loam	8	8.3	0.9	13.0

Table 2. Steps for identifying marked soil-cooling rains, together with the number of events for all the SMOSMANIA stations from 2008 to 2016.

Step	Event to be identified	Total number of events (and number per year and per station)	Definition
1	Rainfall event	123215 (652)	Continuous time series of non-zero accumulated liquid precipitation values at time intervals of 12 minutes
2	Fully documented rainfall event	104178 (551)	Rainfall event with complete in situ $T_{5\text{cm}}$ and $\text{VSM}_{5\text{cm}}$ observation time series
3	Marked rainfall event	5714 (30)	Fully documented rainfall event with accumulated precipitation and changes in $\text{VSM}_{5\text{cm}}$ larger than 5 mm and equal to or above $0.05\text{ m}^3\text{ m}^{-3}$ ($\text{VSM}_{5\text{cm}}$ change range $\geq 0.05\text{ m}^3\text{ m}^{-3}$), respectively
4	Marked rainfall event affecting $T_{5\text{cm}}$ topsoil temperature	1577 (8)	Marked rainfall event with changes in $T_{5\text{cm}}$ equal to or above $1\text{ }^{\circ}\text{C}$ ($T_{5\text{cm}}$ change range $\geq 1\text{ }^{\circ}\text{C}$)
5	Intense soil-cooling during a marked rainfall event	122 (0.65)	A 12-minute slot during a marked rainfall event affecting $T_{5\text{cm}}$ with minimum $\Delta T_{5\text{cm}}$ (drop of $T_{5\text{cm}}$ within 12 minutes) equal to or below $-1.5\text{ }^{\circ}\text{C}$
6	Rainwater temperature retrieval slot	13 (0.07)	Intense soil-cooling during a marked rainfall event with rises in $\text{VSM}_{5\text{cm}}$ and $\text{VSM}_{10\text{cm}}$ equal to or above 0.10 and $0.05\text{ m}^3\text{ m}^{-3}$, respectively

5

Table 3. Soil characteristics at a depth of 5 cm for the 21 stations of the SMOSMANIA network. The volumetric fractions of sand, clay and silt at 5 cm (f_{sand} , f_{clay} and f_{silt}) are measured, and the volumetric fractions of gravel and soil organic matter (SOM) (f_{gravel} and f_{SOM}) at 5 cm are derived from measurements at 10 cm. VSM_{sat} is the porosity representing VSM at saturation ($\text{VSM}_{\text{sat}} = 1 - f_{\text{sand}} - f_{\text{clay}} - f_{\text{silt}} - f_{\text{gravel}} - f_{\text{SOM}}$). Stations are listed from (top) west to (bottom) east.

5

Station	VSM_{sat} ($\text{m}^3 \text{m}^{-3}$)	f_{sand} ($\text{m}^3 \text{m}^{-3}$)	f_{clay} ($\text{m}^3 \text{m}^{-3}$)	f_{silt} ($\text{m}^3 \text{m}^{-3}$)	f_{gravel} ($\text{m}^3 \text{m}^{-3}$)	f_{SOM} ($\text{m}^3 \text{m}^{-3}$)
SBR	0.440	0.501	0.021	0.016	0.001	0.021
URG	0.472	0.079	0.078	0.338	0.005	0.029
CRD	0.487	0.413	0.027	0.029	0.000	0.045
PRG	0.505	0.045	0.119	0.121	0.186	0.024
CDM	0.457	0.076	0.211	0.227	0.011	0.018
LHS	0.415	0.140	0.178	0.186	0.052	0.029
SVN	0.459	0.134	0.072	0.166	0.159	0.010
MNT	0.457	0.117	0.062	0.235	0.099	0.029
SFL	0.401	0.143	0.075	0.111	0.257	0.013
MTM	0.440	0.103	0.072	0.070	0.277	0.038
LZC	0.472	0.107	0.066	0.070	0.270	0.015
NBN	0.511	0.058	0.103	0.061	0.236	0.030
PZN	0.513	0.199	0.069	0.126	0.051	0.042
PRD	0.479	0.044	0.051	0.069	0.336	0.020
LGC	0.411	0.254	0.045	0.048	0.220	0.022
MZN	0.609	0.168	0.037	0.043	0.085	0.058
VLV	0.559	0.244	0.051	0.077	0.027	0.043
BRN	0.455	0.087	0.011	0.015	0.415	0.018
MJN	0.500	0.065	0.023	0.055	0.317	0.040
BRZ	0.579	0.090	0.056	0.094	0.163	0.019
CBR	0.500	0.113	0.058	0.067	0.239	0.023

Table 4. Characteristics of the 122 intense soil-cooling rains. **Response 2.4)**

<u>Characteristic</u>	<u>Event count or fraction</u>
<u>M or MM climate</u>	<u>107</u>
<u>O or SO climate</u>	<u>15</u>
<u>Spring</u>	<u>17</u>
<u>Summer</u>	<u>82</u>
<u>Autumn</u>	<u>19</u>
<u>Winter</u>	<u>4</u>
<u>Starting time at daytime (9:00 am – 21:00 pm)</u>	<u>83 %</u>
<u>Duration less than 2 hours</u>	<u>80 %</u>
<u>Minimum ΔT_{5cm} values ranging from -3 to -1.5 °C 12 min⁻¹</u>	<u>82 %</u>
<u>Maximum number of events per year per station</u>	<u>2.7</u>

Table 45. The estimated rain temperatures (T_{rain}) for 13 intense soil-cooling events, together with the in situ observations of $\text{VSM}_{5\text{cm}}$, $T_{5\text{cm}}$, T_{air} at time t_1 and t_2 , and T_{wb} at time t_1 . The time lapse from time t_1 to t_2 is 12 min. For rain events 9 and 12, Eq. (4) is used to estimate the amount of melting hail at the soil surface. T_{rain} values lower by -5°C than T_{air} at time t_1 are in bold. Stations are listed from west (top) to east (bottom).

Station	Rain event number in Fig. 108	Date (year-month-day)	Accumulated rainfall (mm event ⁻¹)	Peak rainfall intensity (mm 12 min ⁻¹)	$\text{VSM}_{5\text{cm}}$ at t_1 (m ³ m ⁻³)	$\text{VSM}_{5\text{cm}}$ at t_2 (m ³ m ⁻³)	$T_{5\text{cm}}$ at t_1 (°C)	$T_{5\text{cm}}$ at t_2 (°C)	T_{wb} at t_1 (°C)	T_{air} at t_1 (°C)	T_{air} at t_2 (°C)	T_{rain} at t_1 (°C)	Melting hail (kg m ⁻²)
PRG	1	2008-07-26	28.1	16.5	0.232	0.339	21.4	19.9	14.5	16.2	16.2	13.3	0
SFL	2	2015-08-31	29.0	16.1	0.132	0.310	26.3	24.1	16.2	17.2	16.4	18.9	0
LZC	3	2009-10-08	10.0	6.6	0.127	0.262	24.0	21.8	15.3	16.0	14.3	15.6	0
NBN	4	2011-08-14	14.4	10.0	0.141	0.263	26.3	23.5	18.5	19.9	19.3	14.8	0
PZN	5	2015-08-31	29.0	9.6	0.166	0.349	23.6	19.6	18.2	18.7	18.6	10.8	0
PRD	6	2011-07-13	26.2	20.5	0.099	0.338	25.8	22.5	19.8	20.2	19.8	17.7	0
PRD	7	2015-08-23	77.6	27.8	0.252	0.360	21.7	19.0	18.1	19.5	18.1	6.5	0
PRD	8	2015-08-31	16.9	4.8	0.161	0.274	24.4	22.7	19.6	20.7	18.8	16.5	0
PRD	9	2016-04-13	9.3	8.5	0.212	0.340	17.9	12.6	13.7	17.5	15.0	0	1.1
PRD	10	2016-06-15	24.1	20.7	0.126	0.402	22.6	18.0	17.2	17.6	16.2	11.7	0
LGC	11	2016-06-07	13.9	6.5	0.117	0.247	27.5	25.7	17.5	19.9	17.7	20.2	0
MJN	12	2010-03-30	20.3	5.6	0.319	0.442	9.8	7.7	3.4	4.3	2.7	0	0.3
CBR	13	2010-06-30	41.1	16.9	0.170	0.360	31.4	28.6	19.0	21.9	20.7	22.5	0

Table 56. The estimated T_{rain} differences, f_{min} differences and f_{SOM} differences between Exp1 and Control, and between Exp2 and Control. Changes in values of T_{rain} larger than ± 0.5 °C are in bold. Changes in values of volumetric fractions larger than $0.05 \text{ m}^3 \text{ m}^{-3}$ are in bold.

Station	Rain event number in Fig. 408	T_{rain} (°C)		$f_{\text{min}} (\text{m}^3 \text{ m}^{-3}) \times 100$		$f_{\text{SOM}} (\text{m}^3 \text{ m}^{-3}) \times 100$	
		Exp1 - Control	Exp2 - Control	Exp1 - Control	Exp2 - Control	Exp1 - Control	Exp2 - Control
PRG	1	-0.07	-0.50	-0.8	7.0	1.5	0.4
SFL	2	-0.06	0.05	-0.5	-2.0	1.1	0.8
LZC	3	-0.09	-0.32	-0.8	4.2	1.6	0.0
NBN	4	-0.26	-1.23	-1.4	10.5	3.0	0.6
PZN	5	-0.04	-0.14	-0.3	3.7	0.5	-1.9
PRD	6	-0.19	0.09	-1.8	-1.5	3.7	0.1
PRD	7	-0.33	0.17	-1.8	-1.5	3.7	0.1
PRD	8	-0.21	0.10	-1.8	-1.5	3.7	0.1
PRD	9	0	0	-1.8	-1.5	3.7	0.1
PRD	10	-0.22	0.11	-1.8	-1.5	3.7	0.1
LGC	11	-0.06	0.11	-0.7	-1.3	1.3	-0.3
MJN	12	0	0	-3.9	0.6	7.9	-1.2
CBR	13	-0.12	0.03	-1.0	0.9	2.2	-1.0

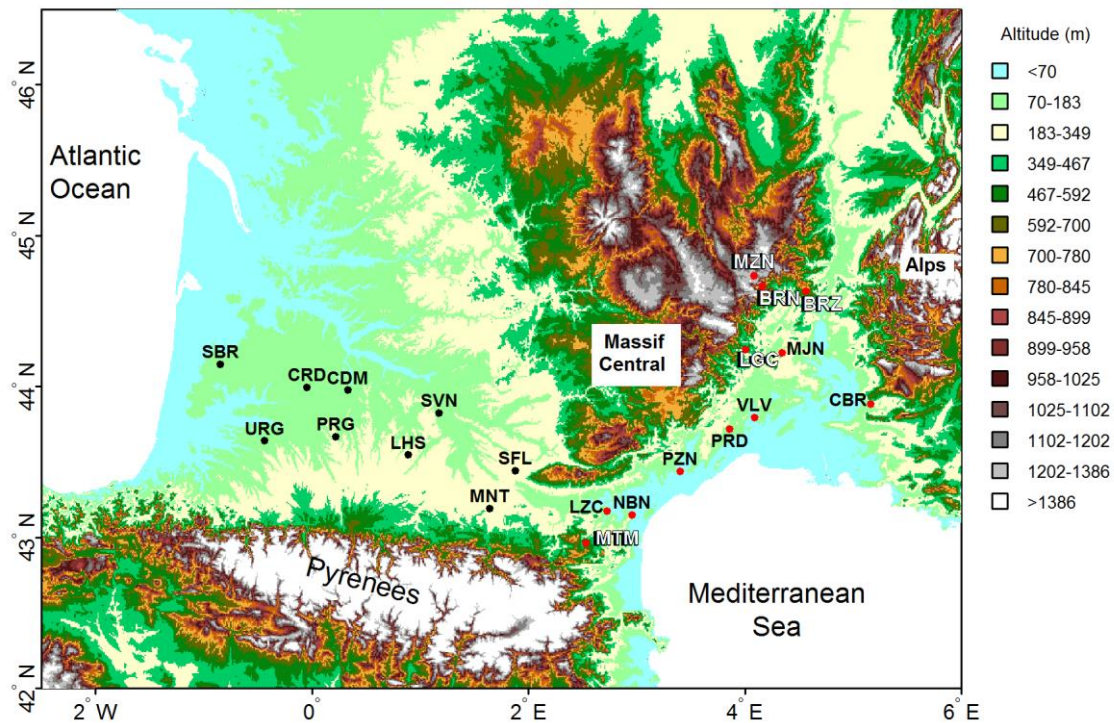
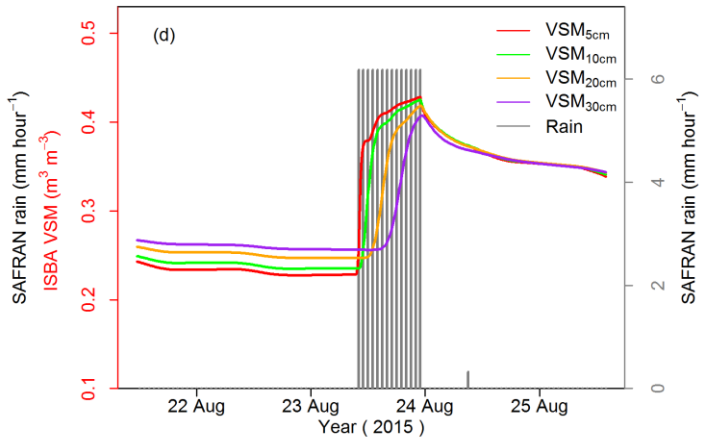
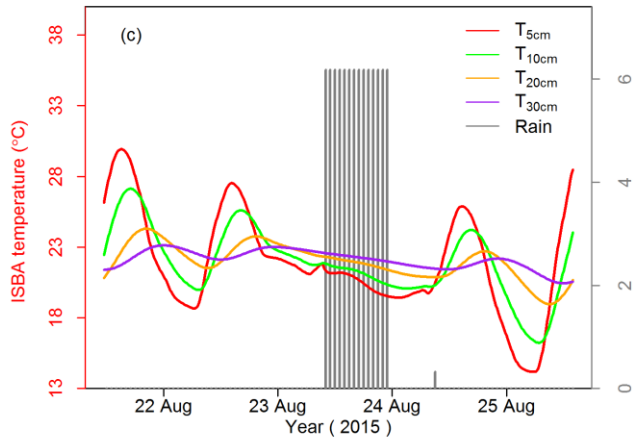
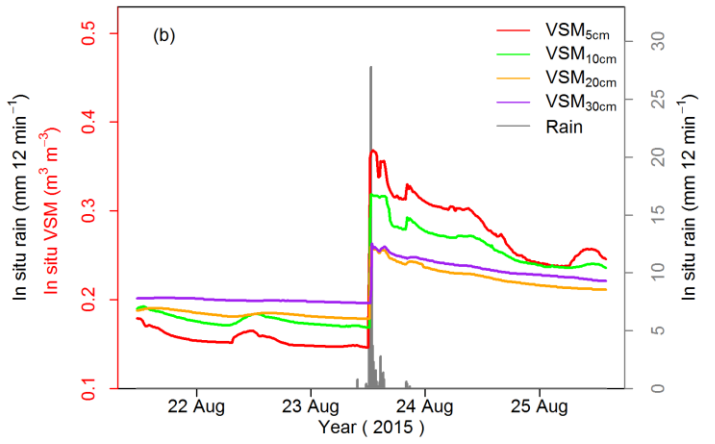
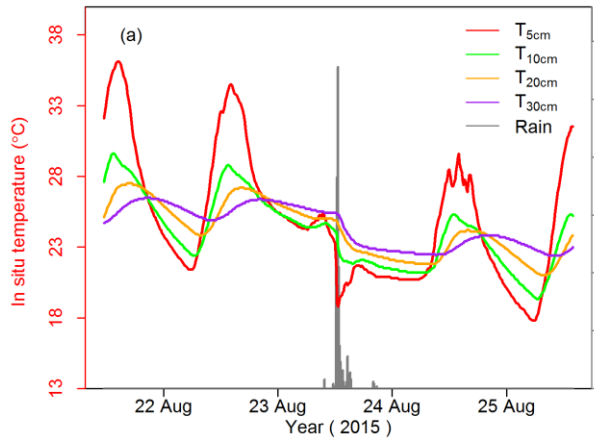


Figure 1. Locations of the 21 SMOSMANIA stations in southern France. Black dots indicate stations under oceanic and semi-oceanic climates. Red dots indicate stations under Mediterranean and Mediterranean-mountain climates. White letters are for names of the five stations under Mediterranean-mountain climates. Background geographic altitudes are from SRTM 90 m digital elevation data (<http://srtm.csi.cgiar.org/>).



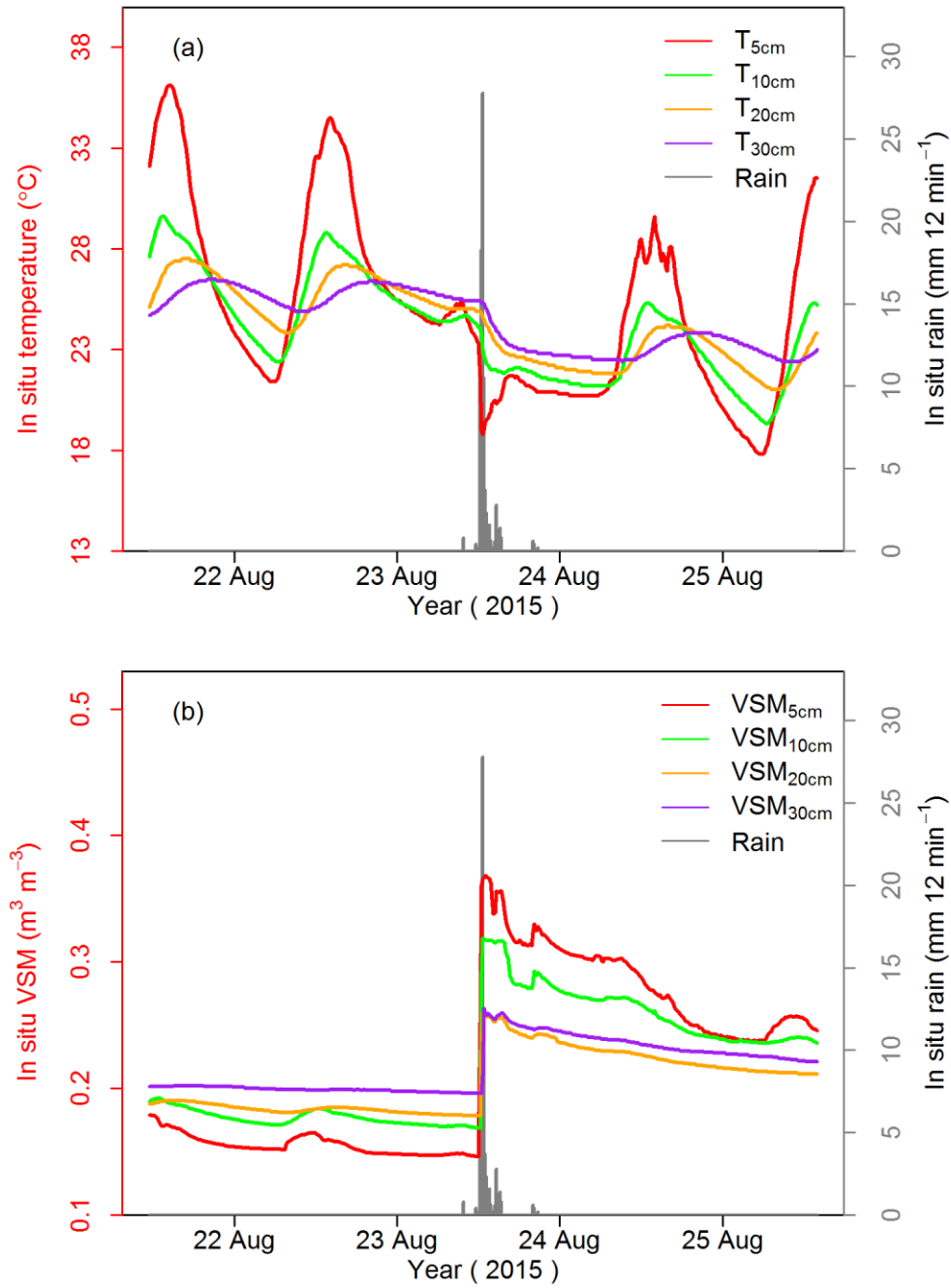
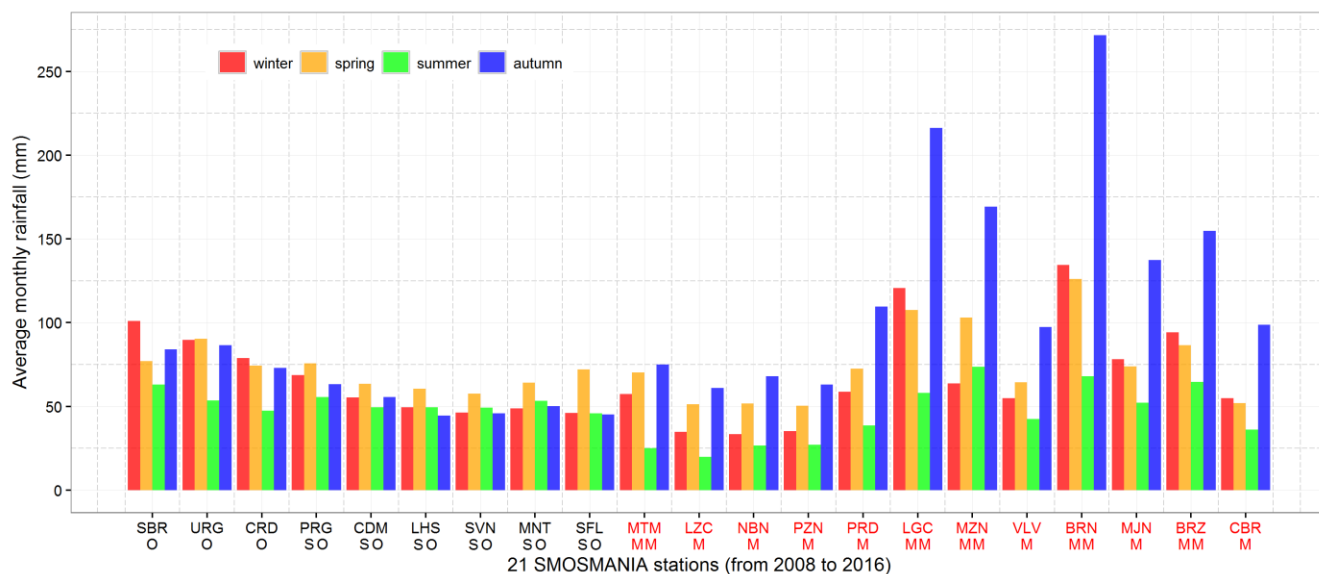


Figure 2. In situ soil temperature (a) and soil moisture (b) measured at the PRD station from 21 to 25 August 2015 at depths of 5, 10, 20 and 30 cm, together with the in situ rainfall observations (mm 12 min⁻¹) shown in grey. ISBA simulations of soil temperature (c) and soil moisture (d), together with the SAFRAN rainfall data (mm hour⁻¹) shown in grey. (e) and soil moisture (d), together with the SAFRAN rainfall data (mm hour⁻¹) shown in grey. (f) and soil moisture (d), together with the SAFRAN rainfall data (mm hour⁻¹) shown in grey.



5 **Figure 3. Average monthly rainfall (in units of mm) for the 21 SMOSMANIA stations across seasons from 2008 to 2016. Stations are sorted from (left) west to (right) east. Symbols “O”, “SO”, “M”, and “MM” indicate Oceanic, Semi-Oceanic, Mediterranean, and Mediterranean-mountain climates, respectively. Winter season is from December to February.**

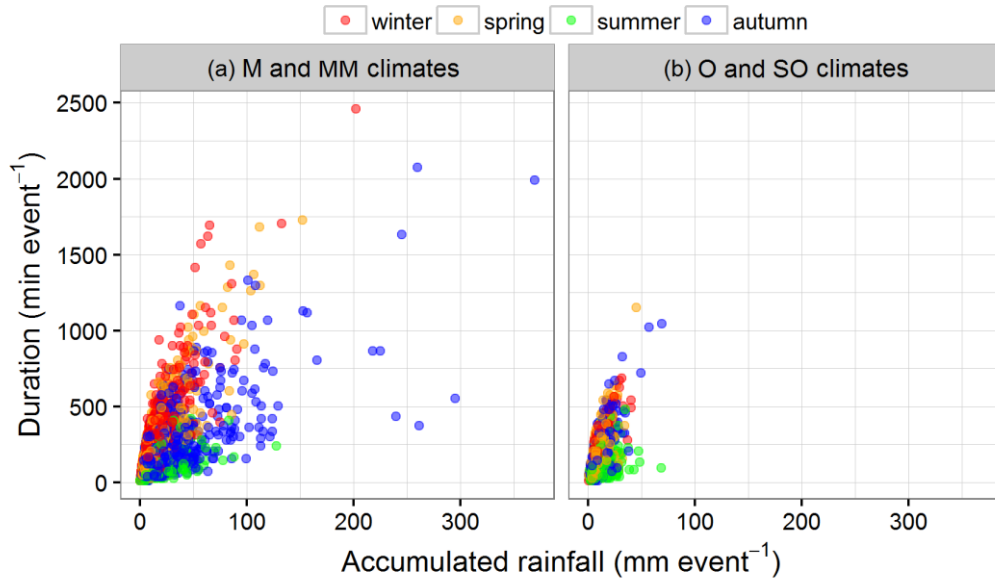


Figure 4. Rainfall duration vs. accumulated rainfall across seasons for each marked rainfall event at Mediterranean (M) and
5 Mediterranean-mountain (MM) stations (a), and oceanic (O) and semi-oceanic (SO) stations (b).

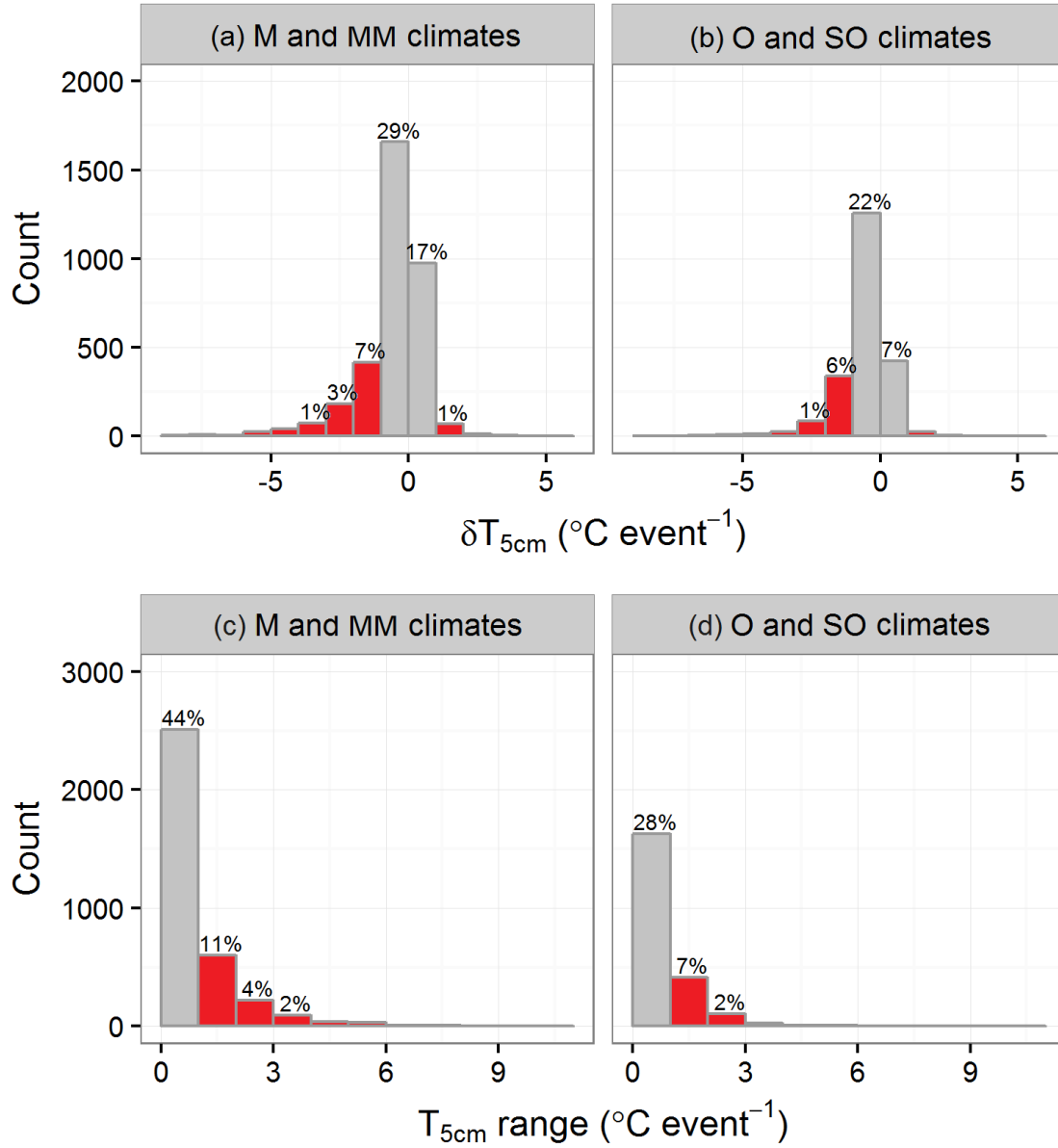


Figure 5. Statistical distributions of $\delta T_{5\text{cm}}$ (a, b) and $T_{5\text{cm}}$ change range (c, d) during 5714 marked rainfall events for Mediterranean (M) and Mediterranean-mountain (MM) stations (a, c) and oceanic (O) and semi-oceanic (SO) stations (b, d). The percent value is the ratio of the count of each bin to the total count in all climate conditions. Bin width is 1°C . Bins for values larger than 1°C or smaller than -1°C are in red.

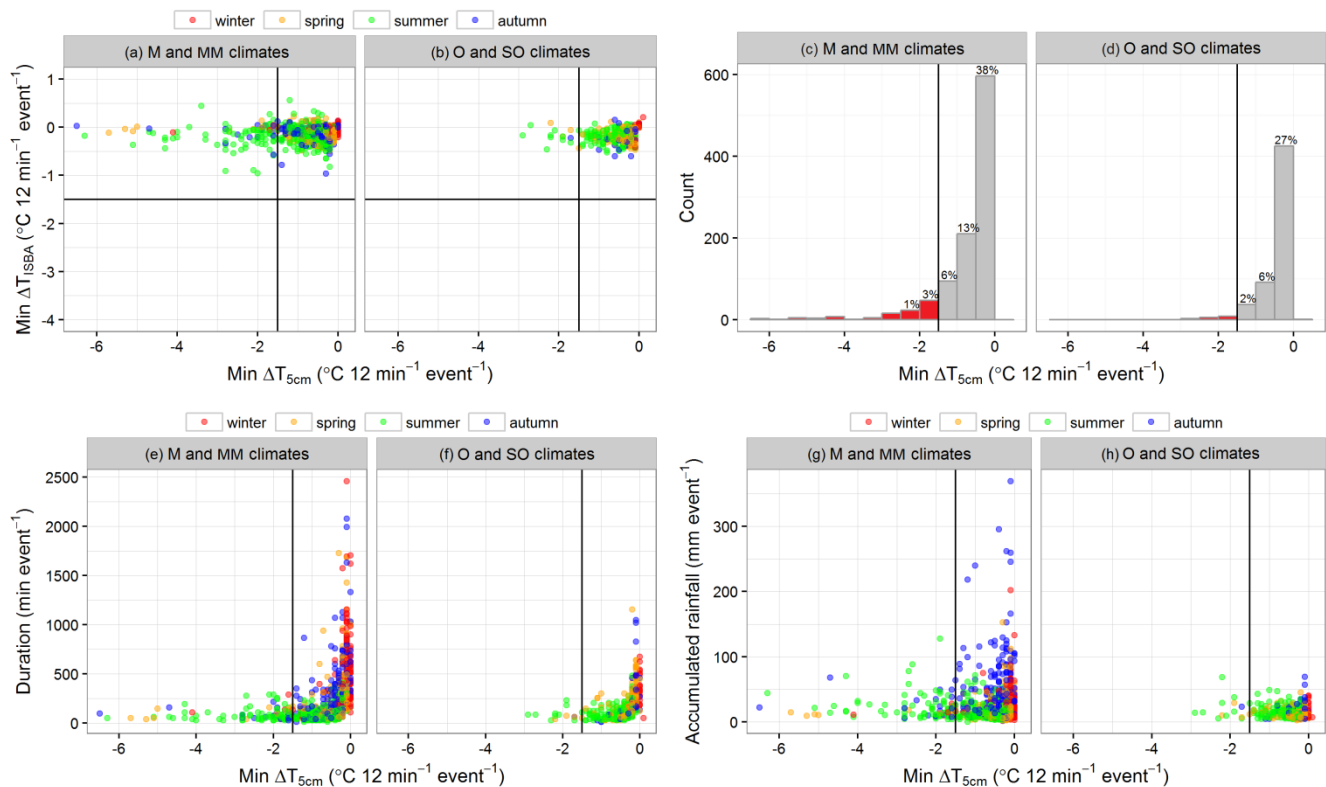


Figure 6. Minimum ΔT_{5cm} during 1577 marked rainfall events affecting T_{5cm} vs. minimum ΔT_{SSA} (a, b), statistical distribution (bins of 0.5 °C) (c, d), vs. rain duration (e, f), and vs. the accumulated rainfall (g, h), for Mediterranean (M) and Mediterranean-mountain (MM) stations (a, c, e, g) and for oceanic (O) and semi-oceanic (SO) stations (b, d, f, h). Dark lines are for the -1.5 °C threshold for intense soil-cooling rains (step 5 in Table 2). (moved to Supplement)

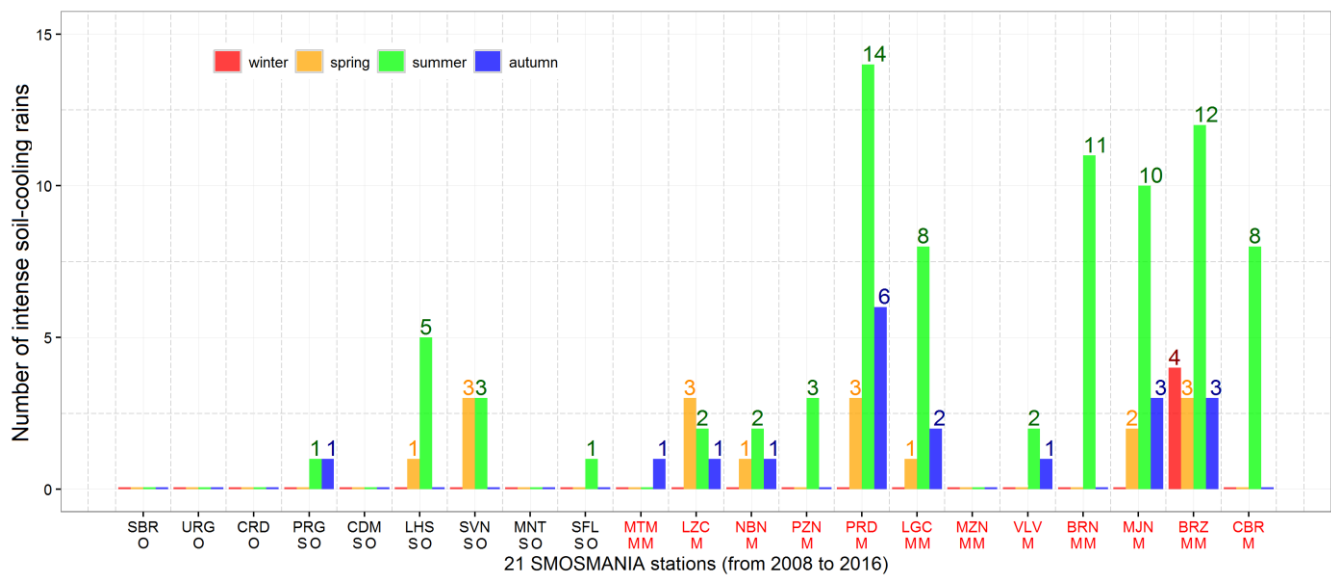
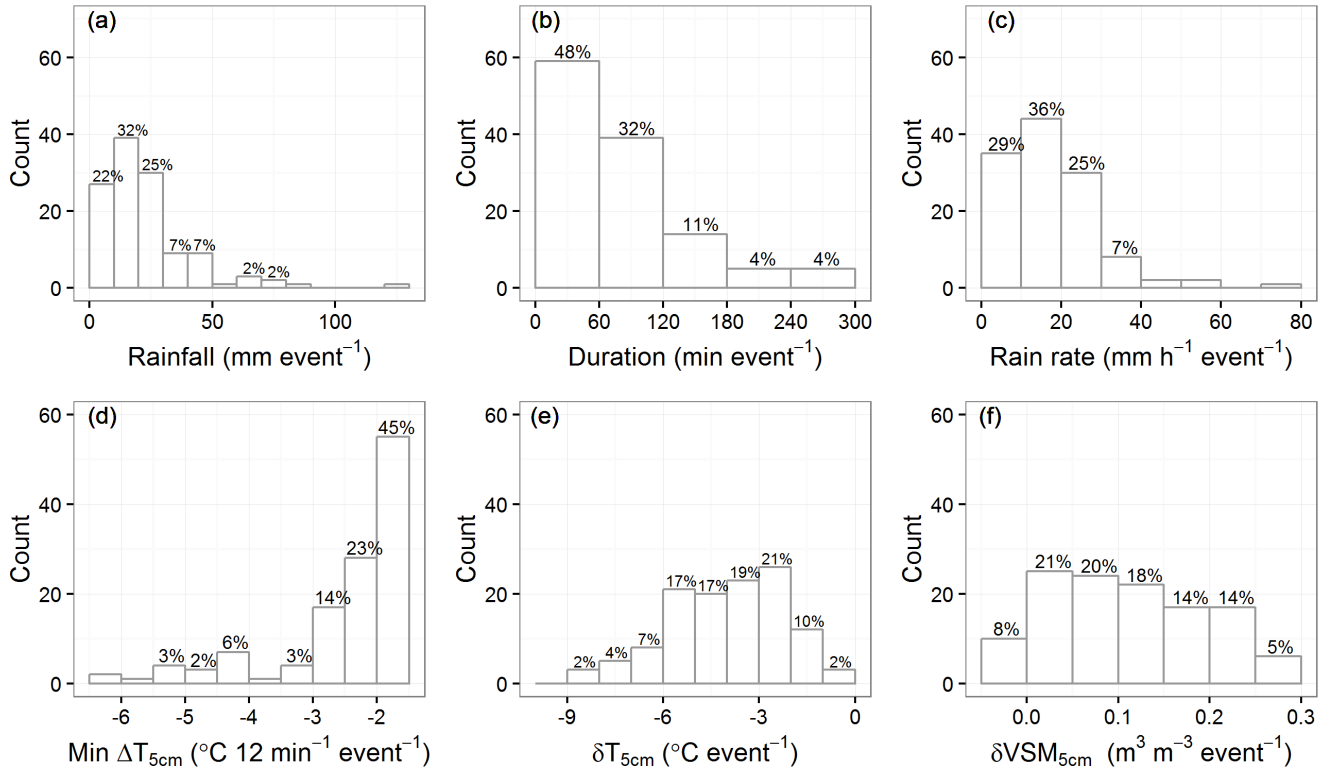


Figure 76. Statistical distribution of the 122 intense soil-cooling rains among stations of the SMOSMANIA network across seasons. Red, orange, green and blue bars are for winter, spring, summer and the autumn, respectively. Symbols “O”, “SO”, “M”, and “MM” indicate Oceanic, Semi-Oceanic, Mediterranean, and Mediterranean/Mountain climates, respectively. Stations are listed from (left) west to (right) east.



5 | **Figure 87.** Statistical distribution of the 122 intense soil-cooling rains in terms of (Sect. 3.3) accumulated rainfall (a), rain duration (b), rain rate (c), minimum ΔT_{5cm} (d), δT_{5cm} (e), and δVSM_{5cm} (f), with bins of 10 mm, 60 min, 10 mm h⁻¹, 1 °C, 1 °C, and 0.05 m³ m⁻³, respectively.

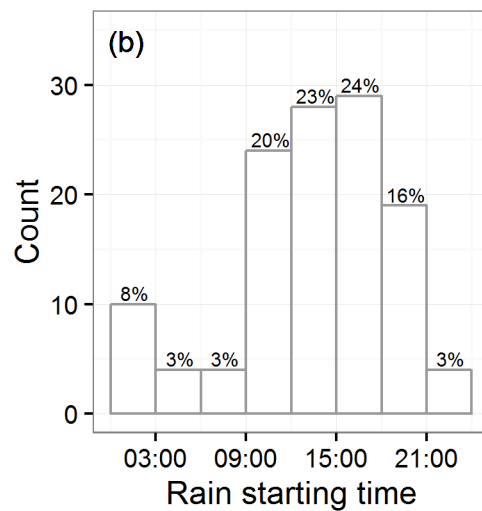
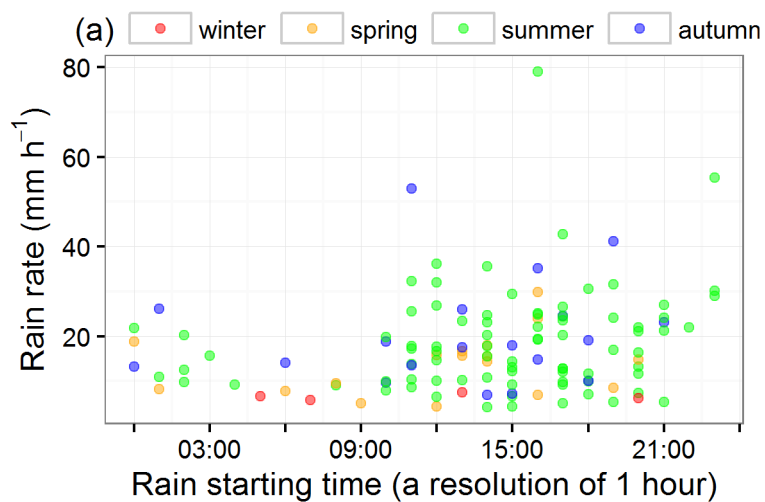


Figure 9. Starting time of the 122 intense soil-cooling rains: vs. rain rate across seasons (a), statistical distribution (with bins of 3 hours): moved to Supplement

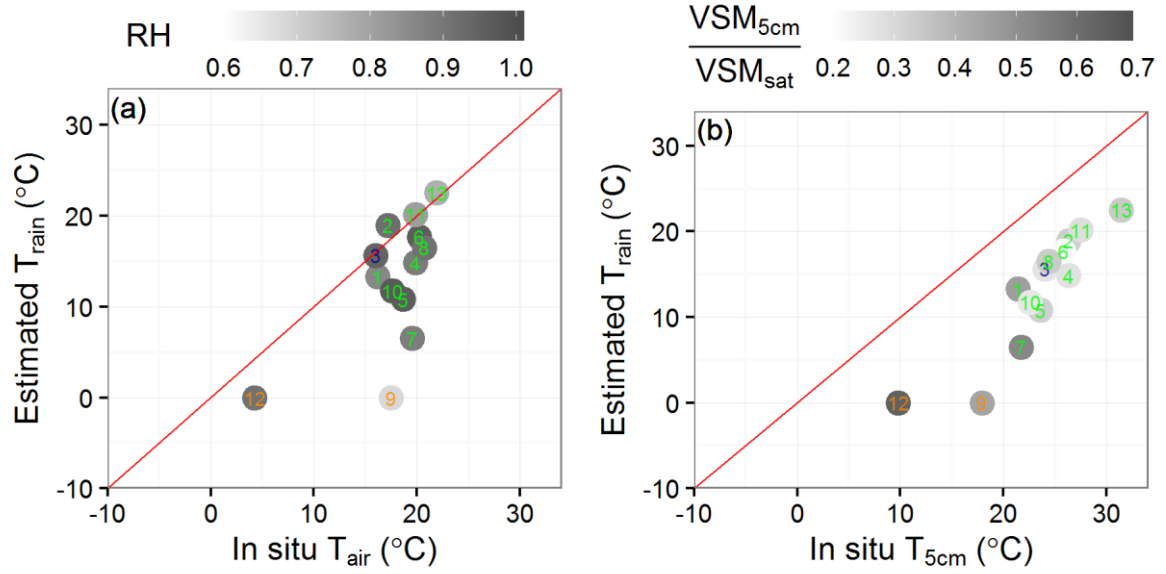
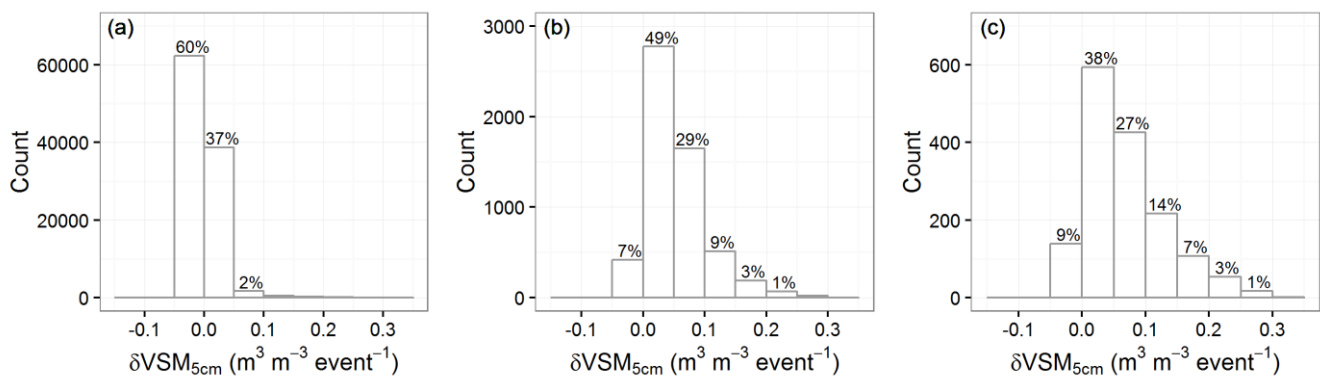


Figure 108. Estimated T_{rain} for the 13 cases listed in Table 45 vs. observed ambient T_{air} (a) and observed $T_{5\text{cm}}$ (b), with levels of grey indicating air relative humidity (RH, dimensionless), and $\text{VSM}_{5\text{cm}}$ to VSM_{sat} ratio (dimensionless) values at time t_1 , respectively.



5 | **Figure 149.** Statistical distribution of δVSM_{5cm} for: 104178 fully documented rainfall events (a), 5714 marked rainfall events (b), and 1577 marked rainfall events affecting topsoil temperature (c) defined in Table 2.

Supplement of

Identification of soil-cooling rains in southern France from soil temperature and soil moisture observations

S. Zhang, C. Meurey, and J.-C. Calvet

Correspondence to: J.-C. Calvet (jean-christophe.calvet@meteo.fr)

Fraction of missing data of in situ observations

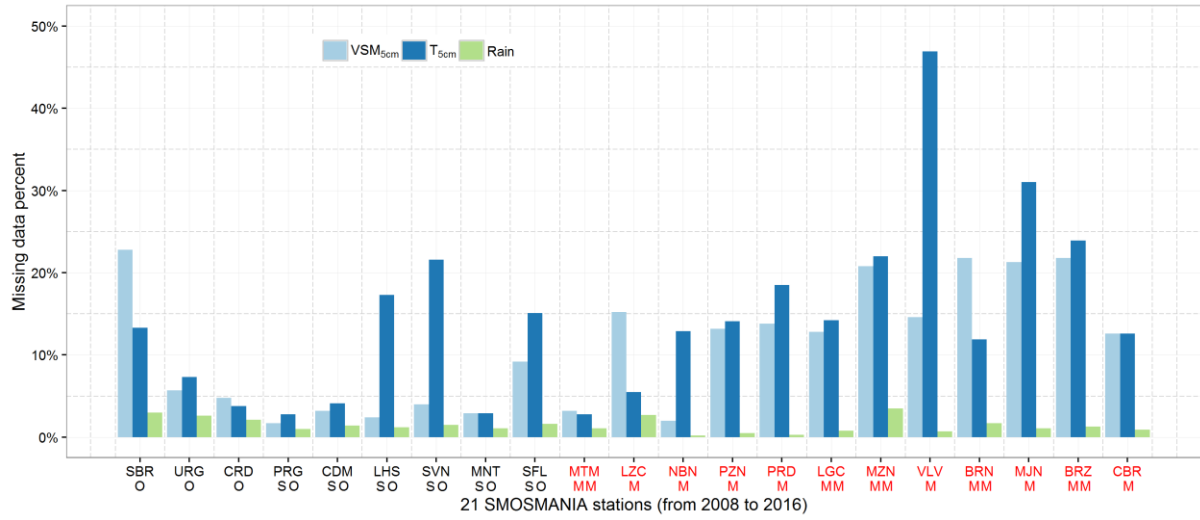


Figure S1. Fraction of missing data for in situ VSM_{5cm} (light blue), T_{5cm} (dark blue) and Rain observations measured every 12 min for the 21 SMOSMANIA stations from 2008 to 2016. Stations are sorted from (left) West to (right) East. Symbols “O”, “SO”, “M”, and “MM” indicate Oceanic, Semi-Oceanic, Mediterranean, and Mediterranean/Mountain climates, respectively.

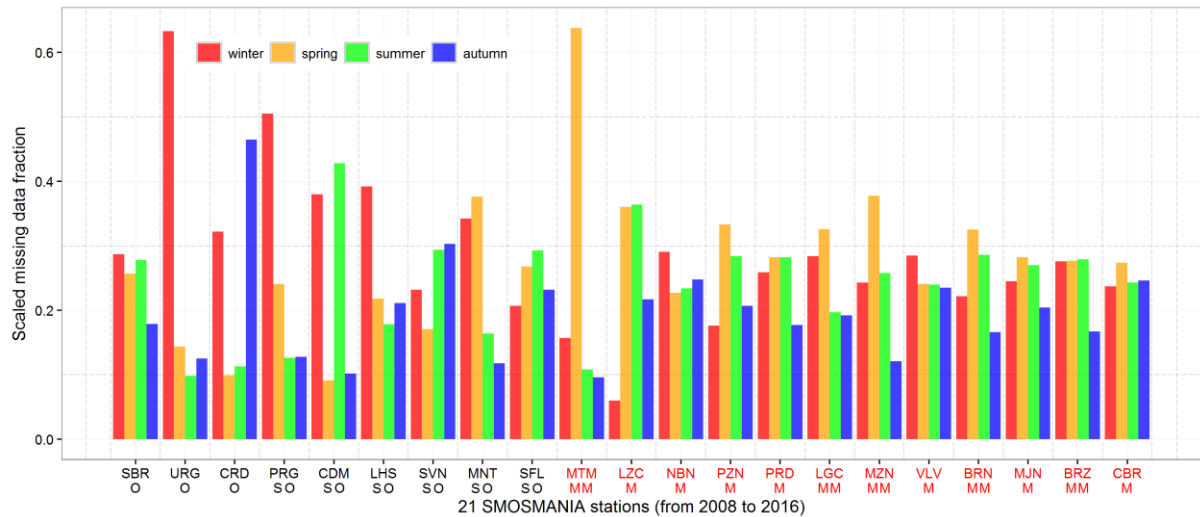


Figure S2. Scaled seasonal distribution of the fraction of missing data of either VSM_{5cm} or T_{5cm} for the 21 SMOSMANIA stations (winter, spring, summer, autumn, corresponding to December-January-February, March-April-May, June-July-August, September-October-November, respectively). Stations are sorted from (left) West to (right) East. Symbols “O”, “SO”, “M”, and “MM” indicate Oceanic, Semi-Oceanic, Mediterranean, and Mediterranean/Mountain climates, respectively.

Table S1. Fraction of missing data, from 0 to 1, of either VSM_{5cm} or T_{5cm} for the 21 SMOSMANIA stations and its seasonal distribution in % (winter, spring, summer, autumn, corresponding to December-January-February, March-April-May, June-July-August, September-October-November, respectively). Fractions larger than 0.1 are in bold. Seasonal grouping of missing data larger than 40 % is in bold. Stations are sorted from (top) West to (bottom) East.

Station (full name)	Mean fraction of missing data	Winter	Spring	Summer	Autumn
SBR (Sabres)	0.24	29 %	26 %	28 %	18 %
URG (Urgons)	0.07	64 %	15 %	9 %	12 %
CRD (Créon d'Armagnac)	0.06	32 %	11 %	11 %	47 %
PRG (Peyrusse Grande)	0.03	48 %	24 %	14 %	14 %
CDM (Condom)	0.04	38 %	10 %	43 %	10 %
LHS (Lahas)	0.18	39 %	22 %	18 %	21 %
SVN (Savenès)	0.23	23 %	17 %	29 %	30 %
MNT (Montaut)	0.03	34 %	38 %	17 %	10 %
SFL (Saint-Félix-de-Lauragais)	0.19	21 %	27 %	29 %	23 %
MTM (Mouthoumet)	0.05	16 %	64 %	10 %	10 %
LZC (Lézignan-Corbières)	0.16	6 %	36 %	36 %	22 %
NBN (Narbonne)	0.13	29 %	22 %	23 %	25 %
PZN (Pézenas)	0.14	18 %	33 %	28 %	21 %
PRD (Prades-le-Lez)	0.20	26 %	28 %	28 %	18 %
LGC (La-Grand-Combe)	0.15	28 %	33 %	20 %	19 %
MZN (Mazan-L'Abbaye)	0.23	24 %	38 %	26 %	12 %
VLV (Villevieille)	0.48	29 %	24 %	24 %	24 %
BRN (Barnas)	0.22	22 %	32 %	29 %	16 %
MJN (Méjannes-le-Clap)	0.31	24 %	28 %	27 %	20 %
BRZ (Berzème)	0.31	28 %	28 %	28 %	17 %
CBR (Cabrières-d'Avignon)	0.13	24 %	28 %	24 %	24 %
Mean value	0.17	29%	28%	24%	20%

Soil characteristics

Table S2. Reconstructed soil characteristics at a depth of 5 cm for the 21 stations of the SMOSMANIA network, assuming a zero fraction of gravels. Stations are sorted from (top) West to (bottom) East.

Station	VSM_{sat} ($m^3 m^{-3}$)	f_{sand} ($m^3 m^{-3}$)	f_{clay} ($m^3 m^{-3}$)	f_{silt} ($m^3 m^{-3}$)	f_{gravel} ($m^3 m^{-3}$)	f_{SOM} ($m^3 m^{-3}$)
SBR	0.440	0.502	0.021	0.016	0	0.021
URG	0.472	0.079	0.078	0.341	0	0.029
CRD	0.487	0.413	0.027	0.029	0	0.045
PRG	0.497	0.073	0.193	0.197	0	0.039
CDM	0.457	0.078	0.215	0.232	0	0.019
LHS	0.413	0.154	0.196	0.205	0	0.032
SVN	0.457	0.191	0.103	0.235	0	0.014
MNT	0.453	0.145	0.077	0.290	0	0.036
SFL	0.396	0.253	0.132	0.196	0	0.024
MTM	0.419	0.211	0.148	0.144	0	0.079
LZC	0.464	0.222	0.138	0.145	0	0.031
NBN	0.495	0.116	0.206	0.122	0	0.060
PZN	0.510	0.224	0.077	0.141	0	0.047
PRD	0.460	0.130	0.150	0.202	0	0.057
LGC	0.405	0.410	0.072	0.078	0	0.035
MZN	0.600	0.219	0.049	0.056	0	0.075
VLV	0.557	0.261	0.054	0.082	0	0.046
BRN	0.424	0.385	0.047	0.066	0	0.078
MJN	0.460	0.192	0.068	0.161	0	0.119
BRZ	0.572	0.148	0.092	0.155	0	0.032
CBR	0.488	0.222	0.113	0.132	0	0.045

Table S3. Observed soil characteristics at a depth of 10 cm for the 21 stations of the SMOSMANIA network. Adapted from Table 1 in Calvet et al. (2016). Stations are sorted from (top) West to (bottom) East.

Station	VSM_{sat} ($m^3 m^{-3}$)	f_{sand} ($m^3 m^{-3}$)	f_{clay} ($m^3 m^{-3}$)	f_{silt} ($m^3 m^{-3}$)	f_{gravel} ($m^3 m^{-3}$)	f_{SOM} ($m^3 m^{-3}$)
SBR	0.352	0.576	0.026	0.013	0.002	0.032
URG	0.474	0.076	0.078	0.341	0.005	0.025
CRD	0.437	0.457	0.027	0.033	0.000	0.045
PRG	0.431	0.051	0.138	0.138	0.214	0.028
CDM	0.413	0.073	0.241	0.231	0.012	0.030
LHS	0.416	0.102	0.202	0.189	0.051	0.039
SVN	0.445	0.128	0.073	0.176	0.162	0.017
MNT	0.447	0.135	0.066	0.230	0.102	0.020
SFL	0.413	0.127	0.071	0.118	0.250	0.021
MTM	0.405	0.110	0.081	0.076	0.297	0.032
LZC	0.429	0.129	0.066	0.068	0.292	0.015
NBN	0.401	0.063	0.135	0.075	0.290	0.036
PZN	0.495	0.222	0.074	0.131	0.055	0.023
PRD	0.494	0.038	0.052	0.069	0.326	0.021
LGC	0.428	0.254	0.044	0.042	0.214	0.019
MZN	0.560	0.212	0.037	0.045	0.097	0.049
VLV	0.506	0.294	0.054	0.086	0.031	0.029
BRN	0.379	0.105	0.009	0.016	0.474	0.016
MJN	0.506	0.064	0.029	0.056	0.317	0.028
BRZ	0.508	0.097	0.074	0.110	0.191	0.020
CBR	0.501	0.120	0.057	0.068	0.241	0.013

Examples of significant soil-cooling rains

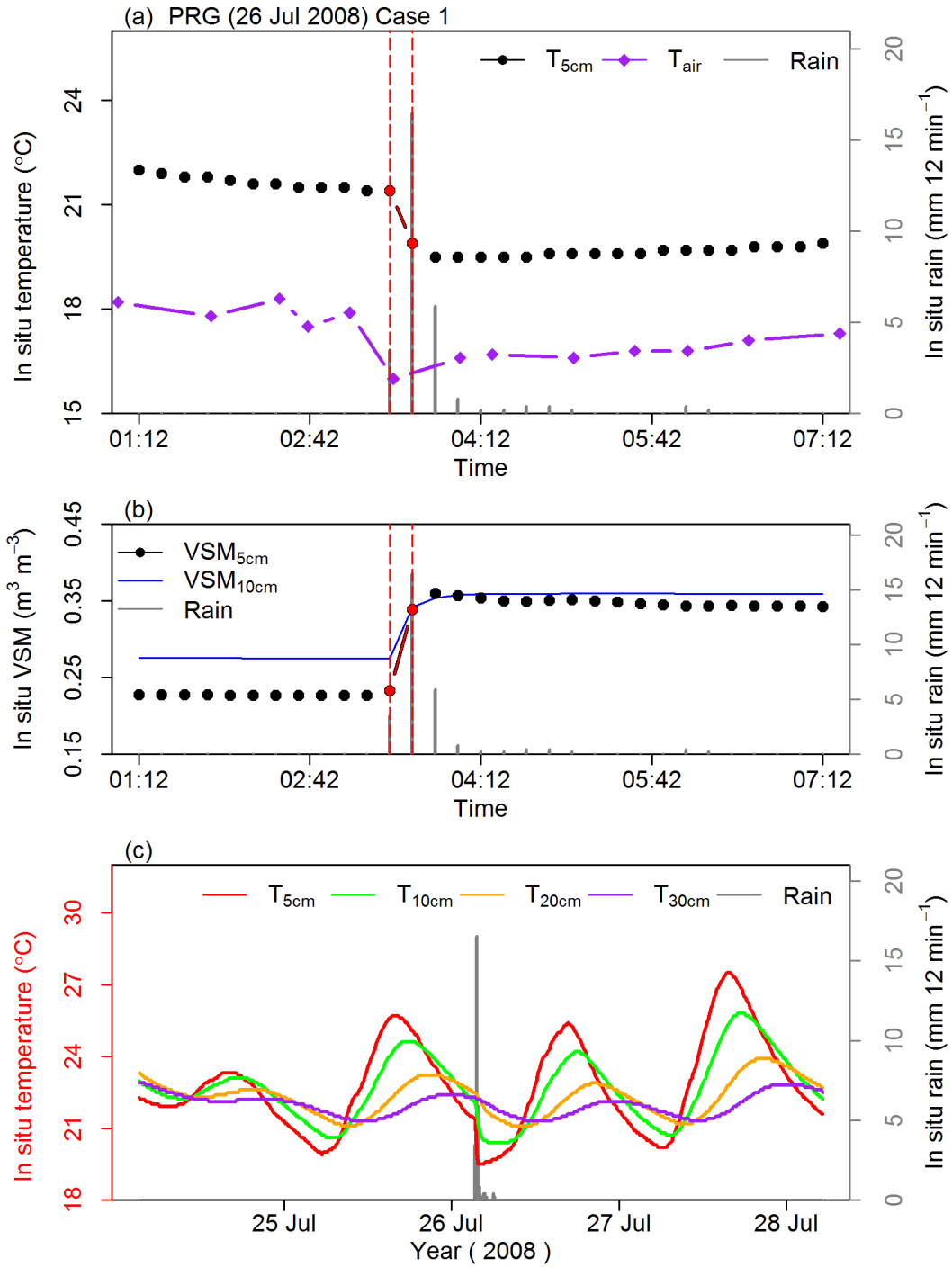


Figure S3. (a) In situ T_{5cm} (black) and accumulated rainfall (grey) observations measured every 12 min, and the maximum and minimum T_{air} values in an hour (purple); (b) in situ VSM_{5cm} (black), VSM_{10cm} (blue) observations also measured every 12 min, from case 1 (see Table 45) at PRG station on 26 July 2008. The red dashed lines show the duration from time t_1 to t_2 , and the corresponding T_{5cm} and VSM_{5cm} are highlighted by red. (c) In situ soil temperature measured from 24 to 28 July 2008 at depths of 5, 10, 20 and 30 cm, together with the in situ rainfall observations ($\text{mm } 12 \text{ min}^{-1}$) shown in grey.

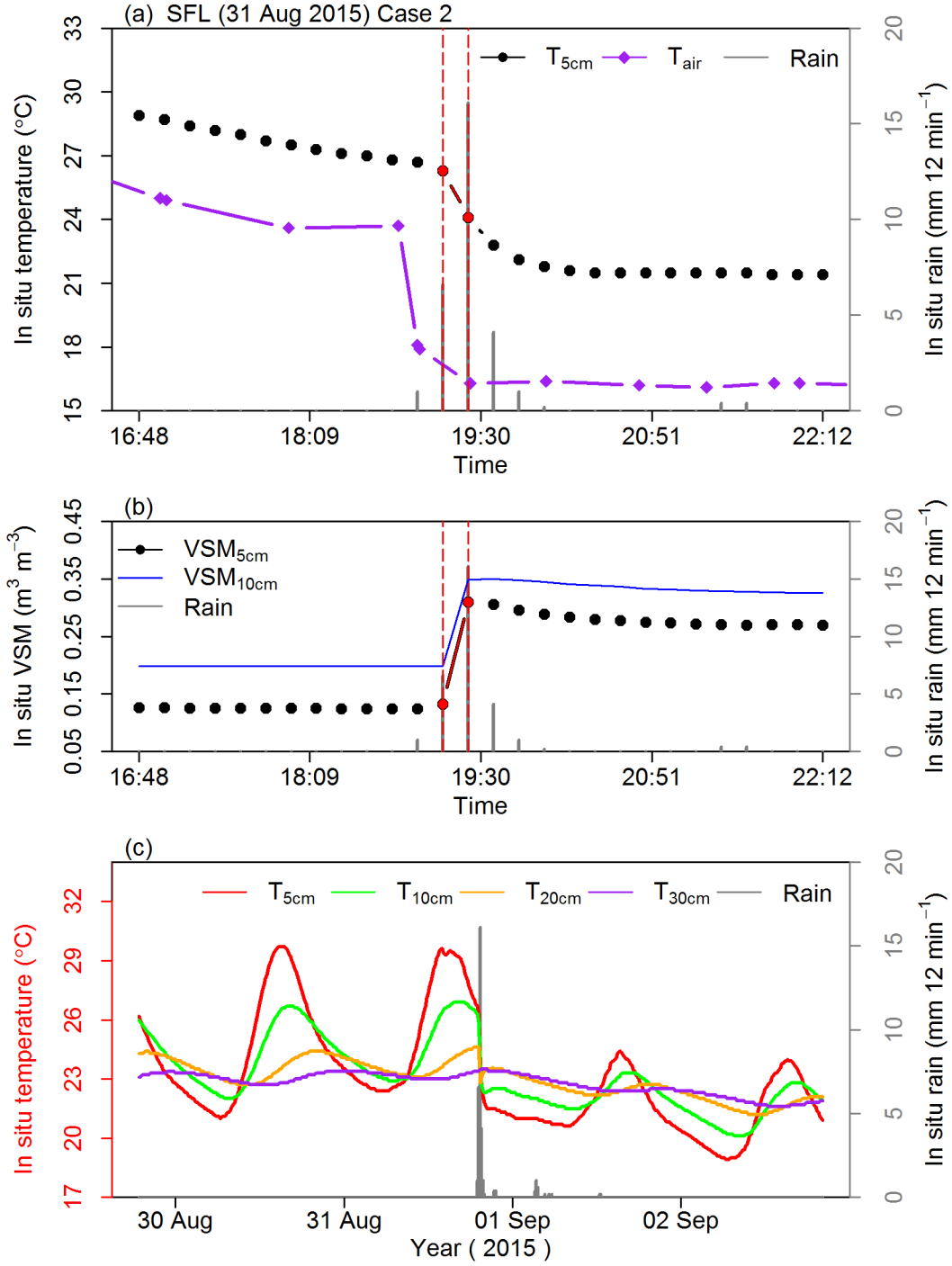


Figure S4. (a) In situ $T_{5\text{cm}}$ (black) and accumulated rainfall (grey) observations measured every 12 min, and the maximum and minimum T_{air} values in an hour (purple); (b) in situ $\text{VSM}_{5\text{cm}}$ (black), $\text{VSM}_{10\text{cm}}$ (blue) observations also measured every 12 min, from case 2 (see Table 45) at SFL station on 31 August 2015. The red dashed lines show the duration from time t_1 to t_2 , and the corresponding $T_{5\text{cm}}$ and $\text{VSM}_{5\text{cm}}$ are highlighted by red. (c) In situ soil temperature measured from 29 August to 2 September 2015 at depths of 5, 10, 20 and 30 cm, together with the in situ rainfall observations ($\text{mm } 12 \text{ min}^{-1}$) shown in grey.

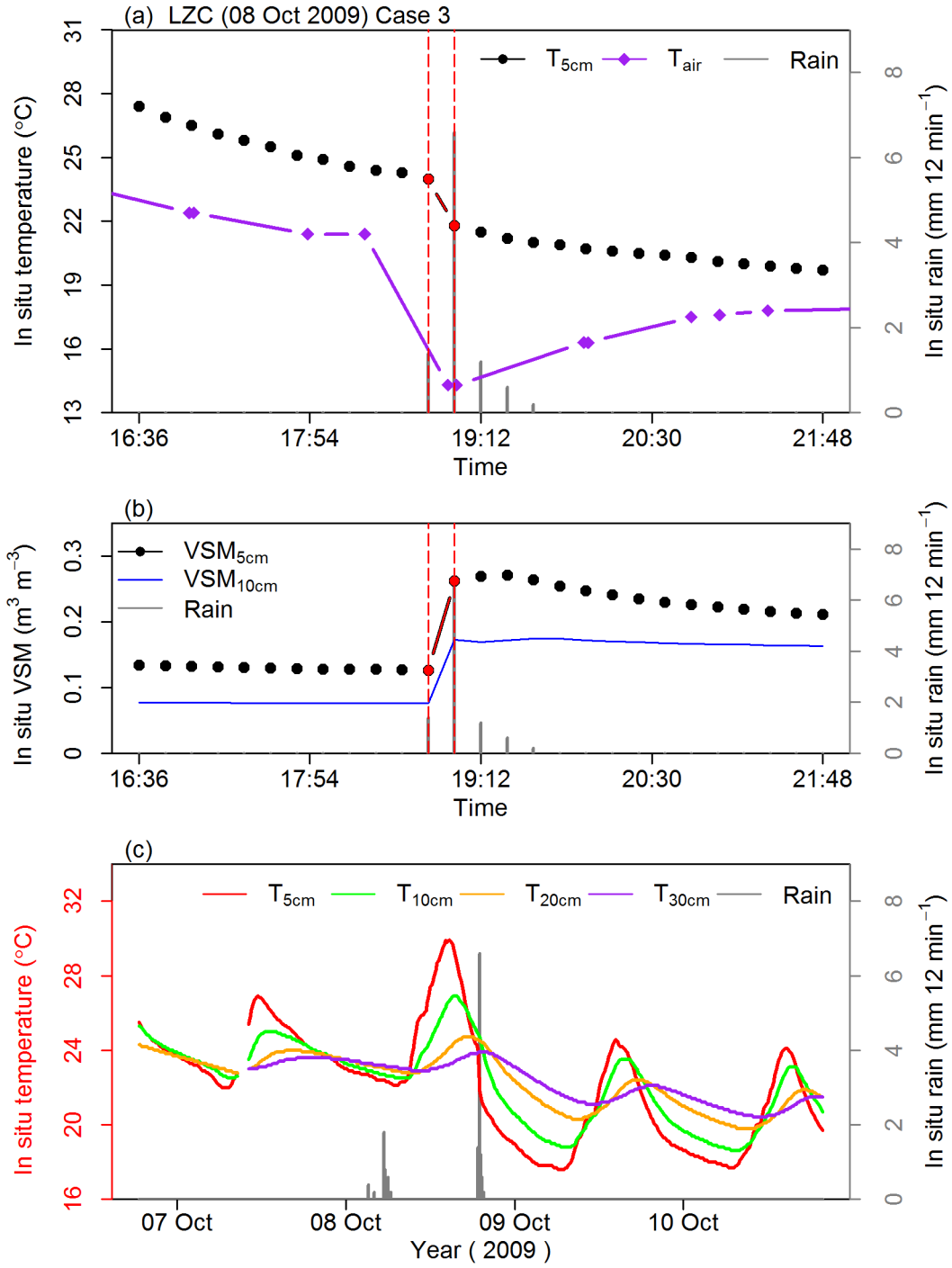


Figure S5. (a) In situ $T_{5\text{cm}}$ (black) and accumulated rainfall (grey) observations measured every 12 min, and the maximum and minimum T_{air} values in an hour (purple); (b) in situ $\text{VSM}_{5\text{cm}}$ (black), $\text{VSM}_{10\text{cm}}$ (blue) observations also measured every 12 min, from case 3 (see Table 45) at LZC station on 8 October 2009. The red dashed lines show the duration from time t_1 to t_2 , and the corresponding $T_{5\text{cm}}$ and $\text{VSM}_{5\text{cm}}$ are highlighted by red. (c) In situ soil temperature measured from 6 to 10 October 2009 at depths of 5, 10, 20 and 30 cm, together with the in situ rainfall observations ($\text{mm } 12 \text{ min}^{-1}$) shown in grey.

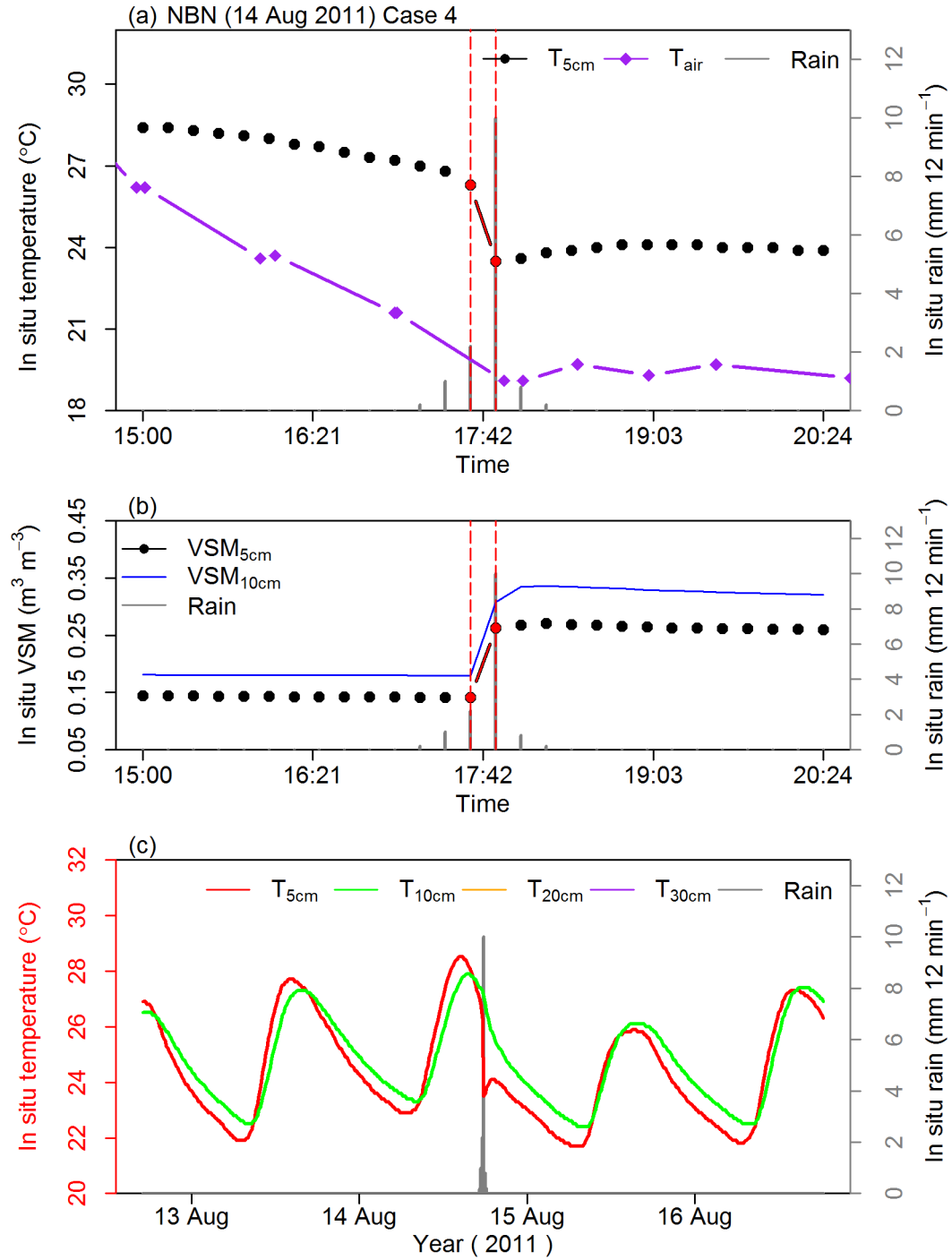


Figure S6. (a) In situ T_{5cm} (black) and accumulated rainfall (grey) observations measured every 12 min, and the maximum and minimum T_{air} values in an hour (purple); (b) in situ VSM_{5cm} (black), VSM_{10cm} (blue) observations also measured every 12 min, from case 4 (see Table 45) at NBN station on 14 August 2011. The red dashed lines show the duration from time t_1 to t_2 , and the corresponding T_{5cm} and VSM_{5cm} are highlighted by red. (c) In situ soil temperature measured from 12 to 16 August 2011 at depths of 5, 10, 20 and 30 cm, together with the in situ rainfall observations ($mm\ 12\ min^{-1}$) shown in grey. In situ soil temperatures at depths of 20 and 30 cm are missing.

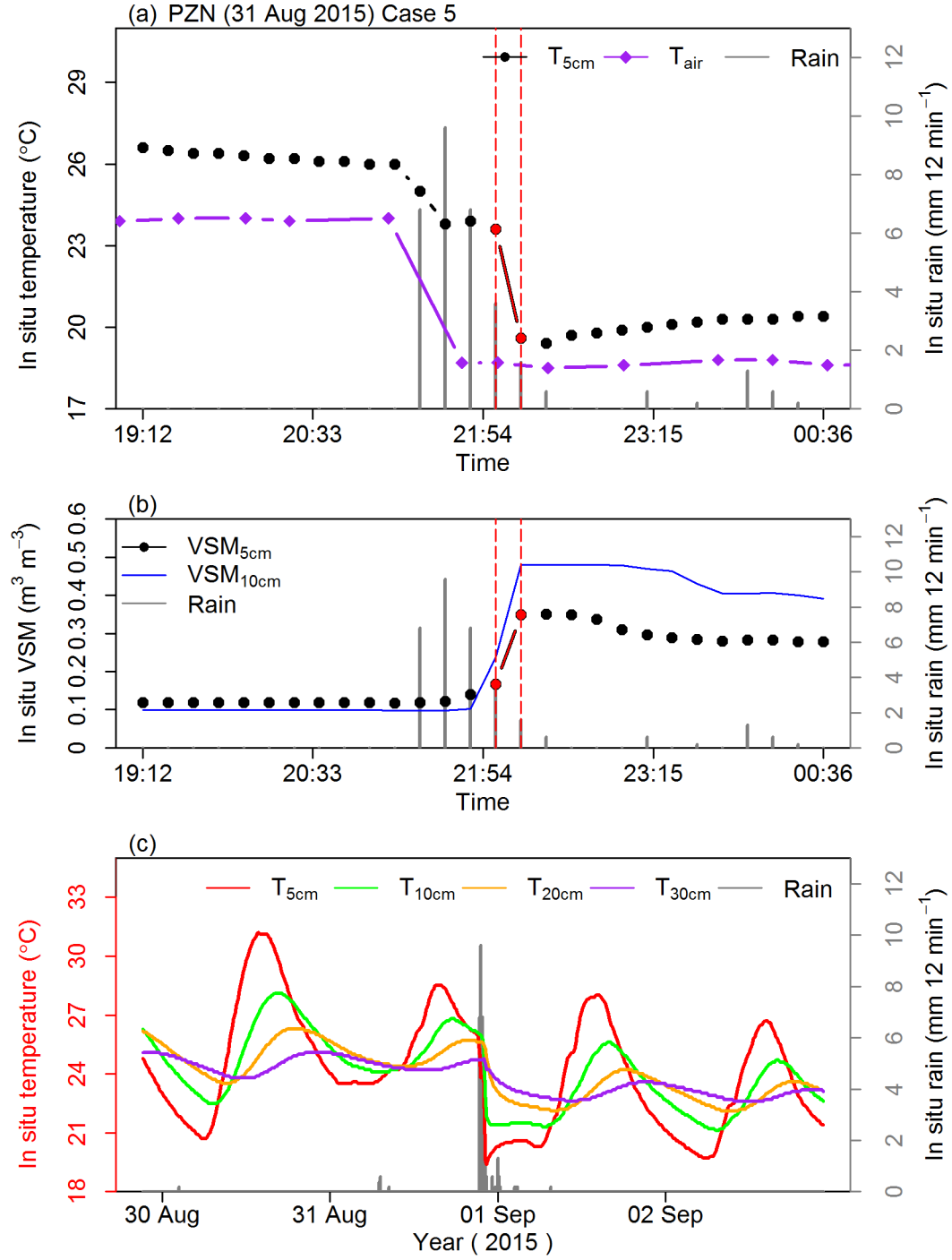


Figure S7. (a) In situ $T_{5\text{cm}}$ (black) and accumulated rainfall (grey) observations measured every 12 min, and the maximum and minimum T_{air} values in an hour (purple); (b) in situ $\text{VSM}_{5\text{cm}}$ (black), $\text{VSM}_{10\text{cm}}$ (blue) observations also measured every 12 min, from case 5 (see Table 45) at PZN station on 31 August 2015. The red dashed lines show the duration from time t_1 to t_2 , and the corresponding $T_{5\text{cm}}$ and $\text{VSM}_{5\text{cm}}$ are highlighted by red. (c) In situ soil temperature measured from 29 August to 2 September 2015 at depths of 5, 10, 20 and 30 cm, together with the in situ rainfall observations ($\text{mm } 12 \text{ min}^{-1}$) shown in grey.

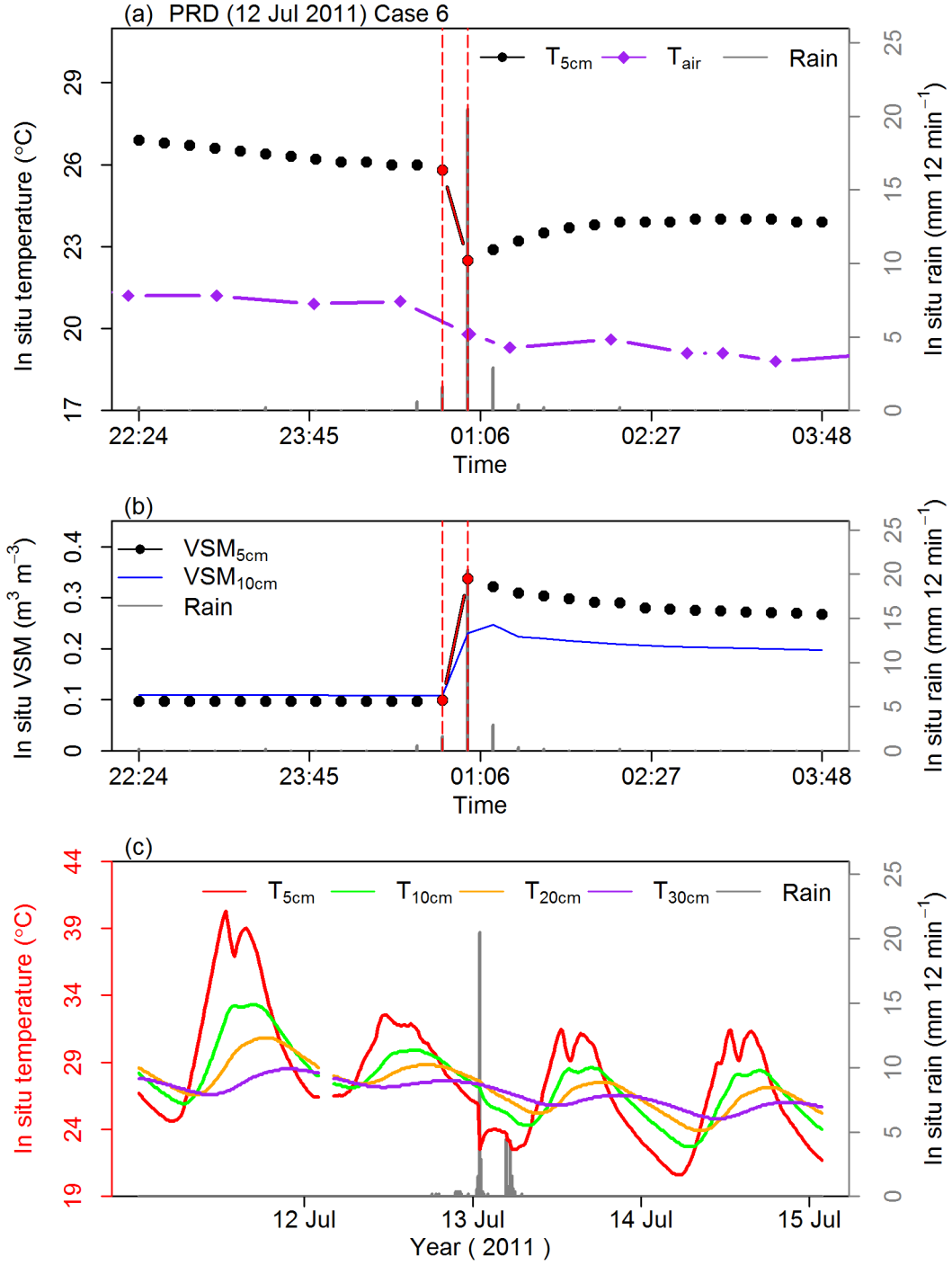


Figure S8. (a) In situ T_{5cm} (black) and accumulated rainfall (grey) observations measured every 12 min, and the maximum and minimum T_{air} values in an hour (purple); (b) in situ VSM_{5cm} (black), VSM_{10cm} (blue) observations also measured every 12 min, from case 6 (see Table 45) at PRD station on 12 and 13 July 2011. The red dashed lines show the duration from time t_1 to t_2 , and the corresponding T_{5cm} and VSM_{5cm} are highlighted by red. (c) In situ soil temperature measured from 11 to 15 July 2011 at depths of 5, 10, 20 and 30 cm, together with the in situ rainfall observations ($mm\ 12\ min^{-1}$) shown in grey.

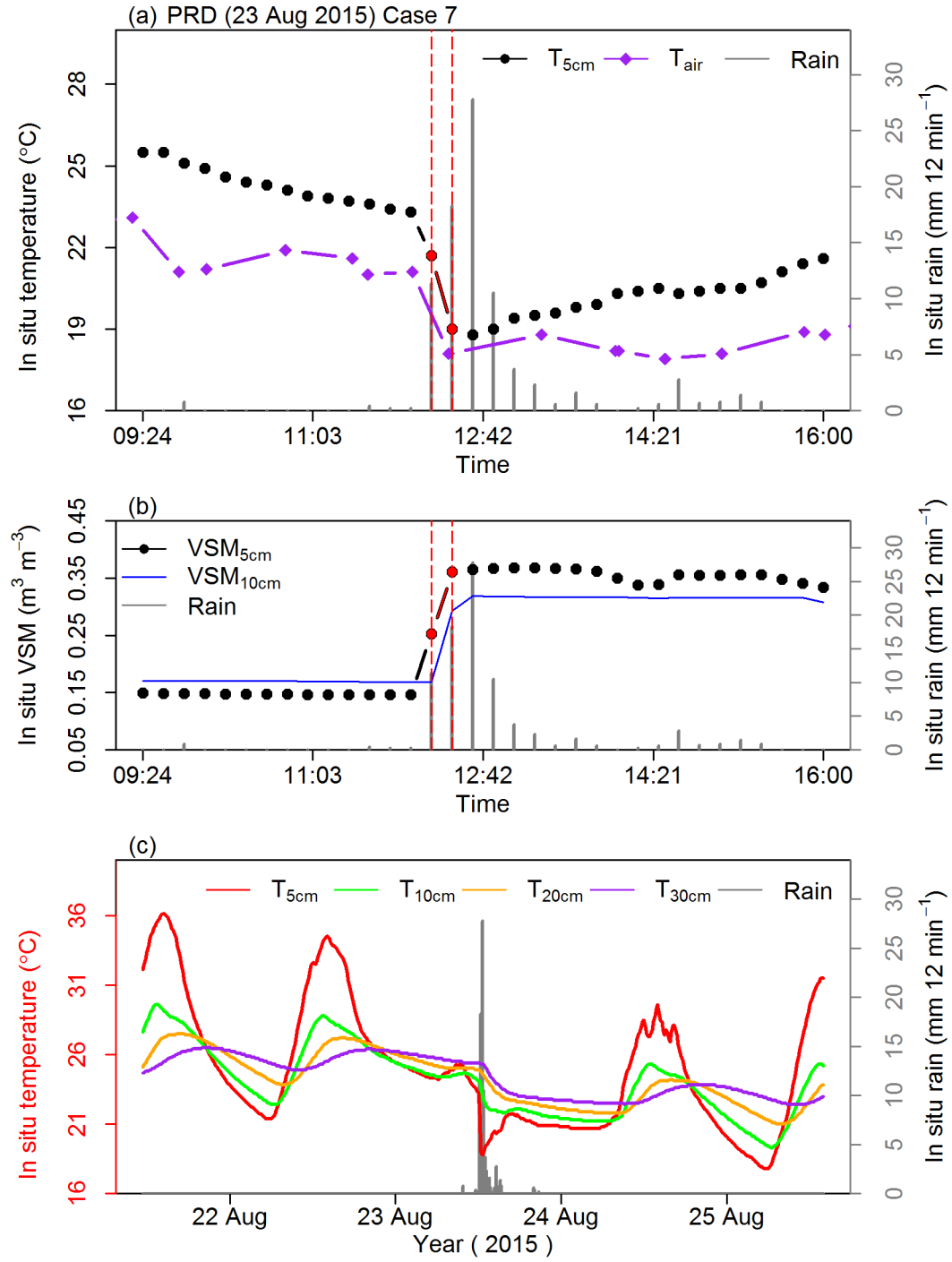


Figure S9. (a) In situ $T_{5\text{cm}}$ (black) and accumulated rainfall (grey) observations measured every 12 min, and the maximum and minimum T_{air} values in an hour (purple); (b) in situ $\text{VSM}_{5\text{cm}}$ (black), $\text{VSM}_{10\text{cm}}$ (blue) observations also measured every 12 min, from case 7 (see Table 45) at PRD station on 23 August 2015. The red dashed lines show the duration from time t_1 to t_2 , and the corresponding $T_{5\text{cm}}$ and $\text{VSM}_{5\text{cm}}$ are highlighted by red. (c) In situ soil temperature measured from 21 to 25 August 2015 at depths of 5, 10, 20 and 30 cm, together with the in situ rainfall observations ($\text{mm } 12 \text{ min}^{-1}$) shown in grey.

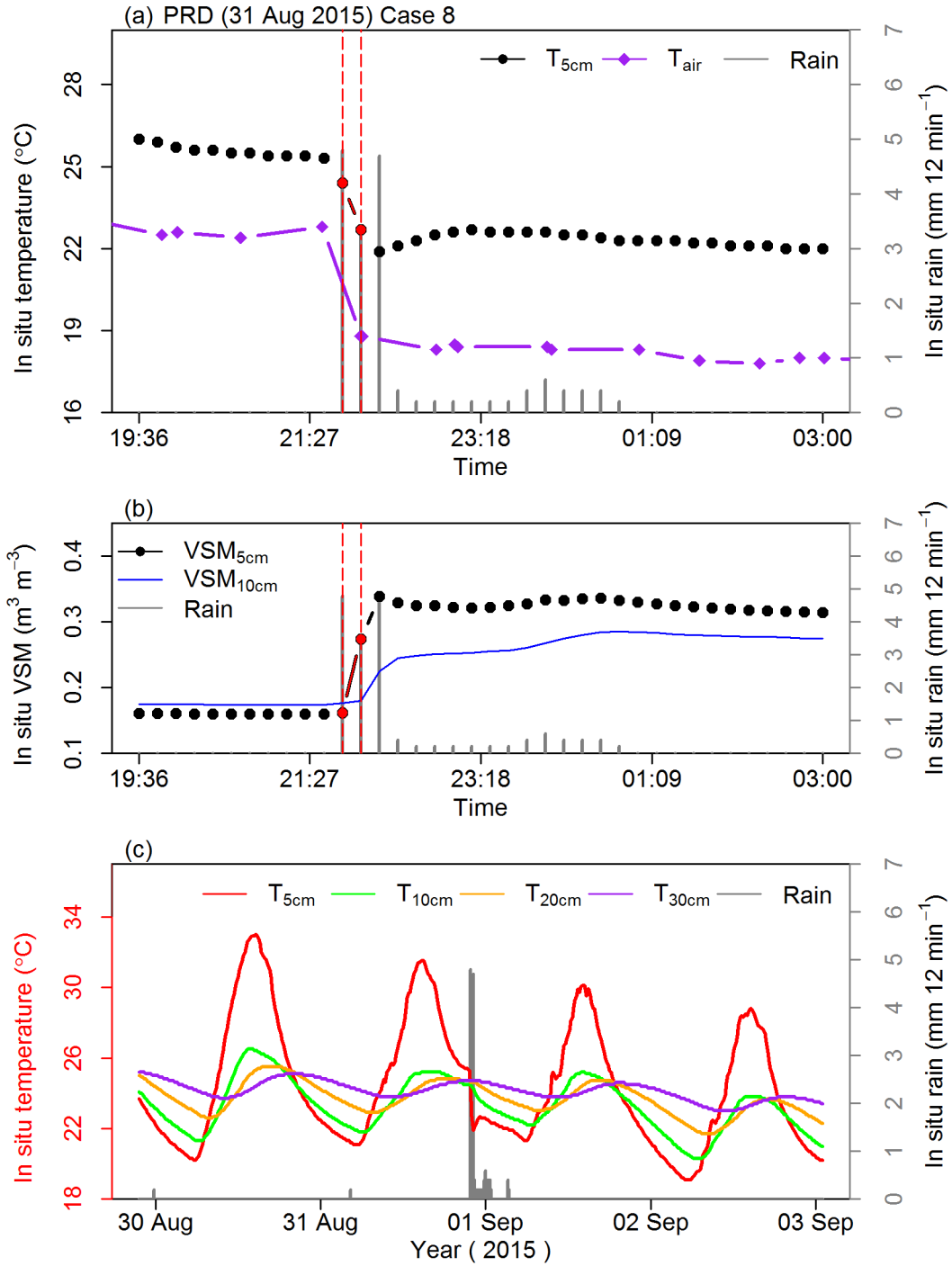


Figure S10. (a) In situ $T_{5\text{cm}}$ (black) and accumulated rainfall (grey) observations measured every 12 min, and the maximum and minimum T_{air} values in an hour (purple); (b) in situ $\text{VSM}_{5\text{cm}}$ (black), $\text{VSM}_{10\text{cm}}$ (blue) observations also measured every 12 min, from case 8 (see Table 45) at PRD station on 31 August and 1 September 2015. The red dashed lines show the duration from time t_1 to t_2 , and the corresponding $T_{5\text{cm}}$ and $\text{VSM}_{5\text{cm}}$ are highlighted by red. (c) In situ soil temperature measured from 29 August to 3 September 2015 at depths of 5, 10, 20 and 30 cm, together with the in situ rainfall observations ($\text{mm } 12 \text{ min}^{-1}$) shown in grey.

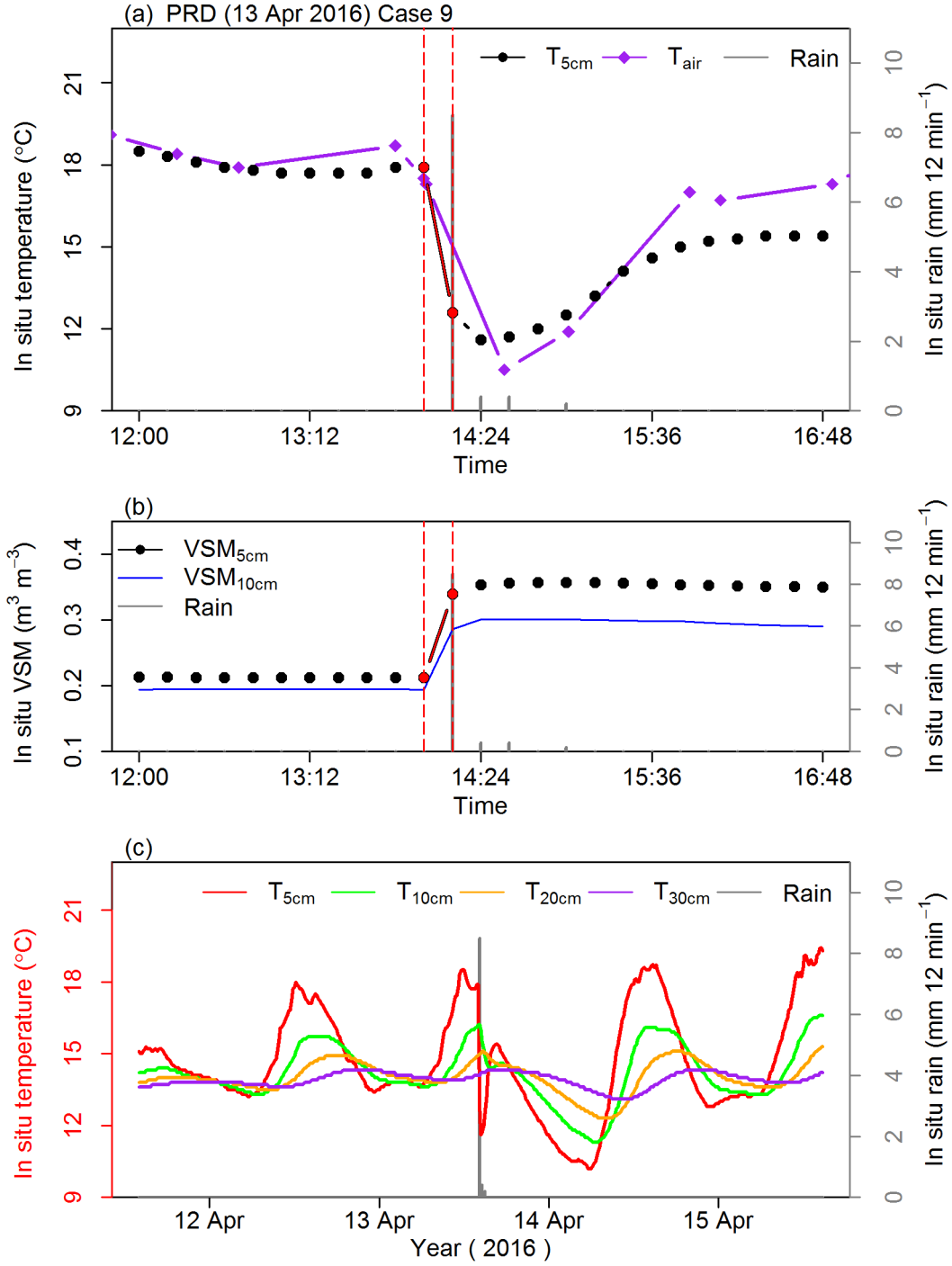


Figure S11. (a) In situ $T_{5\text{cm}}$ (black) and accumulated rainfall (grey) observations measured every 12 min, and the maximum and minimum T_{air} values in an hour (purple); (b) in situ $\text{VSM}_{5\text{cm}}$ (black), $\text{VSM}_{10\text{cm}}$ (blue) observations also measured every 12 min, from case 9 (see Table 45) at PRD station on 13 April 2016. The red dashed lines show the duration from time t_1 to t_2 , and the corresponding $T_{5\text{cm}}$ and $\text{VSM}_{5\text{cm}}$ are highlighted by red. (c) In situ soil temperature measured from 11 to 15 April 2016 at depths of 5, 10, 20 and 30 cm, together with the in situ rainfall observations ($\text{mm } 12 \text{ min}^{-1}$) shown in grey.

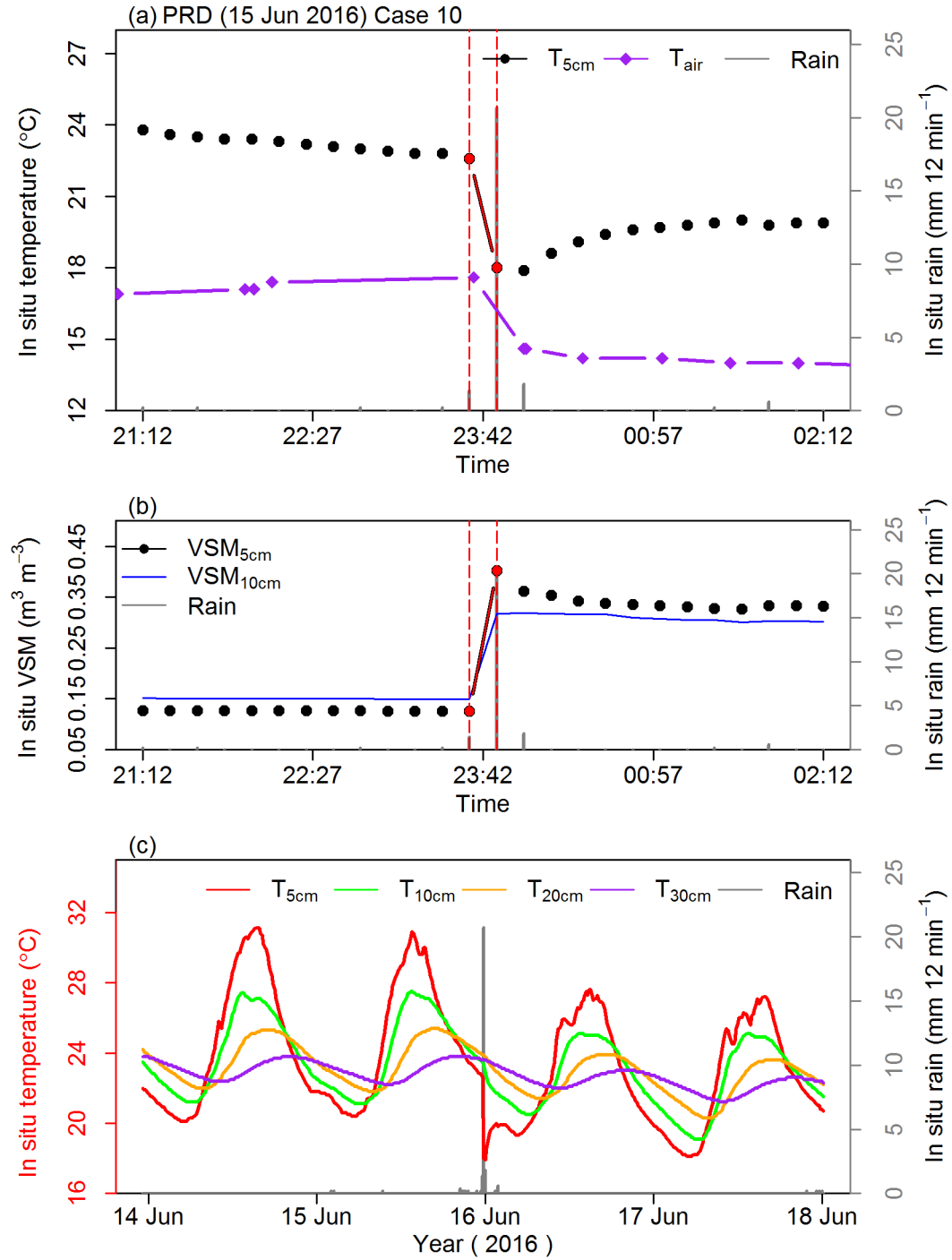


Figure S12. (a) In situ T_{5cm} (black) and accumulated rainfall (grey) observations measured every 12 min, and the maximum and minimum T_{air} values in an hour (purple); (b) in situ VSM_{5cm} (black), VSM_{10cm} (blue) observations also measured every 12 min, from case 10 (see Table 45) at PRD station on 15 and 16 June 2016. The red dashed lines show the duration from time t_1 to t_2 , and the corresponding T_{5cm} and VSM_{5cm} are highlighted by red. (c) In situ soil temperature measured from 13 to 18 June 2016 at depths of 5, 10, 20 and 30 cm, together with the in situ rainfall observations ($mm\ 12\ min^{-1}$) shown in grey.

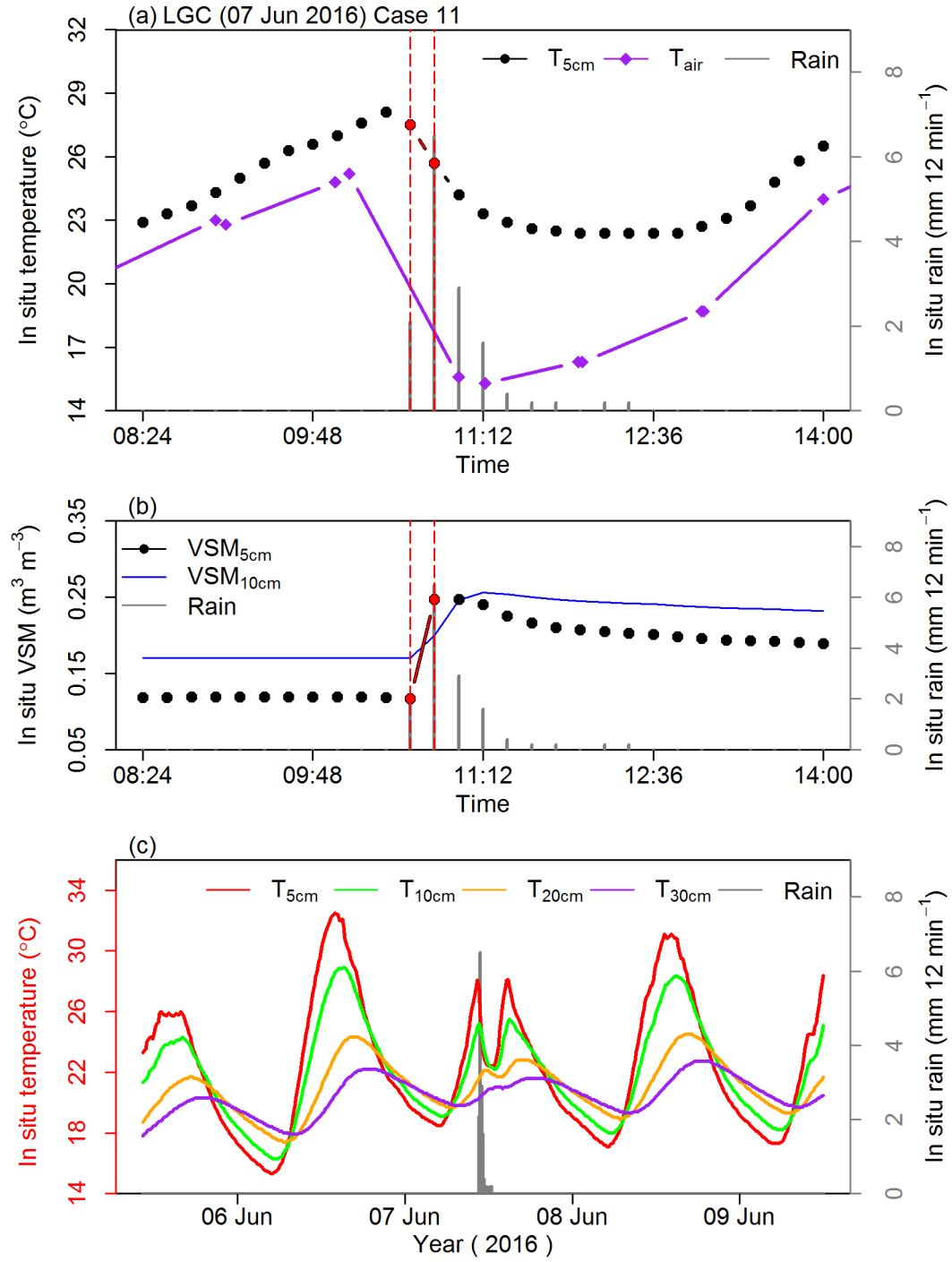


Figure S13. (a) In situ $T_{5\text{cm}}$ (black) and accumulated rainfall (grey) observations measured every 12 min, and the maximum and minimum T_{air} values in an hour (purple); (b) in situ $\text{VSM}_{5\text{cm}}$ (black), $\text{VSM}_{10\text{cm}}$ (blue) observations also measured every 12 min, from case 11 (see Table 45) at LGC station on 7 June 2016. The red dashed lines show the duration from time t_1 to t_2 , and the corresponding $T_{5\text{cm}}$ and $\text{VSM}_{5\text{cm}}$ are highlighted by red. (c) In situ soil temperature measured from 5 to 9 June 2016 at depths of 5, 10, 20 and 30 cm, together with the in situ rainfall observations ($\text{mm } 12 \text{ min}^{-1}$) shown in grey.

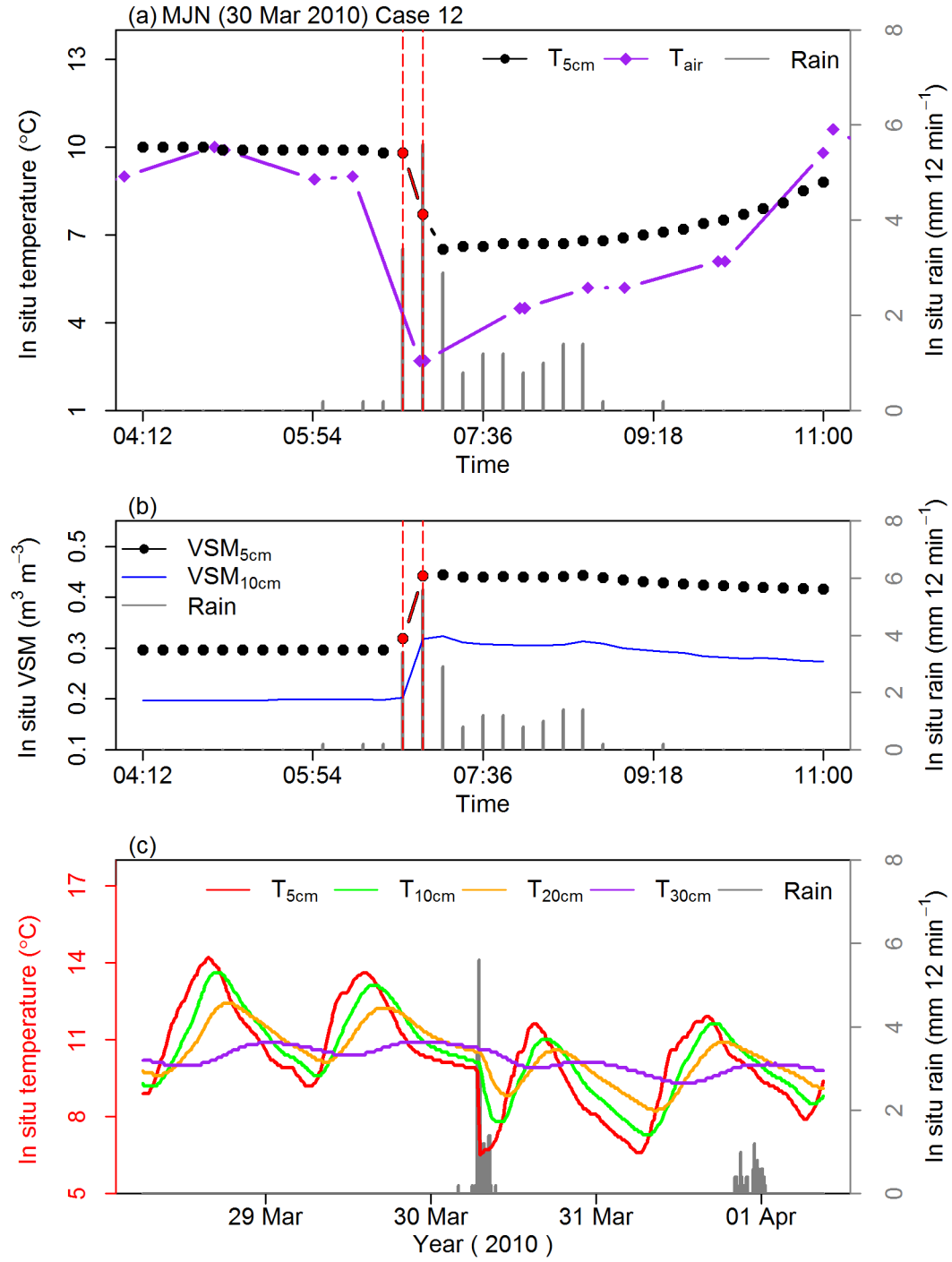


Figure S14. (a) In situ $T_{5\text{cm}}$ (black) and accumulated rainfall (grey) observations measured every 12 min, and the maximum and minimum T_{air} values in an hour (purple); (b) in situ $\text{VSM}_{5\text{cm}}$ (black), $\text{VSM}_{10\text{cm}}$ (blue) observations also measured every 12 min, from case 12 (see Table 45) at MJN station on 30 March 2010. The red dashed lines show the duration from time t_1 to t_2 , and the corresponding $T_{5\text{cm}}$ and $\text{VSM}_{5\text{cm}}$ are highlighted by red. (c) In situ soil temperature measured from 28 March to 1 April 2010 at depths of 5, 10, 20 and 30 cm, together with the in situ rainfall observations ($\text{mm } 12 \text{ min}^{-1}$) shown in grey.

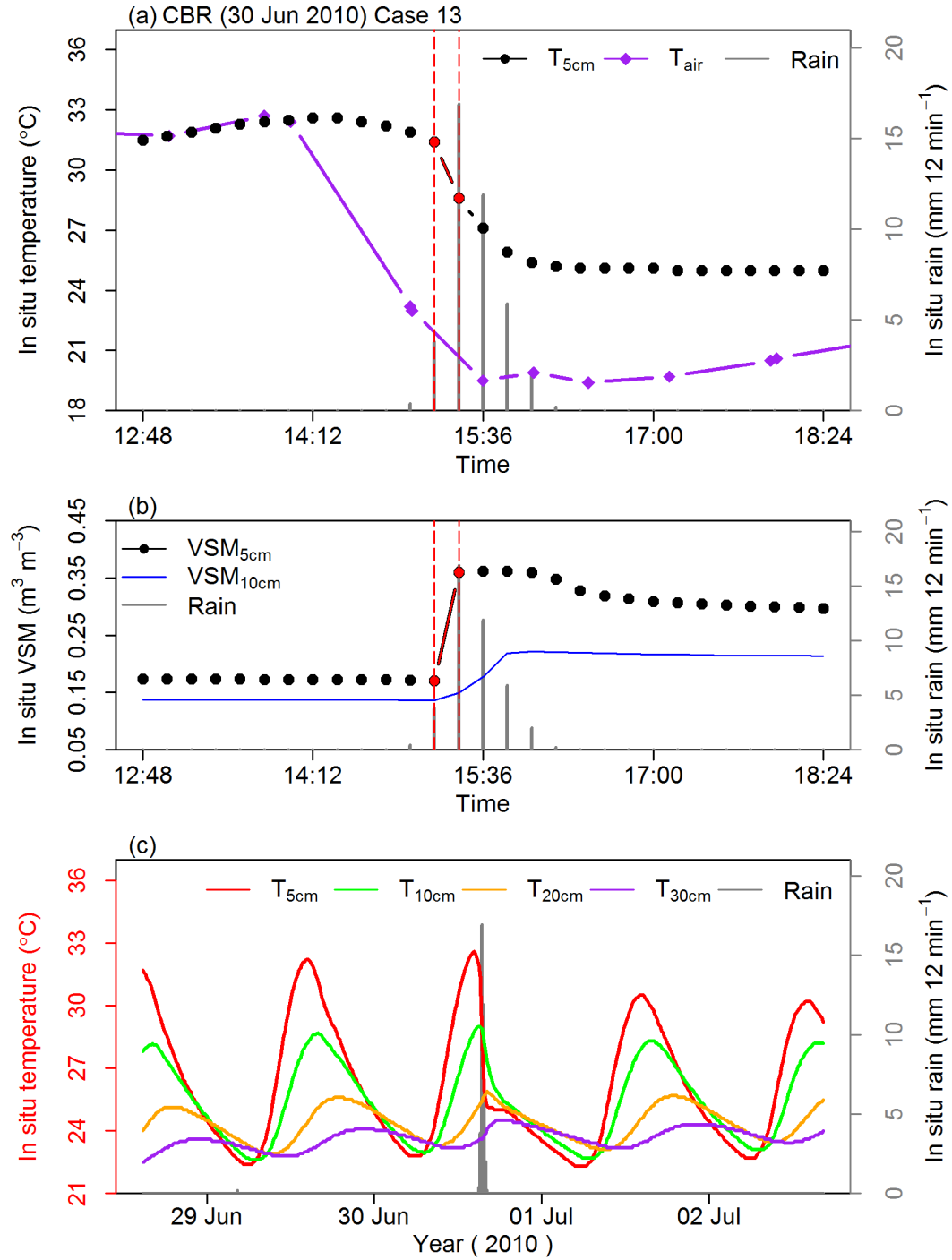


Figure S15. (a) In situ T_{5cm} (black) and accumulated rainfall (grey) observations measured every 12 min, and the maximum and minimum T_{air} values in an hour (purple); (b) in situ VSM_{5cm} (black), VSM_{10cm} (blue) observations also measured every 12 min, from case 13 (see Table 45) at CBR station on 30 June 2010. The red dashed lines show the duration from time t_1 to t_2 , and the corresponding T_{5cm} and VSM_{5cm} are highlighted by red. (c) In situ soil temperature measured from 28 June to 2 July 2010 at depths of 5, 10, 20 and 30 cm, together with the in situ rainfall observations ($mm\ 12\ min^{-1}$) shown in grey.

Examples of VSM_{5cm} response to rain

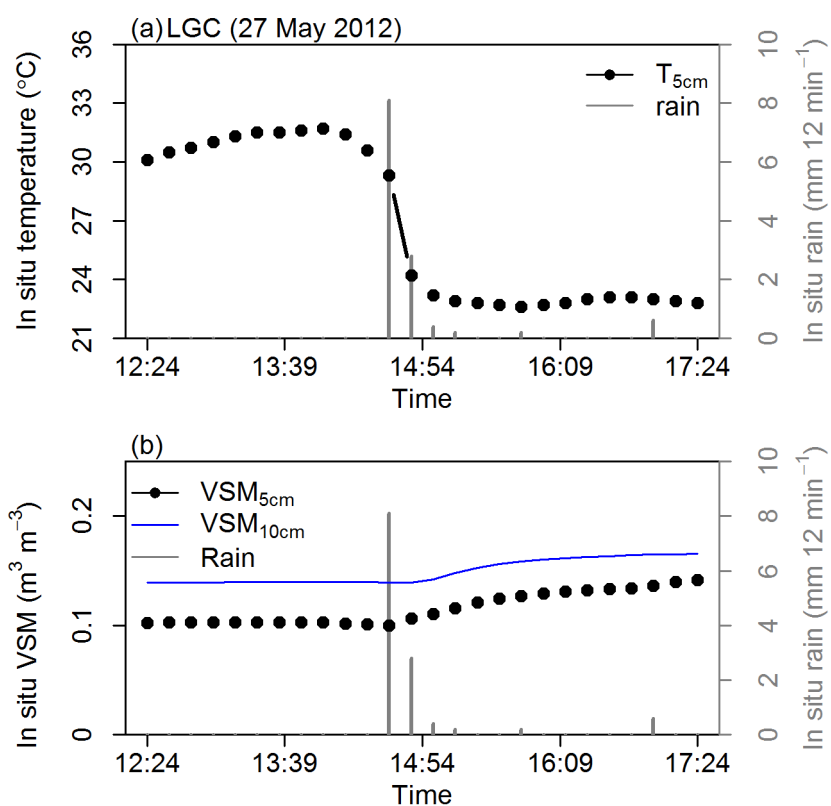


Figure S16. (a) In situ T_{5cm} (black) and rainfall (grey) observations, and (b) in situ VSM_{5cm} (black), VSM_{10cm} (blue) and rainfall (grey) observations are measured every 12 min at LGC station on 27 May 2012.

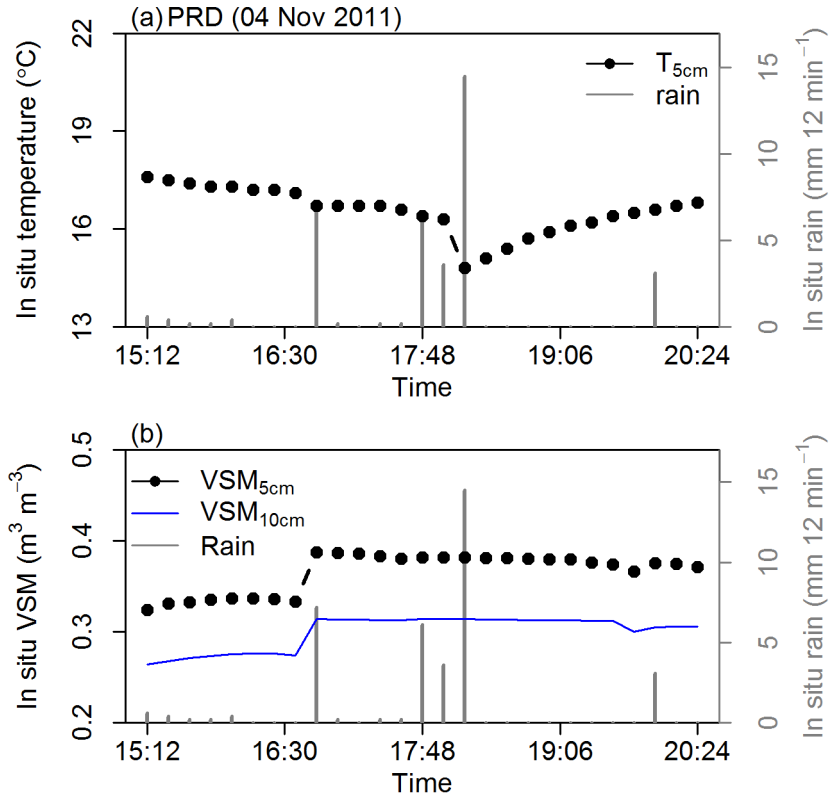


Figure S17. (a) In situ $T_{5\text{cm}}$ (black) and rainfall (grey) observations, and (b) in situ $VSM_{5\text{cm}}$ (black), $VSM_{10\text{cm}}$ (blue) and rainfall (grey) observations are measured every 12 min at PRD station on 4 November 2011.

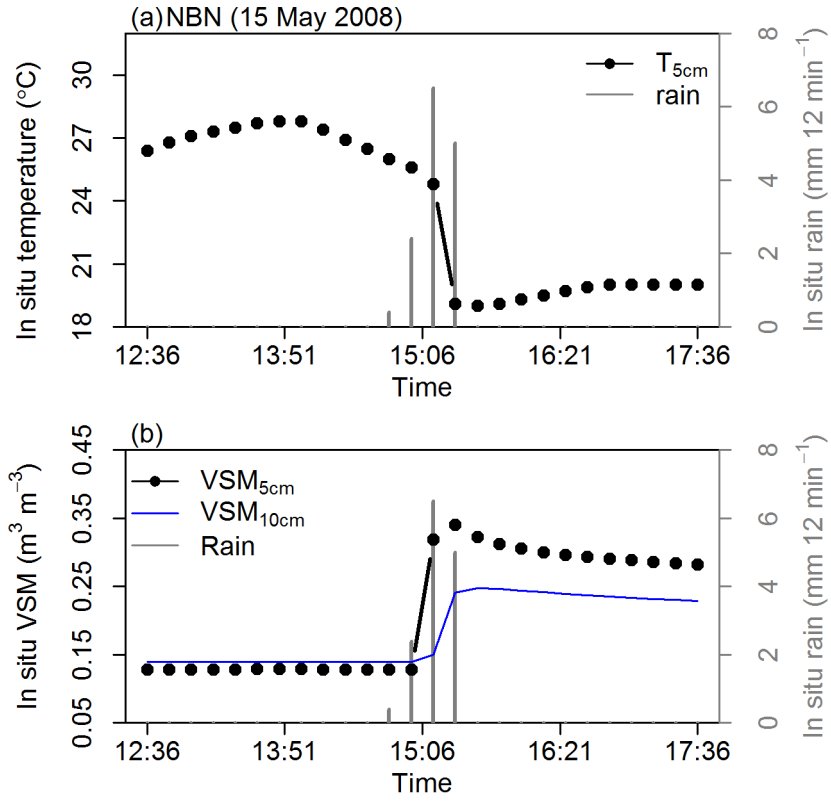


Figure S18. (a) In situ $T_{5\text{cm}}$ (black) and rainfall (grey) observations, and (b) in situ $VSM_{5\text{cm}}$ (black), $VSM_{10\text{cm}}$ (blue) and rainfall (grey) observations are measured every 12 min at NBN station on 15 May 2008.

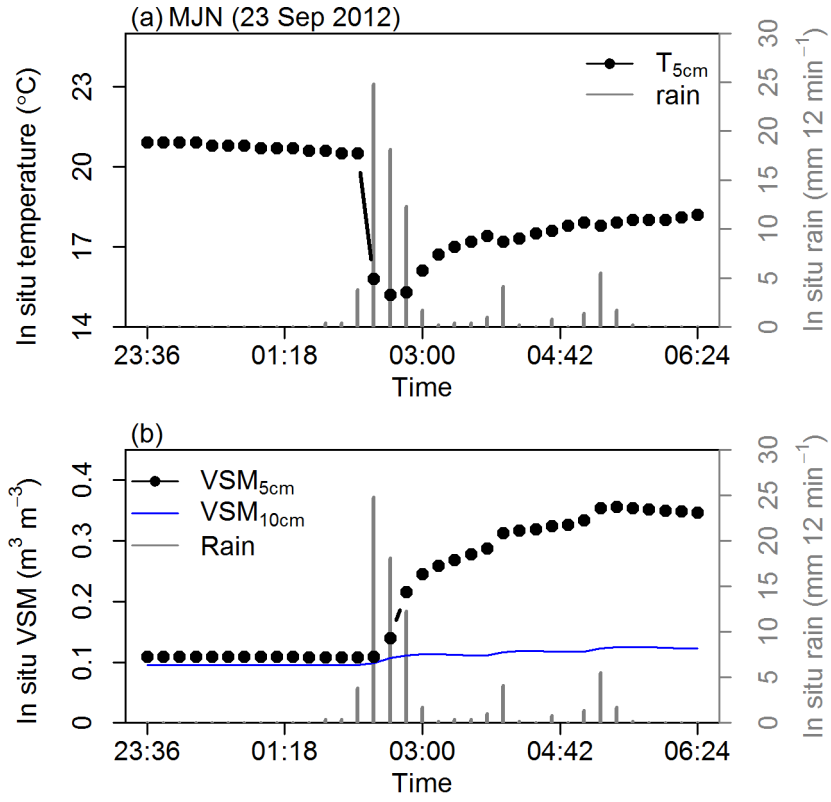


Figure S19. (a) In situ $T_{5\text{cm}}$ (black) and rainfall (grey) observations, and (b) in situ $VSM_{5\text{cm}}$ (black), $VSM_{10\text{cm}}$ (blue) and rainfall (grey) observations are measured every 12 min at MJN station on 23 and 24 September 2012.

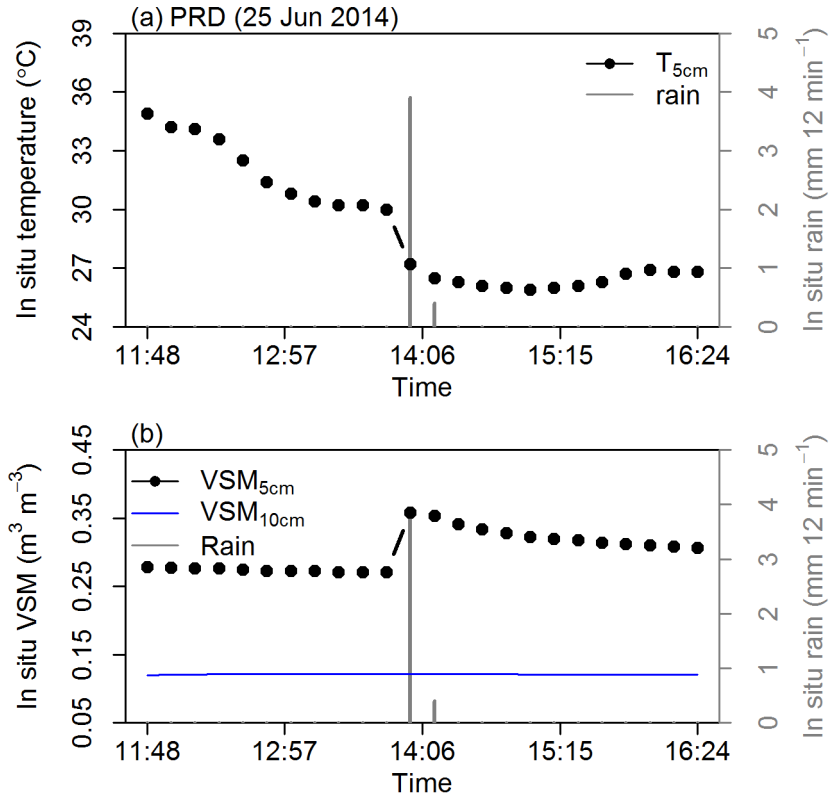


Figure S20. (a) In situ $T_{5\text{cm}}$ (black) and rainfall (grey) observations, and (b) in situ $VSM_{5\text{cm}}$ (black), $VSM_{10\text{cm}}$ (blue) and rainfall (grey) observations are measured every 12 min at PRD station on 25 June 2014. $VSM_{5\text{cm}}$ increase is observed together with the $T_{5\text{cm}}$ decrease, but there is no change in $VSM_{10\text{cm}}$, below $0.15 \text{ m}^3 \text{ m}^{-3}$.

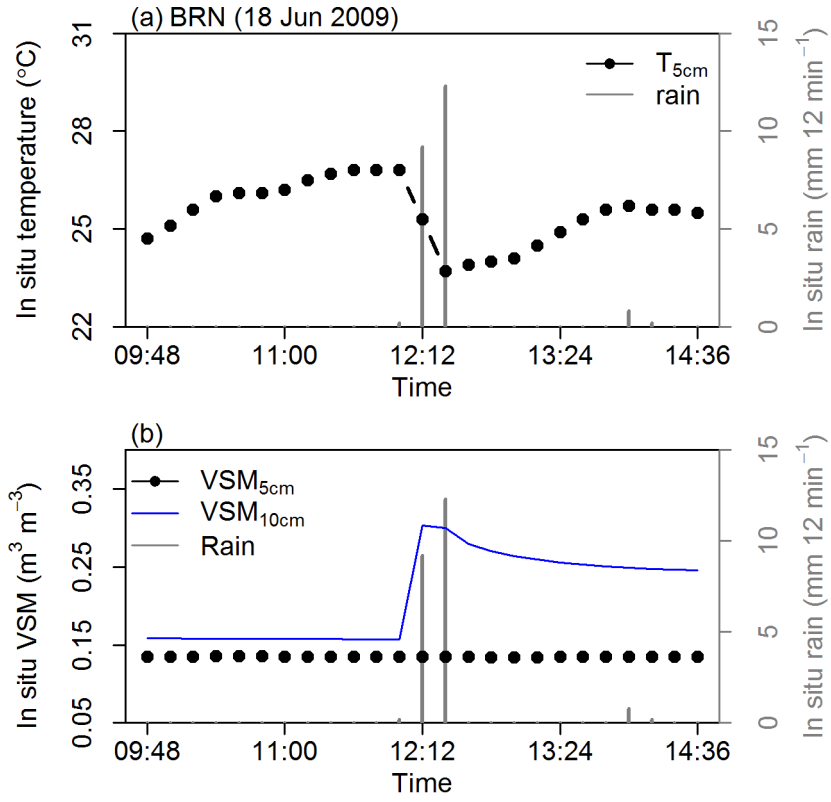


Figure S21. (a) In situ $T_{5\text{cm}}$ (black) and rainfall (grey) observations, and (b) in situ $\text{VSM}_{5\text{cm}}$ (black), $\text{VSM}_{10\text{cm}}$ (blue) and rainfall (grey) observations are measured every 12 min at BRN station on 18 June 2009. $\text{VSM}_{10\text{cm}}$ increase is observed together with the $T_{5\text{cm}}$ decrease, but there is no change in $\text{VSM}_{5\text{cm}}$, below $0.15 \text{ m}^3 \text{ m}^{-3}$.

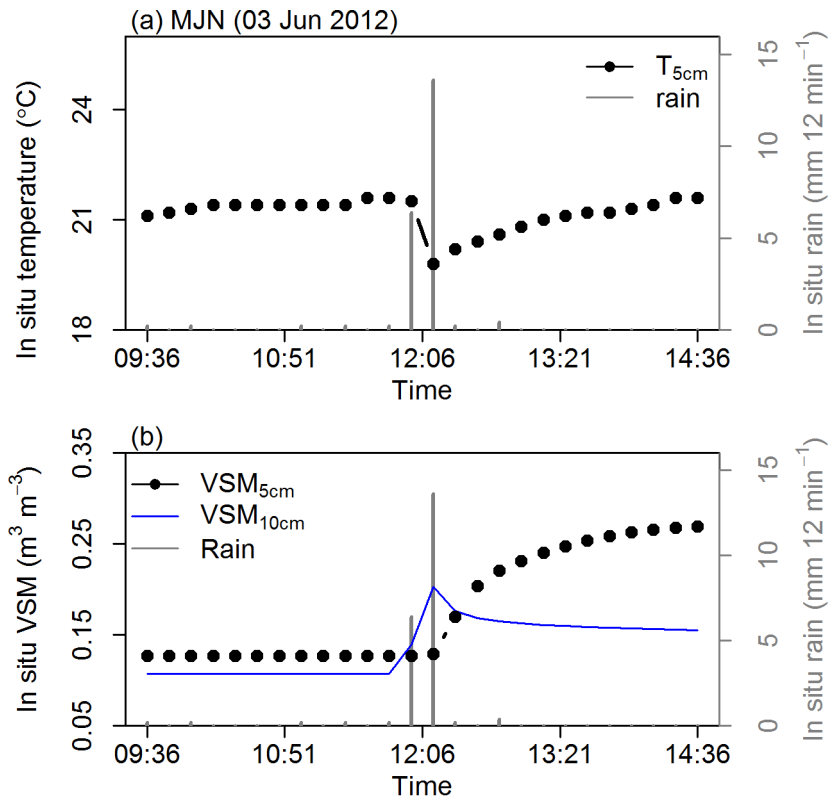


Figure S22. (a) In situ $T_{5\text{cm}}$ (black) and rainfall (grey) observations, and (b) in situ $VSM_{5\text{cm}}$ (black), $VSM_{10\text{cm}}$ (blue) and rainfall (grey) observations are measured every 12 min at MJN station on 3 June 2012.

Starting time of intense soil-cooling rains

Figure S23 investigates the distribution of the starting time of the intense soil-cooling rains at a resolution of 1 hour together with the corresponding average rain rate (in mm h^{-1}) across seasons. For the 4 winter events, the rain rate is relative small (less than 7.5 mm h^{-1}). Only 3 events are found with a rain rate larger than 50 mm h^{-1} , two in summer and one during the autumn. It can be seen that the intense soil-cooling rains tend to occur at daytime. A large proportion (83 %) of the 122 intense soil-cooling rains occur between 09:00 and 21:00 UTC, which is much larger than the fraction of 67 % observed for the 1577 marked rainfall events affecting $T_{5\text{cm}}$. The intense soil-cooling rains are rather uniformly distributed between 09:00 and 21:00 UTC.

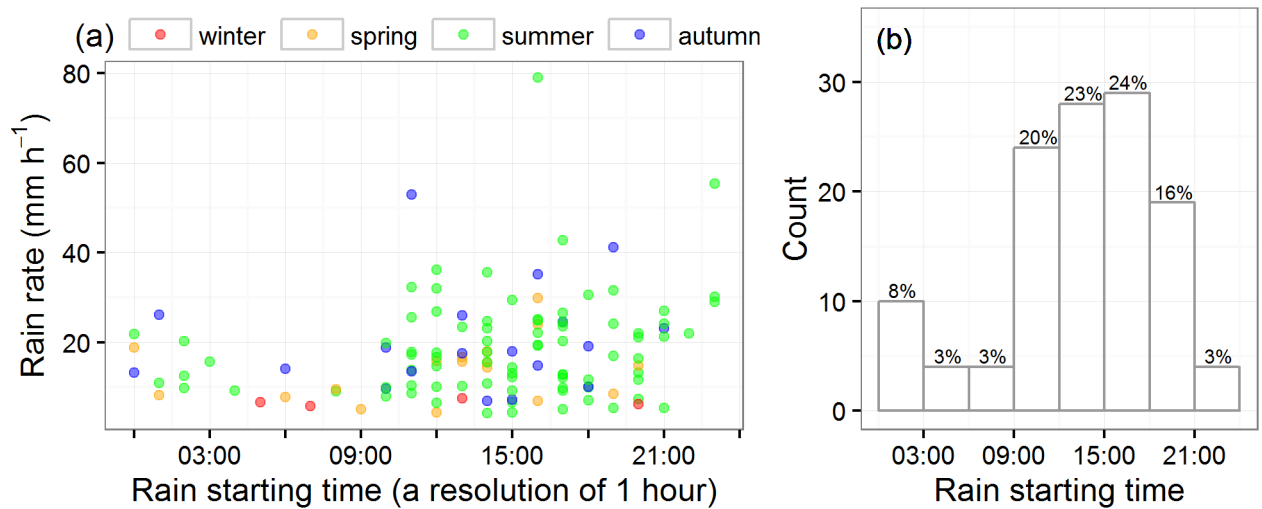


Figure S23. Starting time of the 122 intense soil-cooling rains: vs. rain rate across seasons (a), and statistical distribution with bins of 3 hours (b).

Examples of ISBA simulations

Current versions of the ISBA (Interactions between Soil, Biosphere, and Atmosphere) land surface model (LSM) developed by Centre National de Recherches Météorologiques (CNRM) neglect the precipitation-induced sensible heat flux. Soil temperature and VSM simulations at depths of 5, 10, 20 and 30 cm were performed using the ISBA LSM within the SURFEX (version 8.0) modeling platform (Masson et al., 2013). The ISBA configuration and the hourly SAFRAN atmospheric analysis (Durand et al., 1993, 1999) we used to force the model at a spatial resolution of 8 km x 8 km are described in Lafont et al. (2012) and Decharme et al. (2013). ISBA simulations of topsoil soil moisture and soil temperature profiles for the grassland plant functional type are considered.

Figure S24 presents the ISBA numerical simulations of soil temperature and soil moisture at the PRD station from 21 to 25 August 2015 at depths of 5, 10, 20 and 30 cm. Since ISBA does not represent the heat exchange caused by the mass movement of rainwater, the simulated topsoil temperature is only driven by the surface energy budget, including the evaporation of rainwater intercepted by the vegetation, and by heat conduction from deeper soil layers. As a result, almost no soil temperature change is simulated while changes in soil moisture in response to the rain are simulated. In this example, the rainfall event as a whole is represented well by the SAFRAN atmospheric forcing used to force the ISBA model. In SAFRAN, the rainfall event lasts for 14 h, starting at 10:00 UTC and ending at 23:00 UTC. Over this period of time, the accumulated rainfall of SAFRAN rain is 86.4 mm, very close to the observed accumulated rainfall of in situ rain of 86.1 mm (note that this time period differs from the one used in Table 5). However, SAFRAN is not able to represent the sub-hourly variability of rainfall intensity. While the observed peak rainfall intensity value is 27.8 mm in 12 minutes at 12:36 UTC (Figure 2), SAFRAN indicates a rather constant intensity of about 6 mm h⁻¹. The shown ISBA simulations represent the current state of hourly operational land surface monitoring, available over whole of metropolitan France. This means that the best possible operational simulations currently available are not able to represent the impact of intense precipitation on the soil temperature profile. The ISBA land surface model needs to be improved. The SAFRAN atmospheric analysis could also probably be improved by using more in situ observations together with high resolution atmospheric simulations.

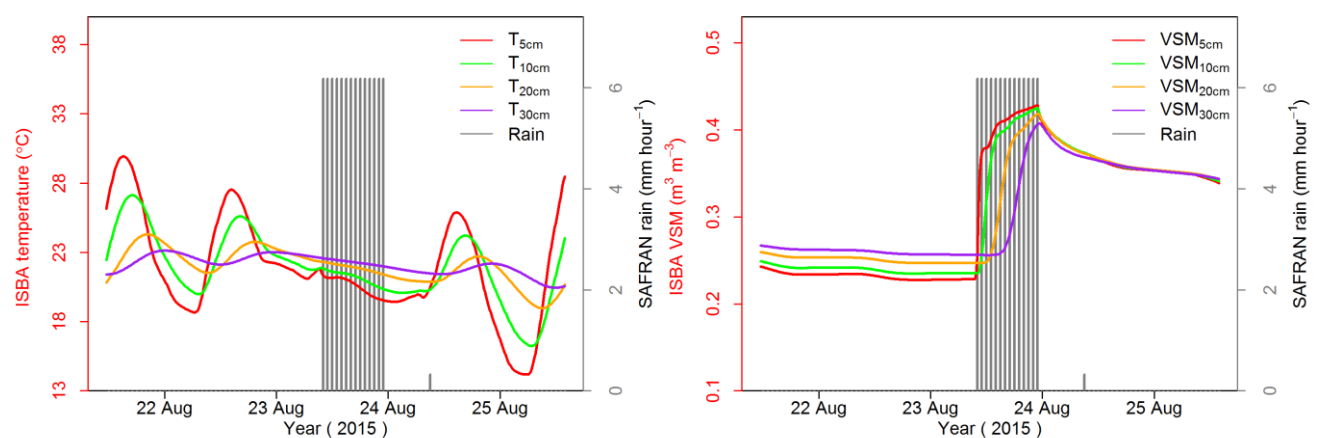


Figure S24. ISBA simulations of soil temperature (left) and soil moisture (right) at the PRD station from 21 to 25 August 2015 at depths of 5, 10, 20 and 30 cm, together with the SAFRAN rainfall data (mm hour⁻¹) shown in grey.

Figure S25 presents the statistical distribution of minimum $\Delta T_{5\text{cm}}$ observations, and the corresponding minimum $\Delta T_{5\text{cm}}$ values simulated by the ISBA model for the 1577 marked rainfall events affecting $T_{5\text{cm}}$. It appears that step 5 tends to remove the longest rainfall events and the selected rainfall events last less than 4 hours. The comparison between observed and simulated values shows that ISBA is not able to simulate $\Delta T_{5\text{cm}}$ values well. In particular, most of the simulated minimum $\Delta T_{5\text{cm}}$ values do not depart much from 0 °C in 12 minutes during intense soil-cooling events, even for very intense ones with observed minimum $\Delta T_{5\text{cm}}$ values lower than -4 °C in 12 minutes. Figure S25 also shows that most of the 122 intense soil-cooling events occur in M or in MM climate conditions.

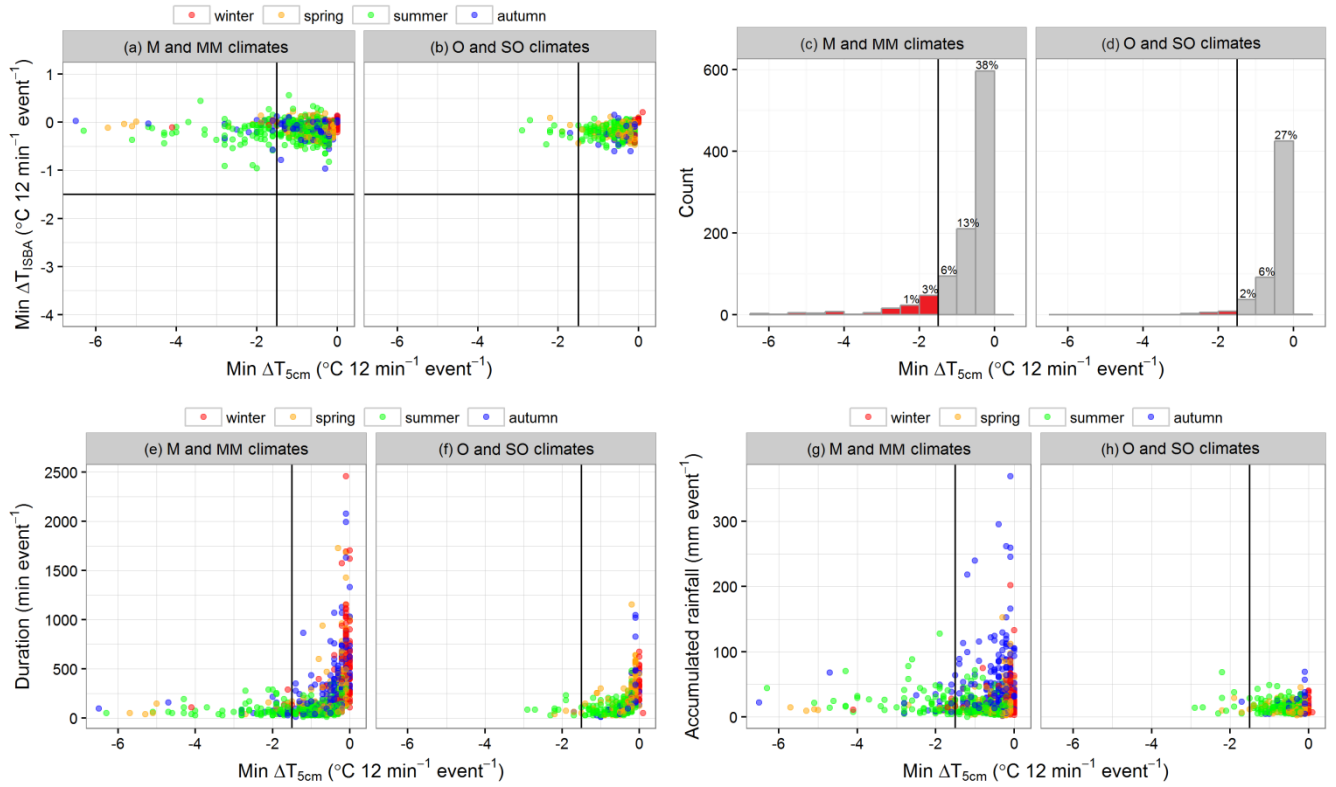


Figure S25. Minimum $\Delta T_{5\text{cm}}$ during 1577 marked rainfall events affecting $T_{5\text{cm}}$: vs. minimum ΔT_{ISBA} (a, b), statistical distribution (bins of 0.5 °C) (c, d), vs. rain duration (e, f), and vs. the accumulated rainfall (g, h), for Mediterranean (M) and Mediterranean-mountain (MM) stations (a, c, e, g) and for oceanic (O) and semi-oceanic (SO) stations (b, d, f, h). Dark lines are for the -1.5 °C threshold for intense soil-cooling rains (step 5 in Table 2).

References

- Durand, Y., Brun, E., Mérindol, L., Guyomarc'h, G., Lesaffre, B., and Martin, E.: A meteorological estimation of relevant parameters for snow models, *Ann. Geophys.*, 18(1), 65–71, <https://doi.org/doi:10.1017/S0260305500011277>, 1993.
- Durand, Y., Giraud, G., Brun, E., Merindol, L., and Martin, E.: A computer-based system simulating snow-pack structures as a tool for regional avalanche forecasting, *Ann. Glaciol.*, 45(151), 469–484, <https://doi.org/doi:10.1017/S0022143000001337>, 1999.
- Lafont, S., Zhao, Y., Calvet, J.-C., Peylin, P., Ciais, P., Maignan, F., and Weiss, M.: Modelling LAI, surface water and carbon fluxes at high-resolution over France: comparison of ISBA-A-gs and ORCHIDEE, *Biogeosciences*, 9, 439–456, <https://doi.org/10.5194/bg-9-439-2012>, 2012.
- Masson, V., Le Moigne, P., Martin, E., Faroux, S., Alias, A., Alkama, R., Belamari, S., Barbu, A., Boone, A., Bouyssel, F., Brousseau, P., Brun, E., Calvet, J.-C., Carrer, D., Decharme, B., Delire, C., Donier, S., Essaouini, K., Gibelin, A.-L., Giordani, H., Habets, F., Jidane, M., Kerdraon, G., Kourzeneva, E., Lafaysse, M., Lafont, S., Lebeaupin Brossier, C., Lemonsu, A., Mahfouf, J.-F., Marguinaud, P., Mokhtari, M., Morin, S., Pigeon, G., Salgado, R., Seity, Y., Taillefer, F., Tanguy, G., Tulet, P., Vincendon, B., Vionnet, V., and Voldoire, A.: The SURFEXv7.2 land and ocean surface platform for coupled or offline simulation of earth surface variables and fluxes, *Geosci. Model Dev.*, 6, 929–960, <https://doi.org/10.5194/gmd-6-929-2013>, 2013.